Three Dimensional Kinematic and Surface Interaction Analysis of a Novel Total Ankle Replacement Surface Design Using a Numerical Model of the Hind Foot.

A Thesis

Submitted to the Faculty

of

Drexel University

by

Wagdi George Mankarious

in partial fulfillment of the

requirements for the degree

of

Masters of Science in Biomedical Engineering

August 2014

Dedications

I dedicate this thesis to my family and friends. They have supported me and gave me the confidence to push myself through struggles and pursue great goals in life.

Acknowledgments

I would like to thank God who through His will guided me through this process and lead me to success. My simple and small efforts by themselves were not what resulted in the success of this study and I pray that He may continue to bless me in my future endeavors.

I would like to thank my dad, George, my mom, Jaclein and my sister Soufia who supported me and offered their help in any way that they could. Their constant support and guidance was the foundation of this work and the backbone of its success. From the constant enthusiastic questions about my progress, to listening to me practice my defense I am grateful for their care and love towards me and my efforts.

I would like to thank Dr. Siegler for his guidance during this study and for giving me many opportunities to improve my work and myself personally. You have not only guided me in this study but have also guided me in making important academic decisions. I truly believe that God has led me to you knowing that you will provide me with great insight and opportunities in academia and I am grateful for that. Special thanks also to Dr. Jason Toy who introduced me to Dr. Siegler and has taken time from his busy schedule to help me during my first days of the study.

Finally, I would like to thank my lab mates who have not left me to my own devices but have always looked out after me and made sure that I don't stumble in my work. I wish that wherever I go to work I have co-workers that act and behave like the teammates you guys are.

Table of Contents

List of Tables

List of Figures

Abstract

Three Dimensional Kinematic and Surface Interaction Analysis of a Novel Total Ankle Replacement Surface Design Using a Numerical Model of the Hind Foot.

Wagdi George Mankarious

Sorin Siegler, Ph.D.

Ankle joint end stage osteoarthritis can be a deliberating condition that is often not treated due to lack of viable treatment options. The current standard of treatment is total ankle fusion which does not only limit mobility but can lead to further complications with neighboring joints. Alternative treatment uses the currently improving Total Ankle Replacements (TAR). Until recently, TAR have been widely unsuccessful due to the accepted design based off a dated assumption which states that the ankle is a one degree of freedom joint with a fixed axis of rotation. Similar to improvements made to knee implants after the proper kinematics of the knee were noted, the TAR have improved when work done by many researchers concluded that the ankle joint is not a one degree of freedom joint and that it doesn't have a fixed axis of rotation for any of its degrees of freedom. This study proposes a novel design for a TAR based off of a novel morphological study done by Siegler et. al. and analyzes the kinematics and interactions of the novel articulating surfaces compared to traditional TAR designs.

The proposed method of analysis uses a currently available 3-D dynamic model of the hind foot to assess ankle joint kinematics and articulating surface interactions by looking at the results of range of motion, kinematic coupling, ligaments strains and spatial distance mapping of the articulating surfaces. Five different models were analyzed. A Natural model of the hind foot, an Inman design based on the dated morphological study done by Inman, a Conic and Cylindrical designs based on current fashions of TAR and a novel Anatomical design based on the morphological study done by Siegler.

The results of the study supported the notion that the ankle is not a one degree of freedom joint and that it did not have a fixed axis of rotation. Range of motion was found to be slightly increased compared to the natural ankle with the novel Anatomical design while the traditional designs have not delivered the same range of motion. Kinematic coupling was found to be similar across the five models, which hinted to the larger role ligaments play in kinematic coupling. Ligament strain analysis found that the Anatomical design allowed for major ankle joint ligaments to be strained similar to that of the Natural model. Articulating surface interactions were similar to that of the Natural model in the Anatomical design due to the anatomically similar saddle geometry of the implant surface design compared to the natural anatomy.

Chapter 1: Introduction

Often overlooked the ankle joint experiences significant forces and moments during daily activities such as walking, climbing stairs or treading uneven ground. Such simple activities can produce forces in ankle up to 8 times the body weight[1]. Over time the cartilage in the ankle joint, specifically the talocrural joint, begin to dry out and break down until bone on bone contact develops and pain results. As a result of this osteoarthritis, physicians favor mitigating symptoms using the common pain medication, steroids and anti-inflammatory medicine. This however is not treating the problem but simply the symptom. In order to treat this end-stage osteoarthritis two competing options take place. The first is fusing the ankle joint and thus significantly limiting the functionality of the joint and also causing other complications. For example, fusing the talocrural joint leads to complication in the neighboring subtalar joint. The other treatment option is Total Ankle Replacements (TAR) where the implications include lack of long term survivability[2].

Similar to the knee joint, initial TAR designs assumed the ankle contained only one degree of freedom and acted like a hinge joint. This assumption led to the development of ankle joints that were oversimplified and failed rapidly. The second attempt was to make ankle implants similar to a hip implant where the tibia was the ball and the talus was the socket of a ball and socket joint. This obviously did not last as it resulted in major ligament strains and tears due to lack of stability. One main finding that improved the TAR was the fact that the ankle does not have a fixed axis of rotation[3]. Similar to knee replacements, which at first were highly unsuccessful due to the assumption that it acted like a hinge joint with a single axis of rotation, the TAR began to be designed to allow this floating axis of rotation and provided he implant with the ability to slide and translate rather than just rotate.

While current TAR are becoming more successful with higher survival rates and increased implantation accuracy, there is still a need for a more successful TAR as the recent TAR survive approximately 5-6 years[4]. Current TAR are based off the study done by Inman, which describe the talar dome as a frustum of a symmetrical cone that apexes medially and contains a saddle[5]. However, studies done by Siegler that show that the talar dome can be approximated as a frustum of a skewed cone that apexes laterally and contains a saddle. The inaccuracy in Inman's apical finding can be realized by identifying a key morphological feature of the talus. When looking at the lateral and medial condyles of the talar dome one can notice how the lateral condyle is superior to the medial condyle. When Inman measured the axis of the cone and looked for the apex, he measured in such a way that relied on this morphological feature which gave Inman the impression that the cone apexes medially when it accurately apexes laterally[5]. In other words the radius of curvature of a best fit circle on the medial and lateral condyles of the talar dome is smaller at the lateral side and not the medial side as Inman suggests[6].

This study is geared towards designing and analyzing the different kinematic behaviors of five different ankle models and relating them to the proposed reasons of failure of current TAR, using an in vitro numerical model. The five models include: 1) A model of the native ankle bones used as a control (Natural model), 2) a symmetrical conic implant surface design that apexes medially based on the measurements Inman used (Inman model), 3) a symmetrical conic implant surface design that apexes laterally (Conic model), 4) a symmetrical cylindrical implant surface design that models current implant types (Cylindrical model), and 5) a novel skewed and saddled conic implant surface design based on the measurements Siegler used (Anatomical model).

Primary Goal and Specific Aims

The primary goal of this study is to develop and analyze four different ankle implant surface designs and compare them to the natural ankle kinematics and surface interaction using a verified dynamic model of the hind foot. The dynamic model will be used to evaluate range of motion of the ankle joint complex (the talocrural and subtalar joints together), kinematic coupling, ligament strains and the surface to surface interaction of the talocrural joint.

In order to accomplish the primary goal, the following specific aims will be set for this study.

1) Create three different implant surface designs based on current TAR and Inman's morphological study.
2) Create novel implant surface design based on Siegler's morphological study.
3) Measure the morphological features of seven MRI scanned 3-D models of the tibia based on the methods used by Siegler.
4) Position or "implant" the surface designs on to a 3-D dynamic model of the hind foot to obtain results on kinematic behavior, ligament strains and surface interaction.
5) Analyze the range of motion, kinematic coupling, ligament strains and surface interaction of the different designs and form conclusion.

Chapter 2: Background

Physiology of the Ankle

The ankle joint contains two major joints, the talocrural and subtalar joints. The talocrural joint is the articulation between the distal ends of the tibia and fibula with the proximal end of the talus. This is also known as the mortise joint because of the geometry of the joint space. The subtalar joint is the articulation between the inferior side of the talus with the superior side of the calcaneus. These two joints make the ankle joint complex (AJC) which is what this study will observe the kinematics of. There are many ligaments in the AJC but only a few will be considered in this study as they are the ones involved with stability and kinematic behavior. The ligaments looked at in this study include the anterior talofibular ligament (ATFL), the anterior tibiotalar ligament (ATTL), the calcaneofibular ligament (CFL), the posterior talofibular ligament (PTFL), the posterior tibiotalar ligament (PTTL), the tibiocalcaneal ligament (TCL) and the tibiospring ligament (TSL).

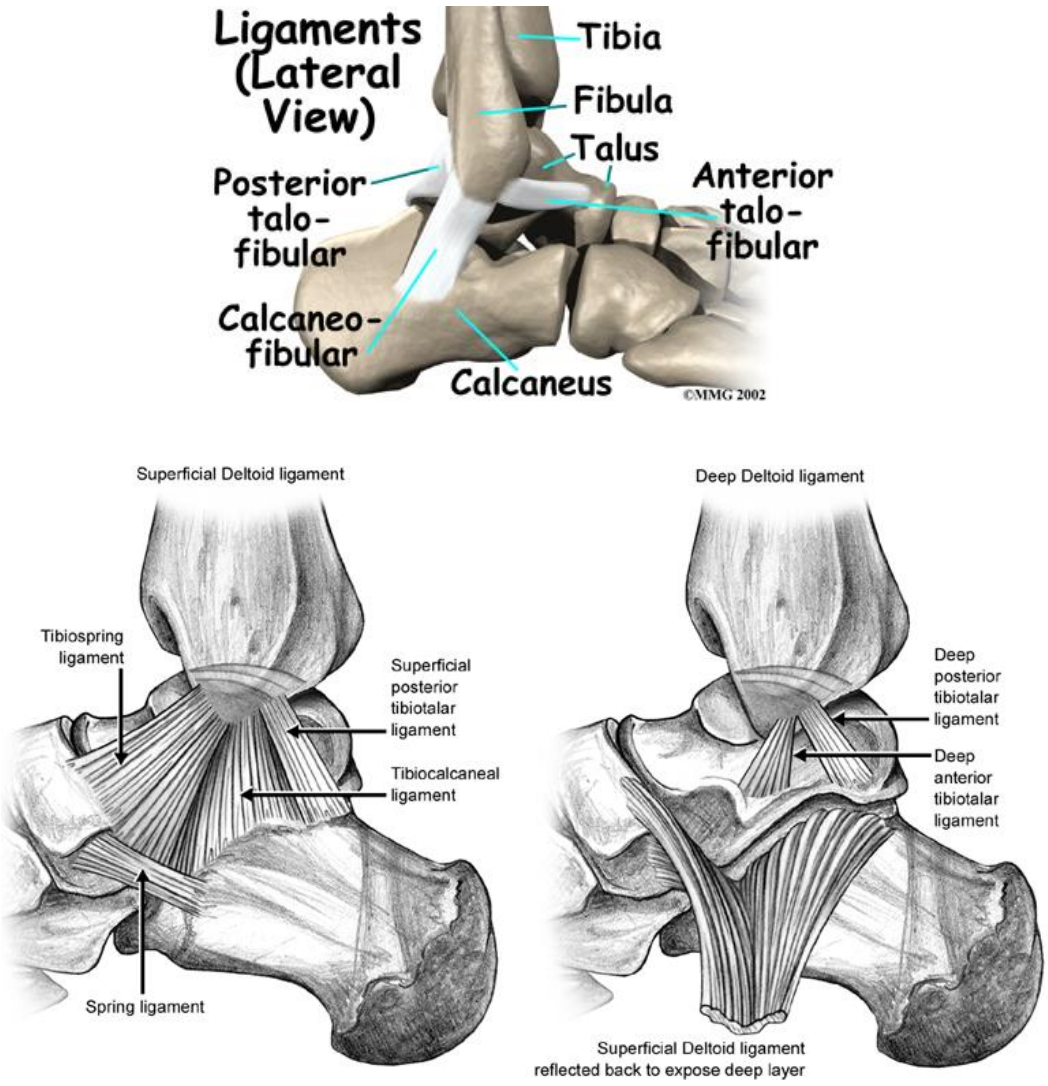

Figure 1: Top image displaying lateral ligaments[7]. Bottom images display the components of deltoid ligaments[8].

The ATFL resists plantar flexion, inversion and internal rotation[9]. The ATTL resists plantar flexion, inversion and external rotation. The CFL resists dorsiflexion, inversion and external rotation. The PTFL resists dorsiflexion and external rotation[10]. The PTTL resists dorsiflexion, inversion and internal rotation[11]. The TCL resists dorsiflexion, eversion and external rotation. The TSL resists plantarflexion, eversion and both internal and external rotation[12].

Grood and Suntay Parameters

A standardized method of measuring and labeling the axis of rotations and translation of the knee have been proposed by Grood and Suntay and have been adopted for use in this study and other studies of ankle joint kinematics[13]. It describes and labels three axes based on the inter-malleolar axis of the ankle. The inter-malleolar axis is described as the axis at runs through the most inferior parts of the tibial and fibular condyles. This axis was used to define the dorsiflexion-plantarflexion moment axis (Alpha, e1). Perpendicular to that axis and facing anteriorly is the inversion-eversion axis (Beta, e2). Perpendicular to both axes and going through the point between the medial and lateral proximal condyles of tibia is the axis for internal and external rotation (Gamma, e3). Figure 2 displays this implemented in the numerical model used to evaluate the different implant surface designs.

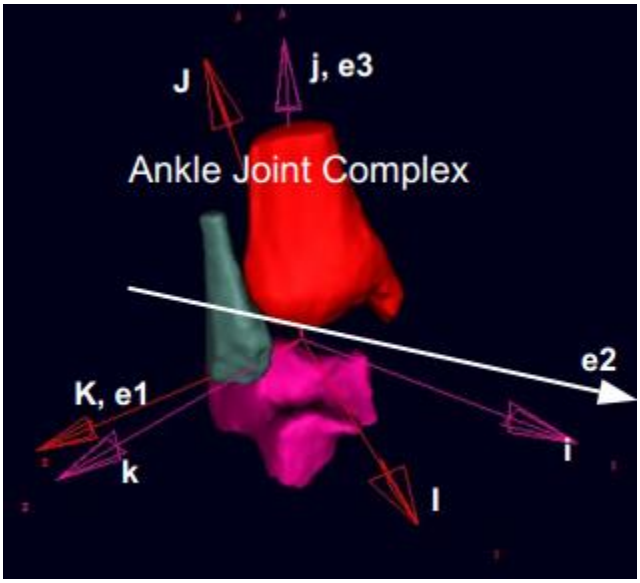

Figure 2: Ankle joint complex with Grood and Suntay Axes[14].

Kinematics of the Ankle

The ankle is a six degree of freedom joint that translates and rotates in all three planes, sagittal, coronal and transverse. There is an assumed fixed axis of rotation for the motions but this is uncertain as it is proved incorrect in this study, and is also supported by this study that found the ankle to roll backwards during plantarflexion and forwards during dorsiflexion[15].

In the sagittal plane the ankle moves into dorsiflexion and plantarflexion. Most of this motion is attributed to the talocrural joint (80%) while the subtalar joint contributes the rest[16]. The range of motion (ROM) in this plane was found to average about 60^{o} in the natural ankle[17]. In the coronal plane the ankle moves into inversion and eversion. Most of this motion is attributed to the subtalar joint (60%) while the talocrural joint contributes the rest[17]. The range of motion averages about in this plane was found to be about 60^{o}. In the transverse plane the ankle moves into internal and external rotation. This motion is split almost evenly and the range of motion in this plane can reach up to 25^{o}[3].

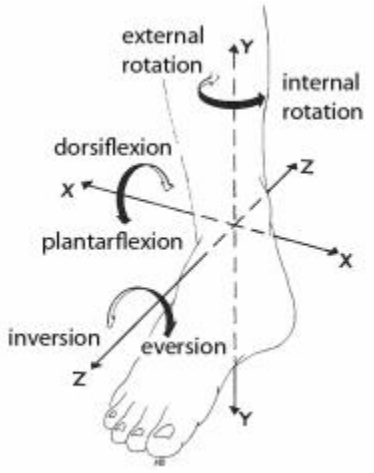

Figure 3: The degrees of freedom in the ankle joint[18].

These motions are coupled with each other in such a way that as the ankle goes into dorsiflexion it also goes into eversion and external rotation, and when the ankle goes into plantarflexion it also goes into inversion and internal rotation[16].

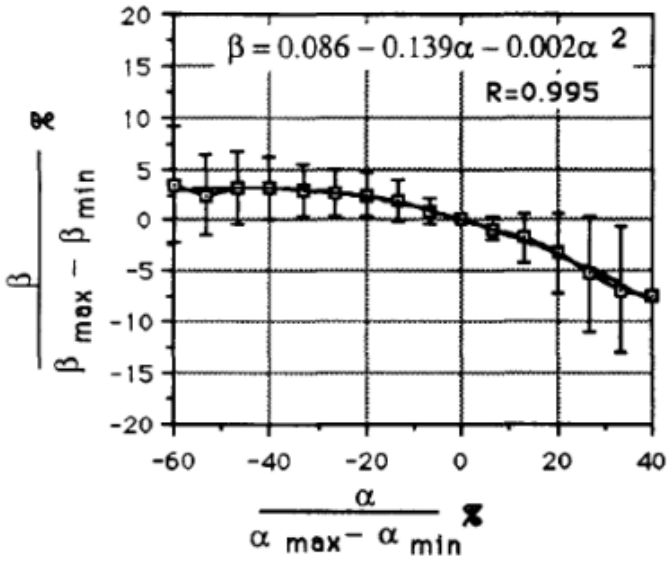

Figure 4: Kinematic Coupling between dorsiflexion-plantarflexion (Alpha) and inversion-eversion (Beta)[16].

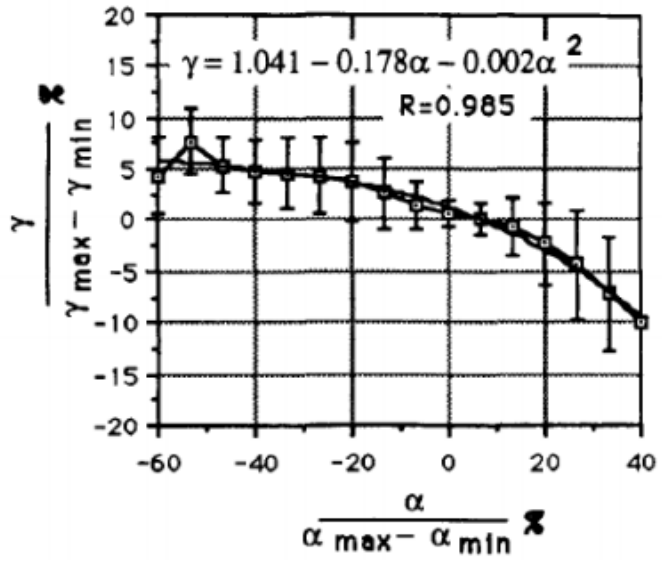

Figure 5: Kinematic Coupling between dorsiflexion-plantarflexion (Alpha) and internal-external rotation (Gamma)[16].

Inman's vs Siegler's Morphology Studies

It has been studied and observed that kinematic behaviors of the ankle joint vary from person to person based on the morphology of their hind foot and ligament structures[19]. Based on Inman's studies, it was concluded that the shape of the talar dome can be approximated by a frustum of a cone that apexes medially. This however was inaccurate as it used the assumption that the ankle is a one degree of freedom joint that rotates about the inter-malleolar axis. This assumption is what led to the incorrect conclusion of the apex of the cone and can also be seen in the method used by Inman to find the apex. 60 years later Siegler did a study where he did not assume a fixed axis of rotation. In his study, Siegler took sagittal measurements of the talus and used best fit circles to estimate the radius of curvature of the talus at the medial and lateral condyles. The centers of these two circles were used as the axis of rotation in the sagittal plane to make coronal sections of the talus and measure again the radii of curvature in the coronal plane.

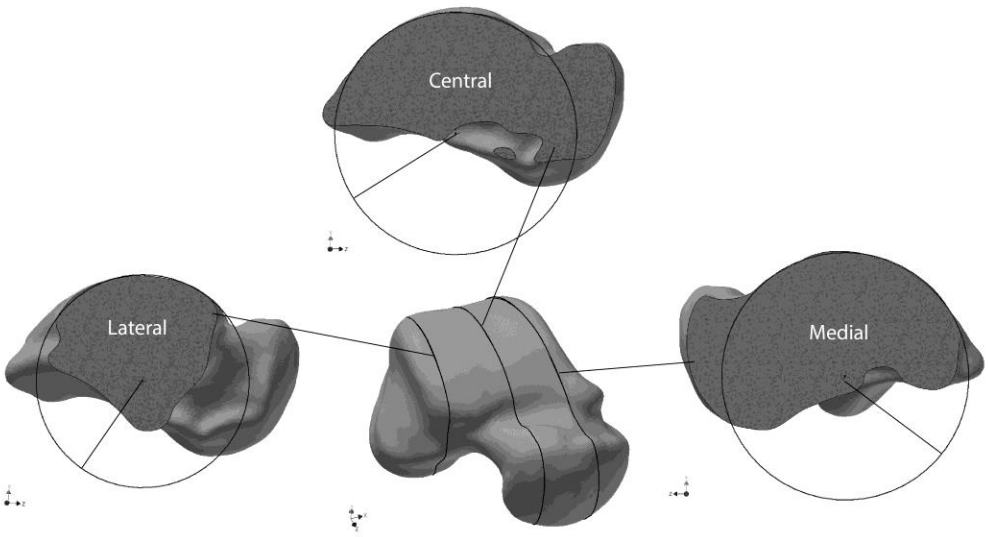

Figure 6: Best fit circles fit over medial, central, and lateral condyles of the talar dome[6].

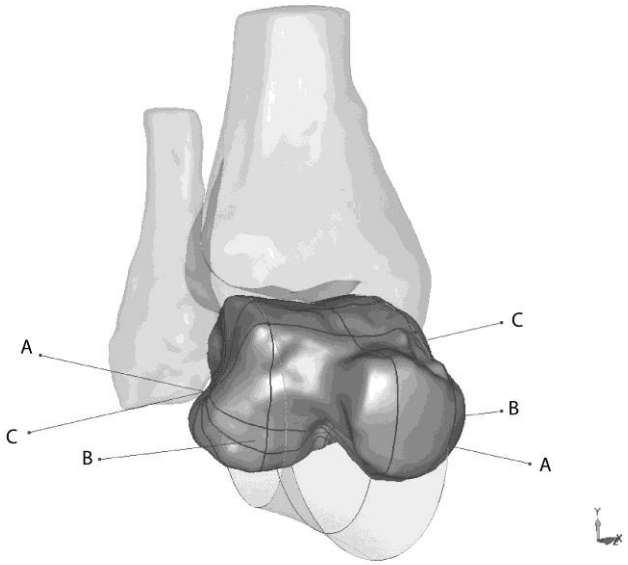

Figure 7: Line C-C labels the inter-malleolar axis, line B-B labels the perpendicular to the medial best fit circle going through its center, line A-A labels the line connecting the centers of the medial and lateral best fit circles[6].

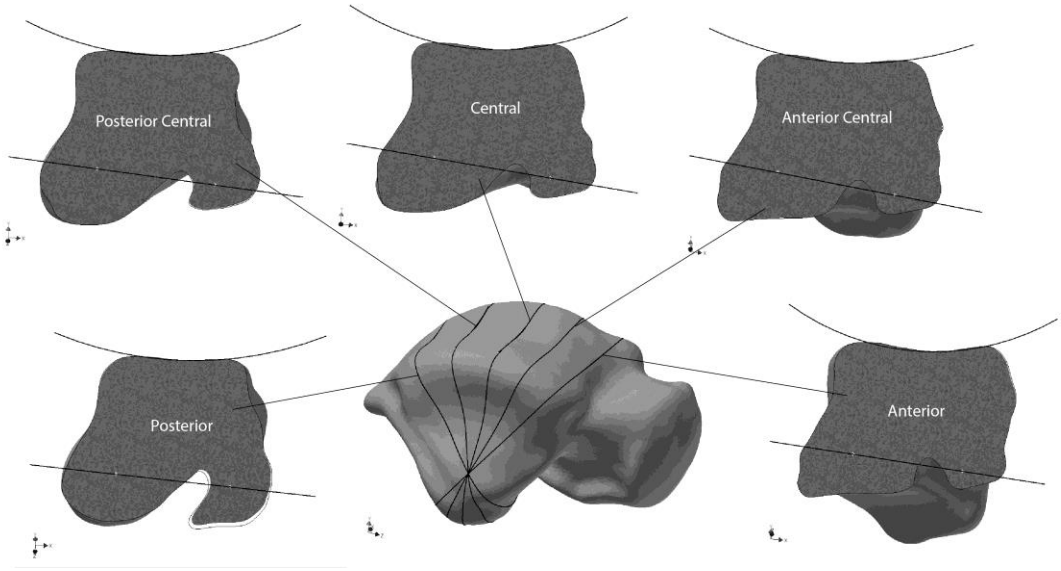

Figure 8: The coronal cuts made to measure the radius of curvature of the talar dome[6].

From these measurements it was found that the talar dome can be approximated by a frustum of a cone that apexes laterally rather than medially. It was also found that the axis of

the cone did not lie on the inter-malleolar axis[6]. From these new findings, novel implant surface designs were created for the talar dome and compared to the designs constructed based on Inman's morphological study.

Dynamic Numerical Model

Carl Imhauser developed a patient specific, numerical dynamic model of the hind foot that was later verified using experimental results[14]. The model used in this study is one of the models Imhauser developed called CAD5L. To summarize, these models were created by first taking MRI scans of cadaver legs in order to obtain the geometry of the bones of the ankle joint. 3DVIEWNIX along with an algorithm called Marching Cubes was then used to construct 3-D models from the MRI scans.

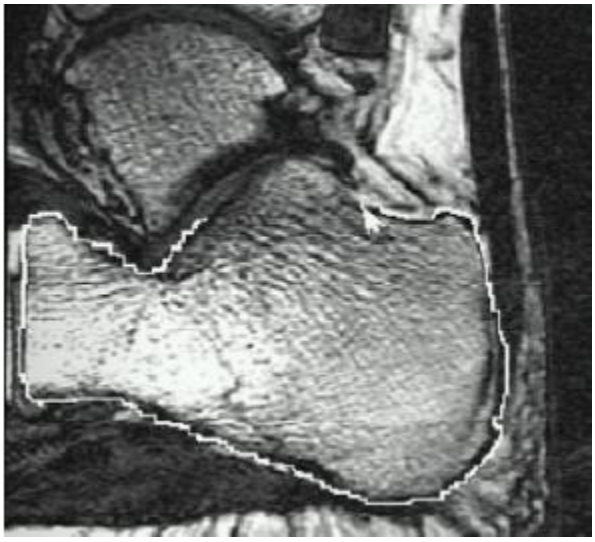

Figure 9: MRI scan being analyzed and segmented to create 3-D model[14].

Insertion points of major ligaments were recorded and used when the dynamic model of the ankle was developed. A reverse engineering software (Geomagic) was then used to refine the bone and smooth out any noise in the image processing phase.

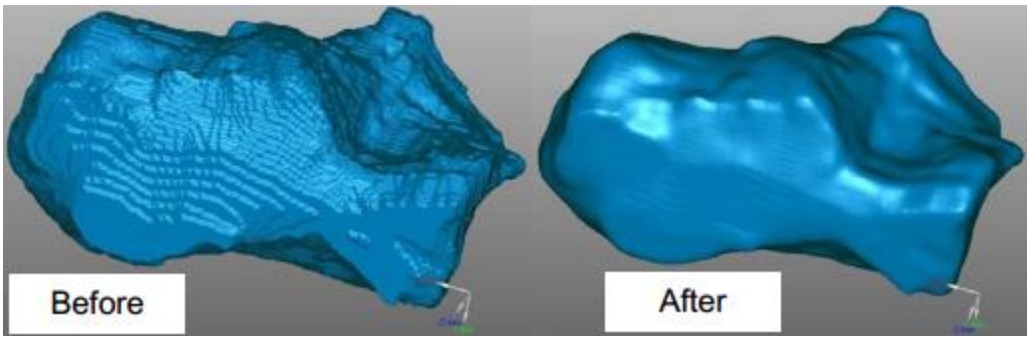

Figure 10: Before and after smoothing operations in Geomagic[14].

A dynamic model software (Adams/View) was then used to apply the ligament locations and tensions and identify the contact between the bones. Grood and Suntay coordinate systems were applied to the model to track kinematic behavior. Moments were inputted into the dynamic model to follow the axes defined by Grood and Suntay.

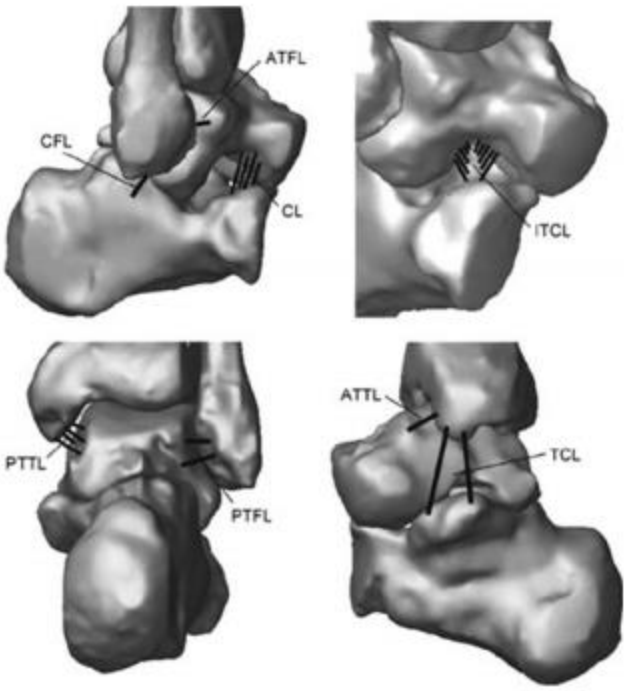

Figure 11: Pictorial representation of ligament insertions in 3-D numerical model in Adams/View[14].

Chapter 3: Methods

Talar and Tibial Measurements and Their Implant Surface Designs

Two sets of implants surface designs and their implantation methods were used. The first set was constructed based on the average of the measurements of seven different ankle models (CAD3R, CAD4L, CAD5L, CAD5R, CAD6R, SAHA, and SIEGLER). The first set was used to run the distance mapping analysis and not for kinematic analysis. The second set of implant surface designs was constructed based on measurements of a specific ankle model (CAD5L) and was used to run kinematic analysis and not distance mapping analysis.

Inman measurements and Implant Surface Design

The Inman measurements were taken by taking cross sectional cuts perpendicular to the inter-malleolar axis. Sections were taken to cover the most surface area of the talar dome. Best fit circles were then fitted to the sections that represent the talar dome at the lateral and medial facets of the talus.

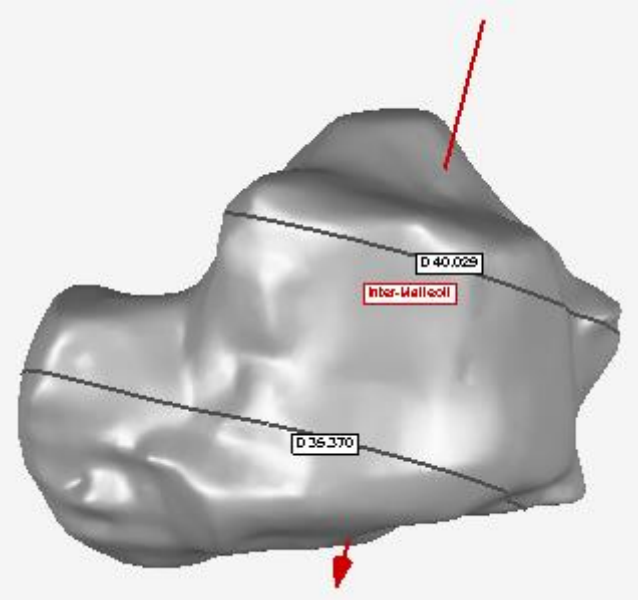

Figure 12: Medial and lateral cuts perpendicular to inter-malleolar axis.

Even though Inman states that there is a skew in the medial and lateral facets of the talar dome this was not taken into account as Inman approximates the talar dome as a symmetrical cone that apexes medially. An Inman cone was constructed that was 1mm thick and a respective tibial aspect implant surface design was constructed as an offset from the talar design to match perfectly and articulate with the talar design in full congruency. Seven equispaced coronal cuts were rotated about the inter-malleolar axis and taken to cover most of

the anterior to posterior surface of the talar dome. These cuts were used to reference the anterior to posterior length of the talar dome and not used to measure saddle curvature.

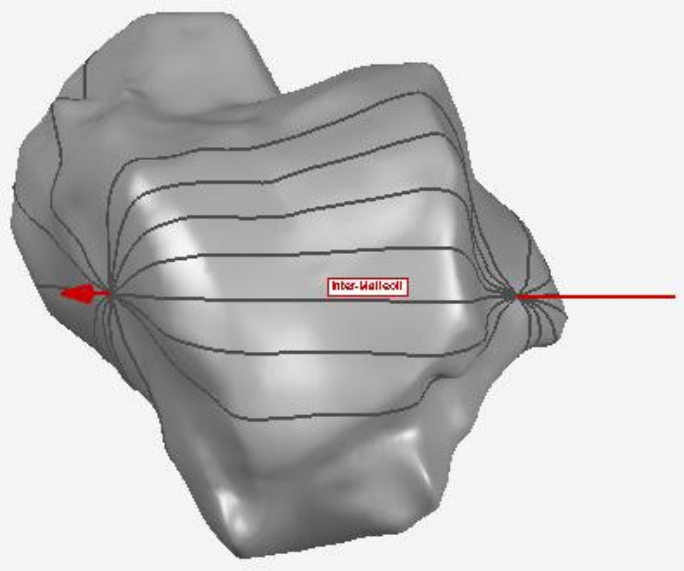

Figure 13: Coronal cuts rotated about the inter-malleolar axis.

In PRO/E Creo Parametric the Inman implant surface design was constructed to follow the measurements taken as described above. Medial and lateral planes were used to sketch the medial and lateral best fit circles. The centers of the circles were aligned on the same axis that was perpendicular to both circles.

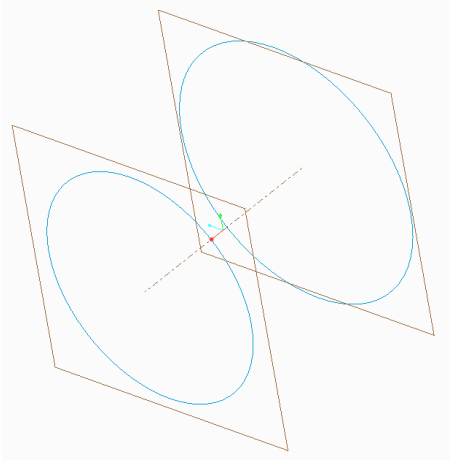

Figure 14: Medial (closer) and lateral planes constructed with the best fit circles aligned with the same axis.

A plane was rotated about the axis of the circles and used to make the seven coronal planes.

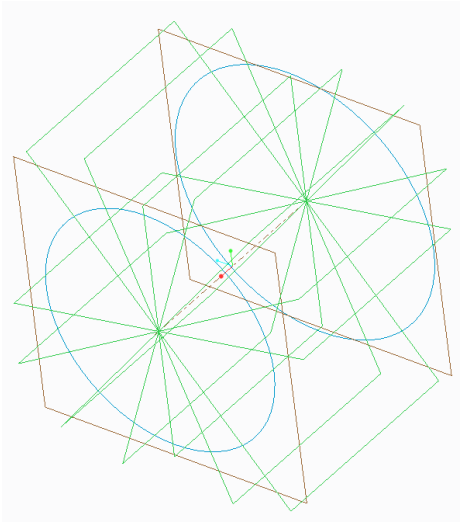

Figure 15: Coronal planes rotated about the cone axis.

The seven coronal planes were used to sketch lines connecting the medial and lateral circles in each of the coronal planes. These lines were offset by 1mm to create depth to the surface design and the seven sketches were then blended into a solid.

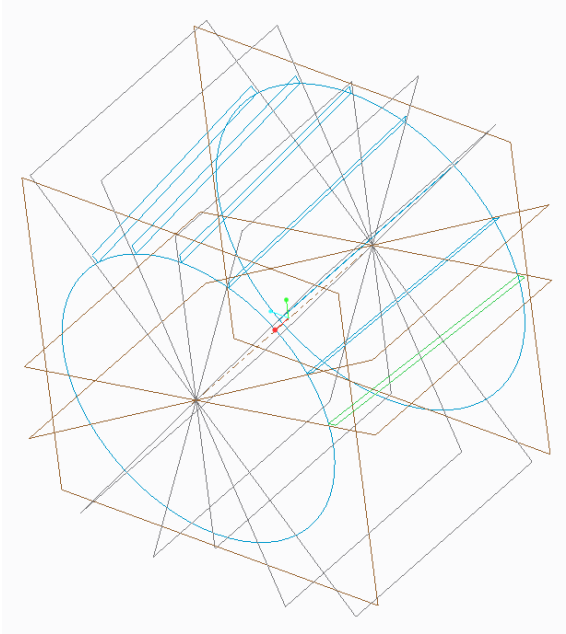

Figure 16: Rectangles sketched on the coronal planes.

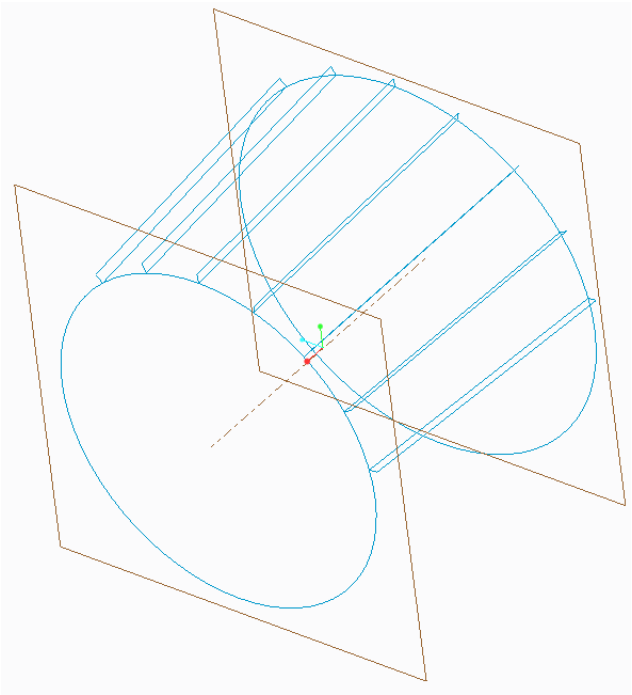

Figure 17: Rectangles used to create rough talar implant surface design.

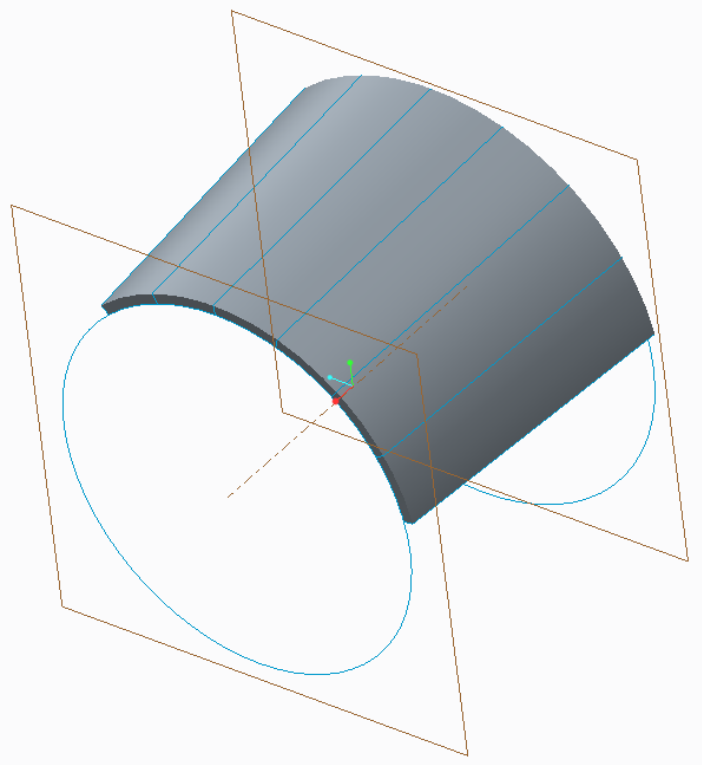

Figure 18: Rough talar implant surface design.

Using chamfers and rounding operations the excess pieces of the surface design were trimmed to fit on the talar dome.

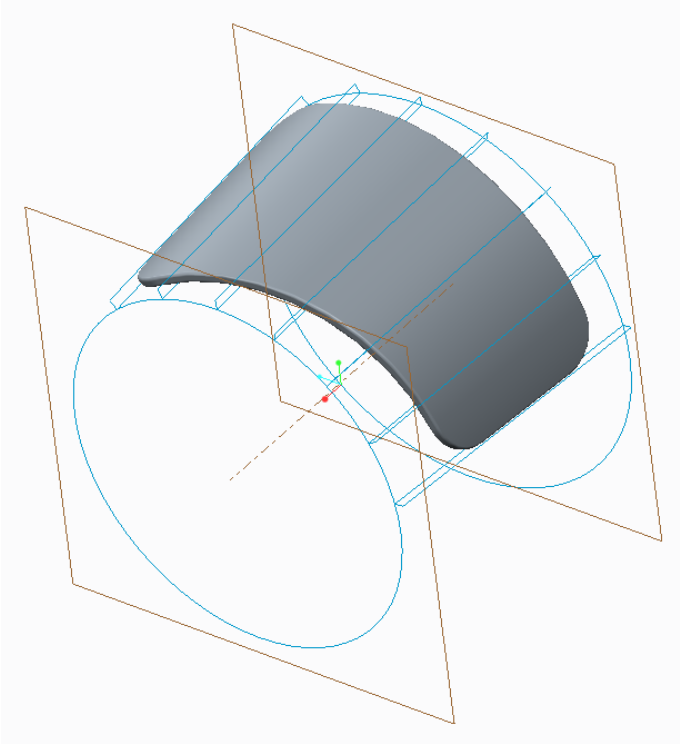

Figure 19: Inman talar implant surface design 1 after trimming and rounding.

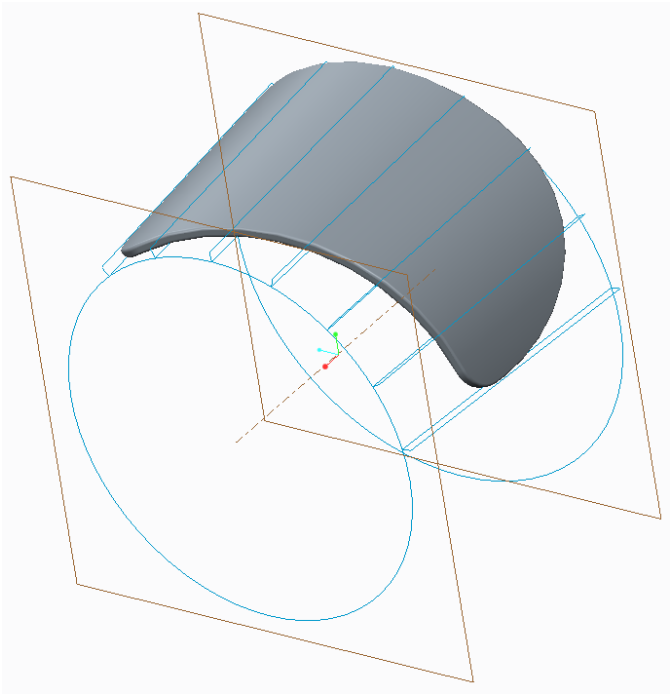

Figure 20: Inman talar implant surface design 2 after trimming and rounding.

To create the tibial aspect of the implant the superior surface of the implant surface design was offset by 1mm.

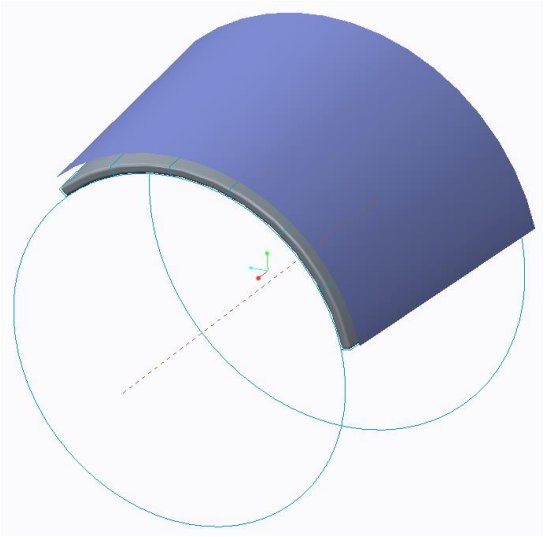

Figure 21: Rough talar implant surface offset for tibial component.

That surface was then thickened to a 1mm depth in the inferior direction. This guaranteed that the inferior surface of the tibial implant was an exact replica of the superior surface of the talar implant.

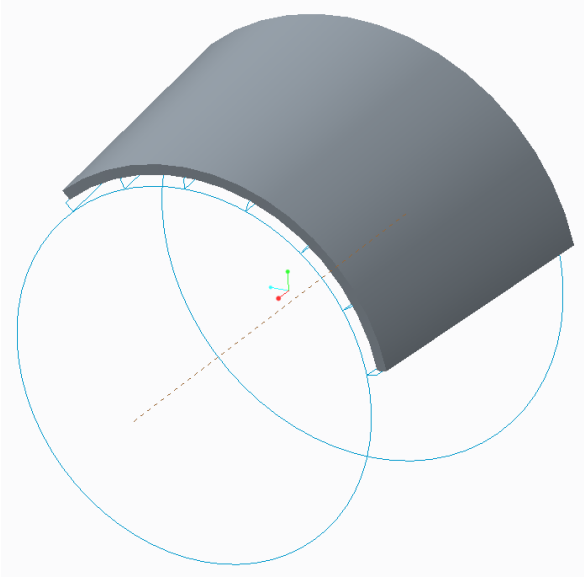

Figure 22: Rough tibial Inman implant surface design.

Using chamfers and rounding operations the excess pieces of the surface design were trimmed to fit on the tibial plafond.

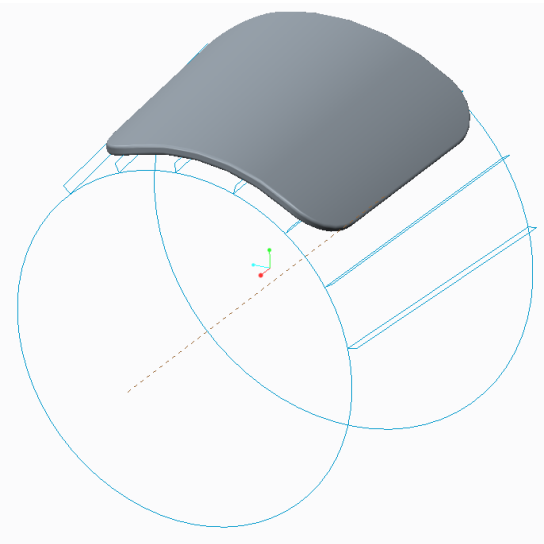

Figure 23: Inman implant surface design after trimming and rounding.

Conic Measurements and Implant Surface Design

The conic measurements were created by taking cross sectional cuts of the talus in parallel to the plane average to the medial and lateral planes. These cuts were made to cover the most medial to lateral talar dome surface.

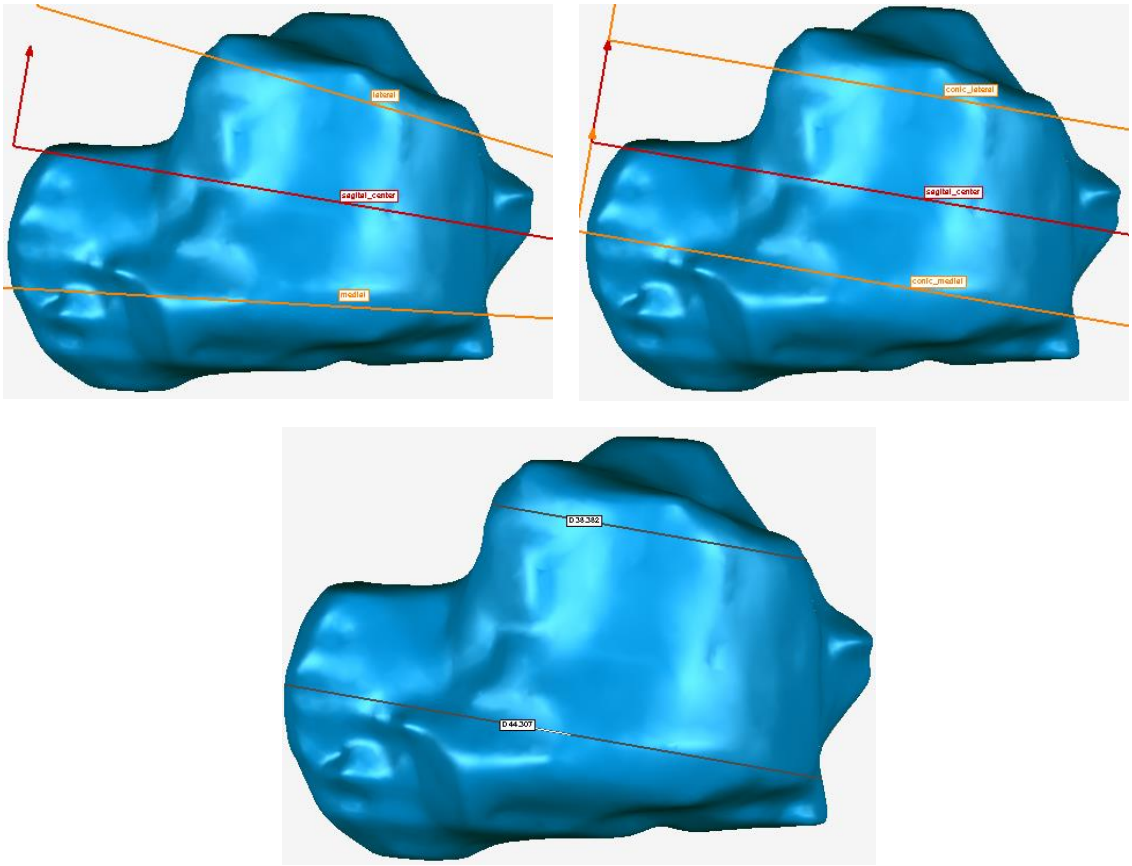

Figure 24: Top left: Medial and lateral sagittal planes rotated in the transverse plane to cover the medial and lateral condyles. The center plane is the average of the medial and lateral planes. Top right: Medial and lateral planes offset from the center plane used to cut and measure the radius of curvature. Bottom: Cuts made for Conic and Cylindrical measurements.

An axis was created by connecting the centers of the two best fit circles to the medial and lateral facets of the talar dome.

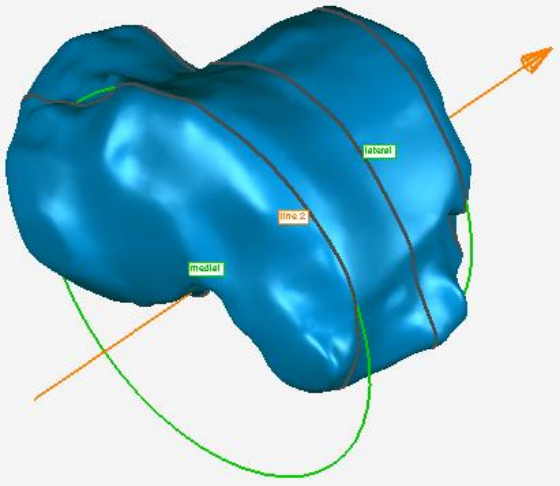

Figure 25: Cone axis connecting the centers of the medial and lateral best fit circles.

Five coronal planes about that axis were created to cover the surface of the talar dome from anterior to posterior.

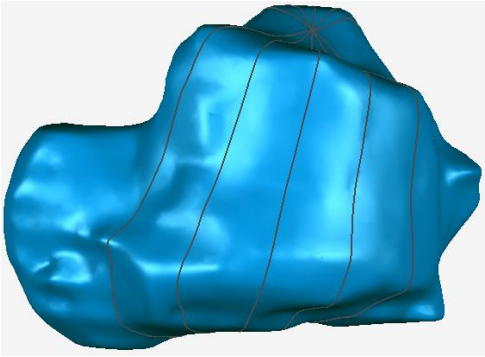

Figure 26: Coronal cuts on the talar dome for Conic and Cylindrical measurements.

In PRO/E Creo Parametric the conic implant surface design was constructed to follow the measurements taken as described above. Medial and lateral planes were used to sketch the medial and lateral best fit circles. The centers of the circles were aligned on the same axis that was perpendicular to both circles.

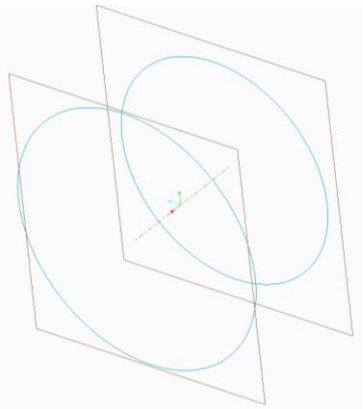

Figure 27: Medial (closer) and lateral planes constructed with the best fit circles aligned with the same axis.

A plane was rotated about the axis of the circles and used to make the five coronal planes.

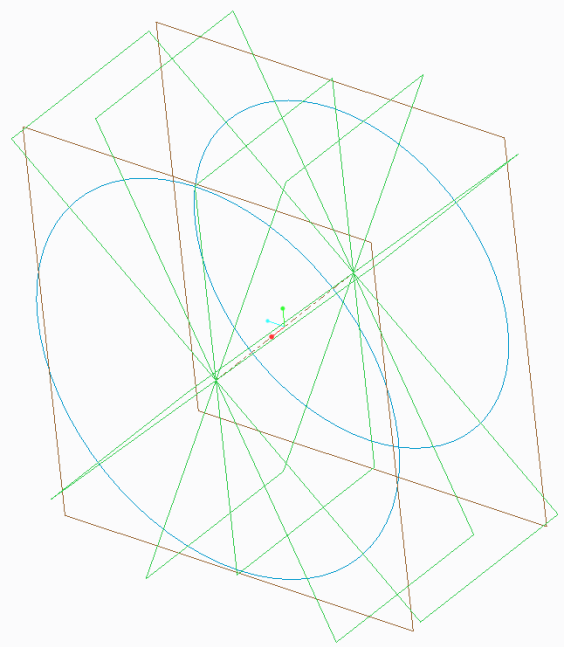

Figure 28: Coronal planes rotated about the cone axis.

The five coronal planes were used to sketch lines connecting the medial and lateral circles in each of the coronal planes. These lines were offset by 1mm to create depth to the surface design and the five sketches were then blended into a solid.

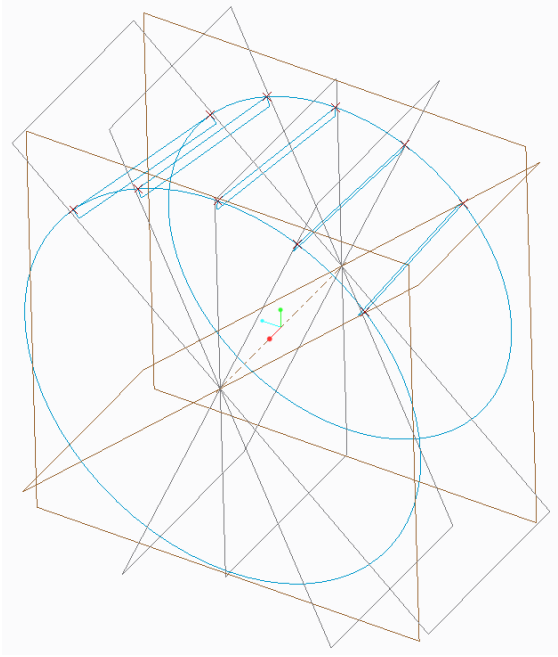

Figure 29: Rectangles sketched on the coronal planes.

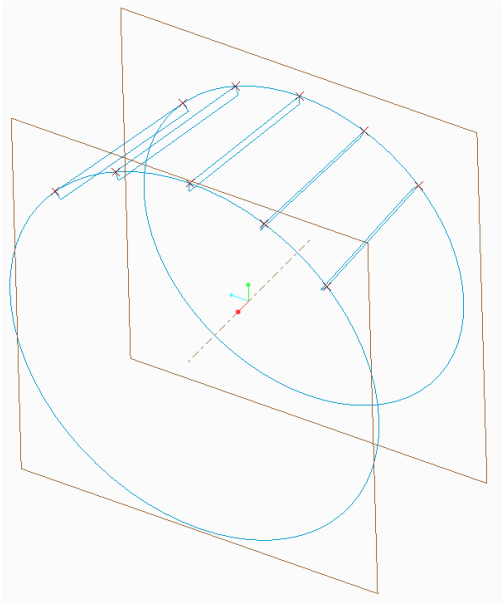

Figure 30: Rectangles used to create rough talar implant surface design.

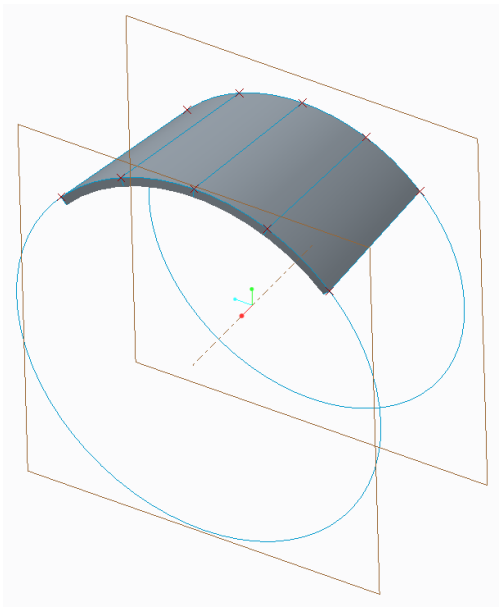

Figure 31: Rough talar implant surface design.

Using chamfers and rounding operations the excess pieces of the surface design were trimmed to fit on the talar dome.

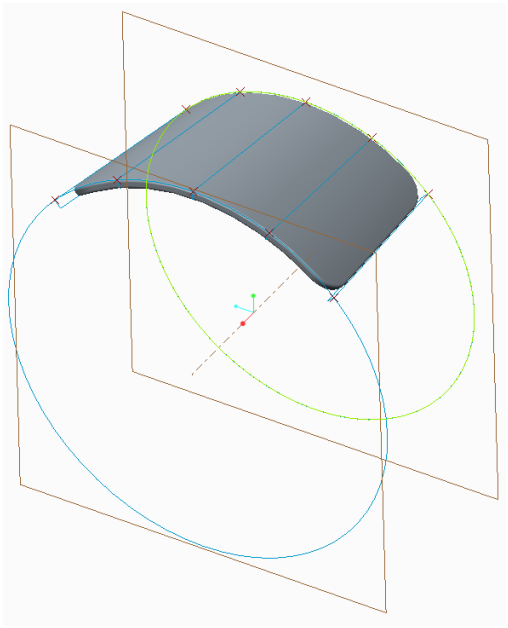

Figure 32: Conic talar implant surface design after trimming and rounding.

To create the tibial aspect of the implant the superior surface of the implant surface design was offset by 1mm.

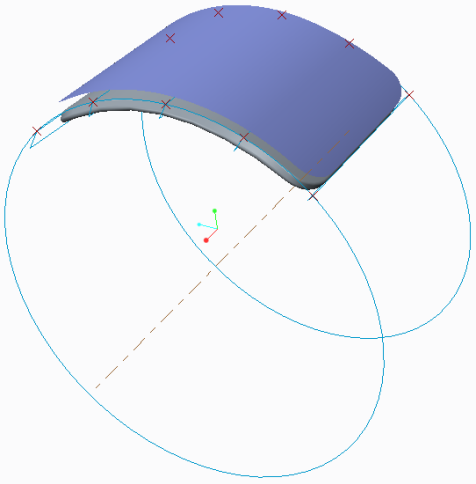

Figure 33: Rough talar implant surface offset for tibial component.

That surface was then thickened to a 1mm depth in the inferior direction. This guaranteed that the inferior surface of the tibial implant was an exact replica of the superior surface of the talar implant.

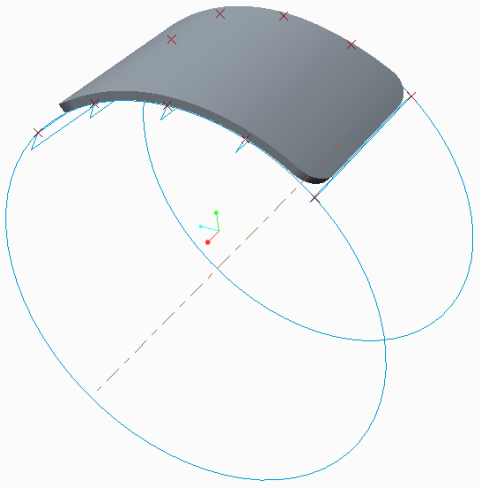

Figure 34: Rough tibial Conic implant surface design.

Using chamfers and rounding operations the excess pieces of the surface design were trimmed to fit on the tibial plafond.

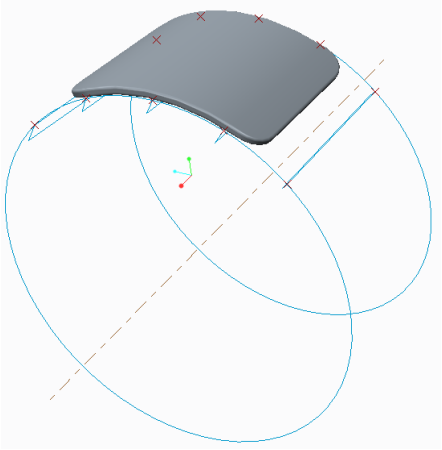

Figure 35: Tibial Conic implant surface design after trimming and rounding.

Cylindrical Measurements and Implant Surface Design

Similar to the conic measurements, the cylindrical measurements were created by taking cross sectional cuts of the talus in parallel to the plane average to the medial and lateral planes. These cuts were made to cover the most medial to lateral talar dome surface. The average of the medial and lateral best fit circles was used as the radius of the cylindrical cone to be constructed. Five coronal planes were created by rotating about the axis connecting the centers of the two best fit circles to the medial and lateral facets of the talar dome.

In PRO/E Creo Parametric the cylindrical implant surface design was constructed to follow the measurements taken as described above. Medial and lateral planes were used to sketch the medial and lateral best fit circles. The centers of the circles were aligned on the same axis that was perpendicular to both circles. A plane was rotated about the axis of the circles and used to make the five coronal planes. The five coronal planes were used to sketch lines

connecting the medial and lateral circles in each of the coronal planes. These lines were offset by 1mm to create depth to the surface design and the five sketches were then blended into a solid. Using chamfers and rounding operations the excess pieces of the surface design were trimmed to fit on the talar dome.

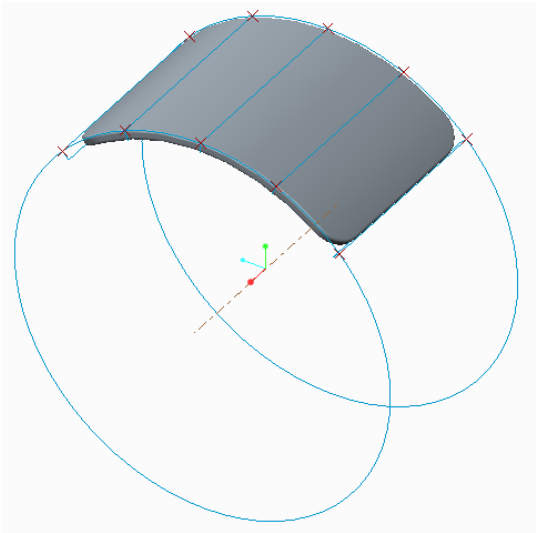

Figure 36: Cylindrical talar implant surface design after trimming and rounding.

To create the tibial aspect of the implant the superior surface of the implant surface design was offset by 1mm. That surface was then thickened to a 1mm depth in the inferior direction. This guaranteed that the inferior surface of the tibial implant was an exact replica of the superior surface of the talar implant. Using chamfers and rounding operations the excess pieces of the surface design were trimmed to fit on the tibial plafond.

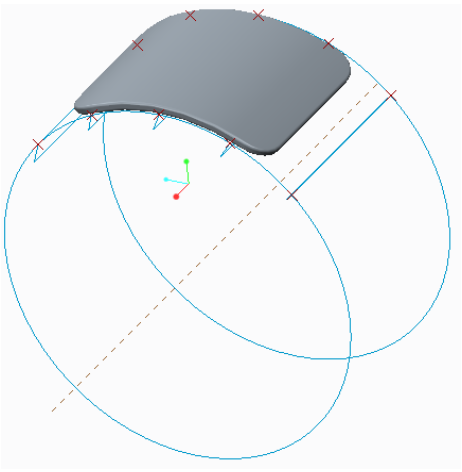

Figure 37: Cylindrical Inman implant surface design after trimming and rounding.

Siegler Measurements and Implant Surface Design

In the Siegler measurements, the axis of the medial and lateral best fit circles did not coincide. This gave the measurement method the flexibility to more accurately measure the morphological features of the talar dome. Medial and lateral planes that coincided with the medial and lateral facets of the talus were used to create cross sectional cuts. Best fit circles were fitted to the two cuts on the talar dome.

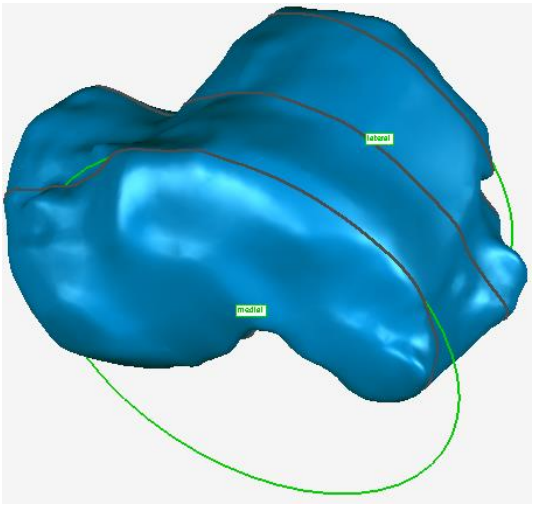

Figure 38: Medial and lateral best fit circles on talus.

The deviation of the axis perpendicular to the medial circle and the axis between the centers of the two circles was also measured. Finally the angle between the medial and lateral planes was measured to recreate the skewedness of the cone.

A plane was rotated about the axis connecting the center of these best fit circles to create five coronal cuts that covered the talar dome anterior to posterior.

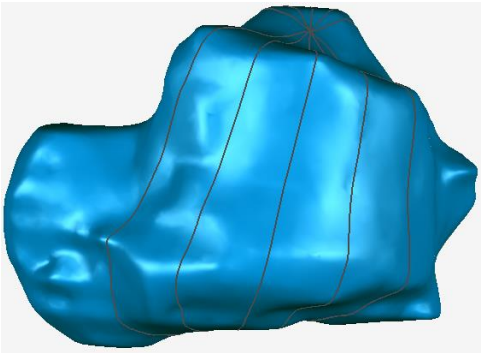

Figure 39: Coronal cuts rotated about axis connecting the centers of the medial and lateral best fit circles.

The radius of curvature in the coronal cuts was measured by means of best fit circles.

In PRO/E Creo Parametric the Anatomical implant surface design was constructed to follow the measurements taken as described above. Medial and lateral planes were used to sketch the medial and lateral best fit circles. The lateral plane was rotated to create the skew and the centers of the circles were aligned to the offset axis that was measured.

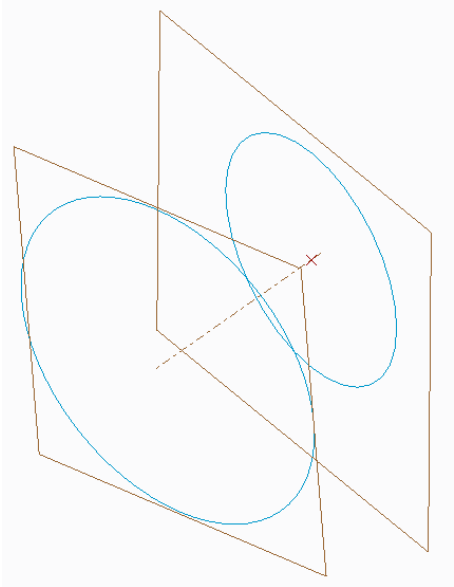

Figure 40: Medial (closer) and lateral planes constructed with the best fit circles aligned with the same axis and with skewed angle.

A plane was rotated about the axis and used to make the five coronal planes.

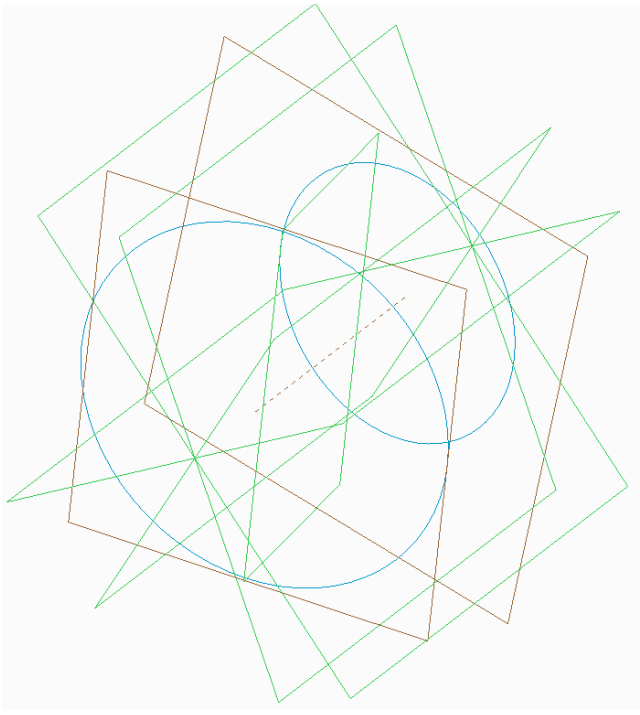

Figure 41: Coronal planes rotated about the cone axis.

The five coronal planes were used to sketch curved lines connecting the medial and lateral circles in each of the coronal planes. The curvature of these lines followed the radius of the best fit circles that were measured. The lines were then offset by 1mm to create depth to the surface design and the five sketches were then blended into a solid.

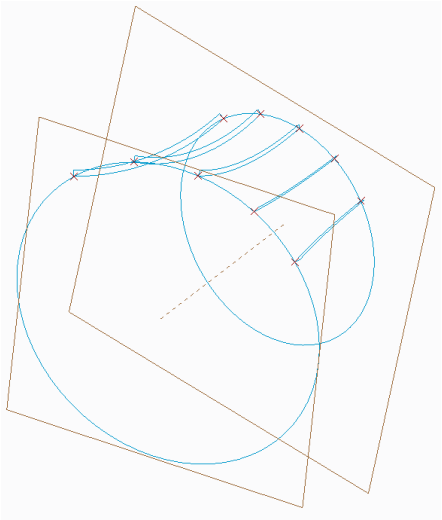

Figure 42: Saddled rectangles sketched on the coronal planes, used to create the rough talar implant surface design.

Using chamfers and rounding operations the excess pieces of the surface design were trimmed to fit on the talar dome.

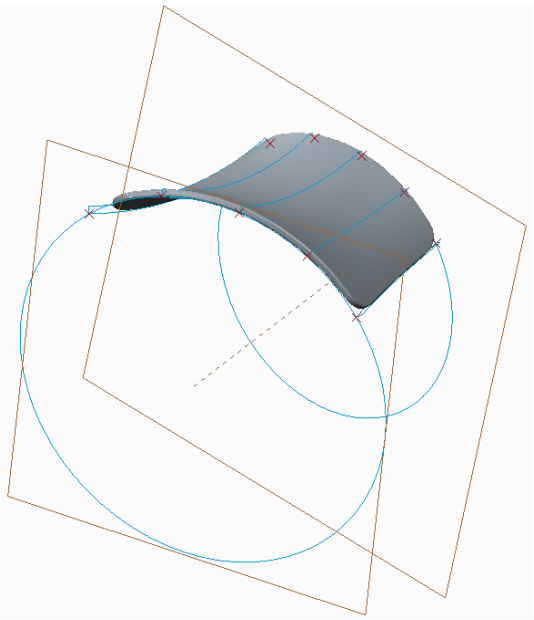

Figure 43: Anatomical talar implant surface design after trimming and rounding.

For the tibial aspect of the surface design a simple offset from the talar design will not work. Since this is a skewed and variably saddled cone, perfect congruency with another surface will only happen in one configuration. This leads to the notion that a separate tibial design constructed from tibial morphological analysis needs to be done.

Tibial Measurements and Implant Surface Design

Similar to the Siegler measurements, cuts on the medial and lateral facets of the tibia were used to estimate the radius of curvature of the tibial plafond in the sagittal plane using best fit circles.

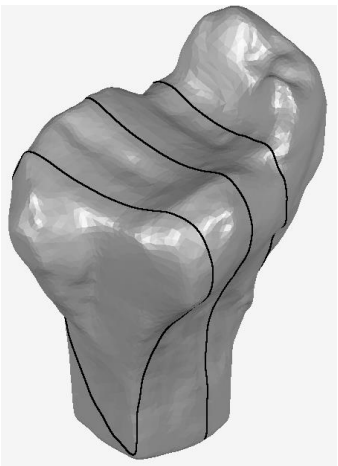

Figure 44: Medial (farther) and lateral (closer) cuts used to measure radius of curvature of the best fit circles.

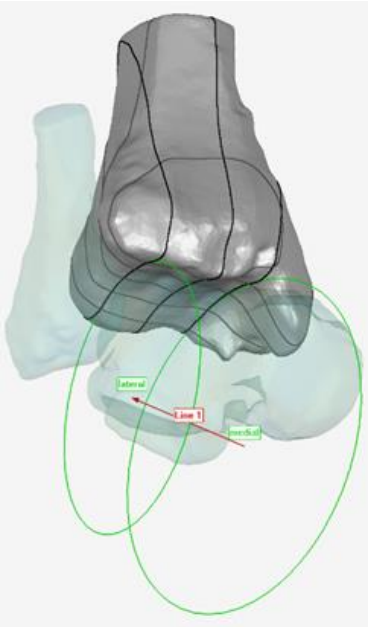

Figure 45: Coronal cuts rotated about the axis connecting the centers of the medial and lateral best fit circles. Sagittal cuts also displayed.

The deviation of the axis perpendicular to the medial circle and the axis connecting the centers of the two circles was also measured. Finally the angle between the medial and lateral planes was measured to recreate the skewedness of the cone.

A Plane was rotated about the axis connecting the center of these best fit circles to create five coronal cuts that covered the tibial plafond anterior to posterior.

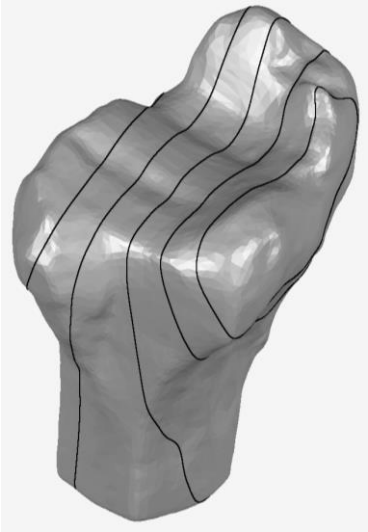

Figure 46: Coronal cuts rotated about the axis connecting the centers of the medial and lateral best fit circles.

This was done to seven different tibia models and the data gathered was used to compare the morphology of the tibial plafond to the talar dome.

In PRO/E Creo Parametric the tibial implant surface design was constructed to follow the measurements taken as described above. Medial and lateral planes were used to sketch the medial and lateral best fit circles. The lateral plane was rotated to create the skew and the centers of the circles were aligned to the offset axis that was measured.

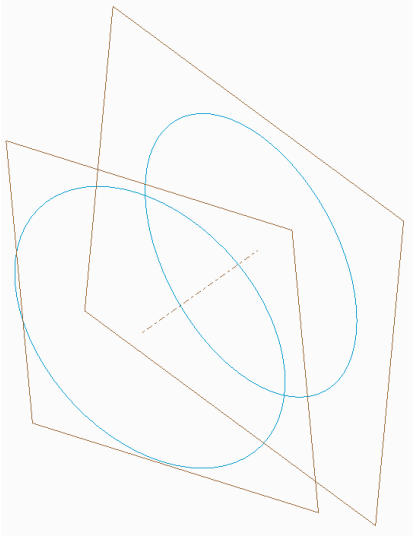

Figure 47: Medial (closer) and lateral planes constructed with the best fit circles aligned with the same axis and with skewed angle.

A plane was rotated about the axis and used to make the five coronal planes.

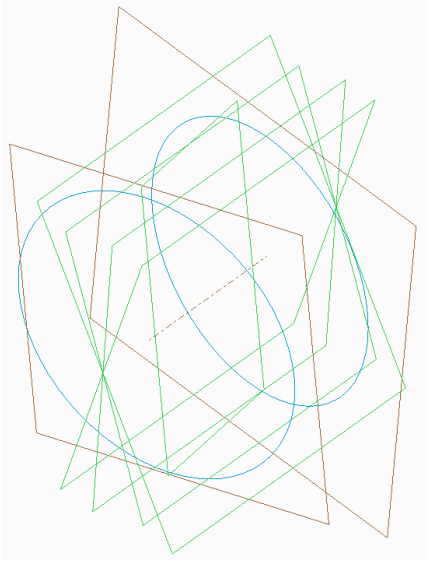

Figure 48: Coronal planes rotated about the cone axis.

The five coronal planes were used to sketch curved lines connecting the medial and lateral circles in each of the coronal planes. The curvature of these lines followed the radius of

the best fit circles that were measured. The lines were then offset by 1mm to create depth to the surface design and the five sketches were then blended into a solid.

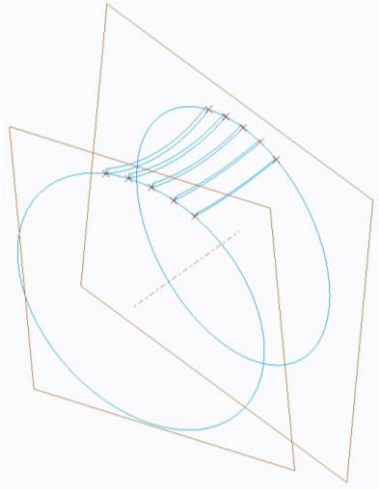

Figure 49: Saddled rectangles used to create rough tibial implant surface design.

Using chamfers and rounding operations the excess pieces of the surface design was trimmed to fit on the tibial plafond.

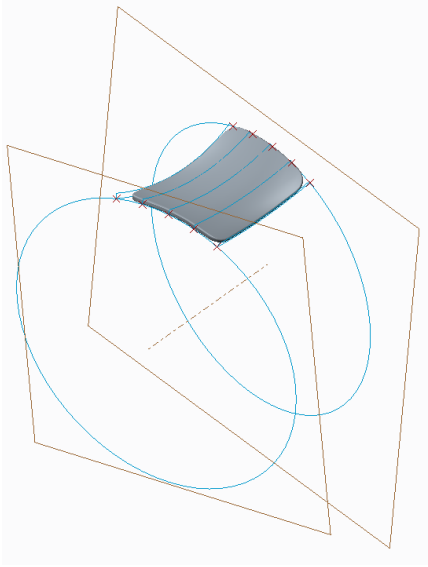

Figure 50: Anatomical tibial implant surface design after trimming and rounding.

Implantation of Surface Designs

Talus Surface Implant Positioning

To align or "implant" the implant surfaces to the bones on which they were made for, Geomagic was utilized. Two sets of implantation methods were used, the first method consisted of simply placing the implant surface on the respective bone without aligning to cuts made for measurements. In Geomagic, the talus was imported in its neutral position and the implant was placed and oriented onto the bone by the manual object mover. This objective method is not consistent when running kinematic analysis since the placement of the surface in a 3-D model space affects the resulting kinematics of the joint. It does not however alter the results of a distance mapping that looks at the behavior of how two articulating surfaces behave on one another.

Below is the first set of implantations for the four different implant surface designs.

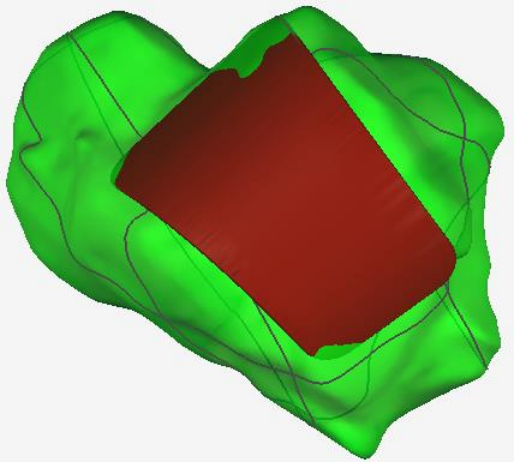

Figure 51: Inman talar implant surface aligned on talus for distance mapping analysis.

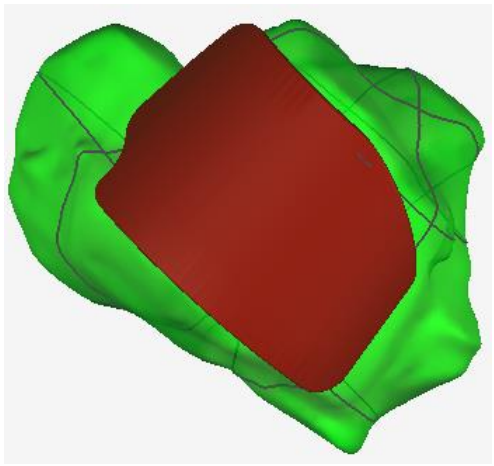

Figure 52: Conic talar implant surface aligned on talus for distance mapping analysis.

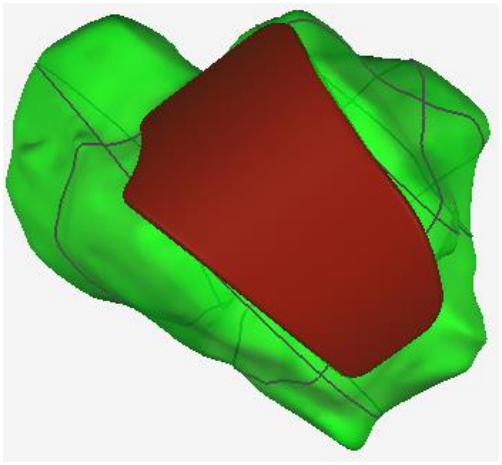

Figure 53: Cylindrical talar implant surface designed by Myers[18], aligned on talus for distance mapping analysis.

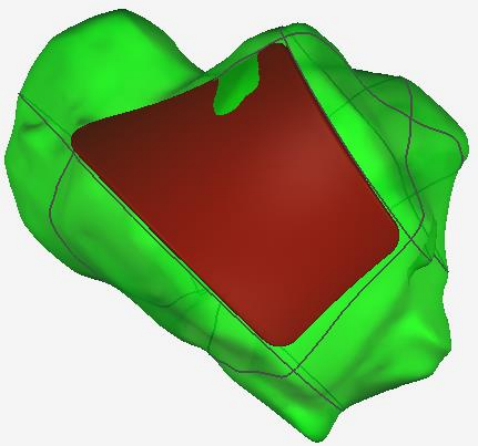

Figure 54: Anatomical talar implant surface aligned on talus for distance mapping analysis.

For the second set of implantations, the talus was once again imported into Geomagic, in its neutral position, and the implant was placed and oriented onto the bone by using the cuts used for measurements as a guide. The Global registration feature in Geomagic was then used to freely re-orient the implant surface until optimal convergence was found. Optimal convergence was defined as finding the minimum distance deviation between the polygons that make up the surface. The implant surface was once again manually re-adjusted to follow the cuts made for measurements and was slightly raised or lowered to replace the surface of the bone so that it sits halfway below and above the bone surface. Below is the second set of implantations for the four different implant surface designs.

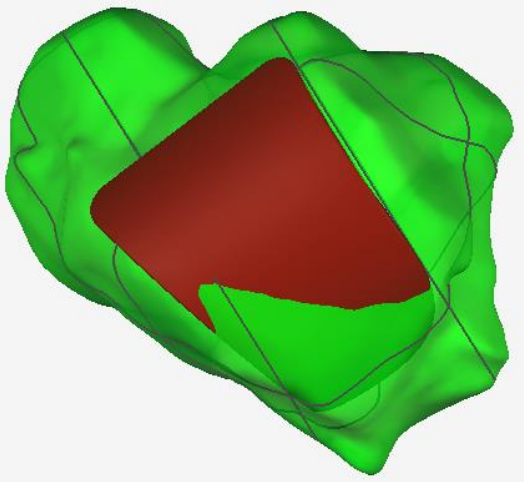

Figure 55: Inman talar implant surface aligned on talus for kinematic analysis.

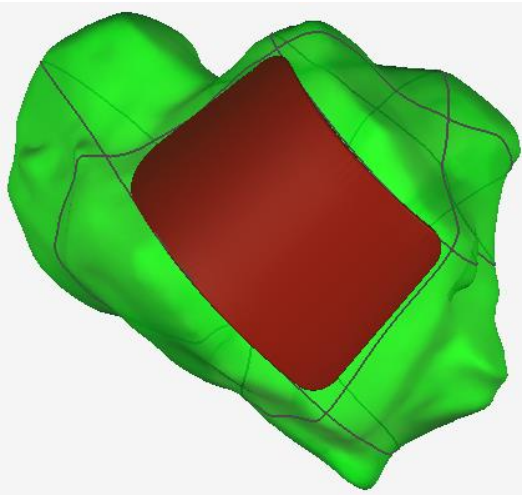

Figure 56: Conic talar implant surface aligned on talus for kinematic analysis.

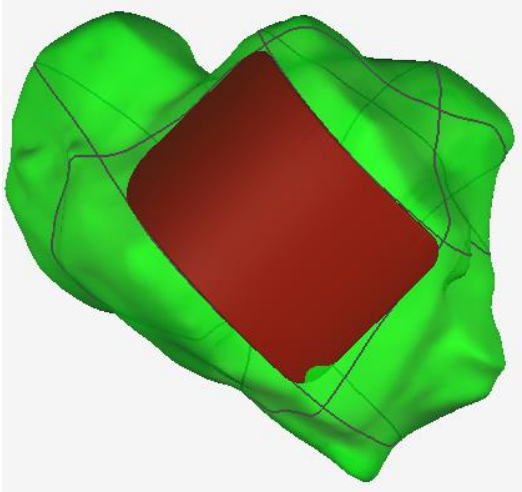

Figure 57: Cylindrical talar implant surface aligned on talus for kinematic analysis.

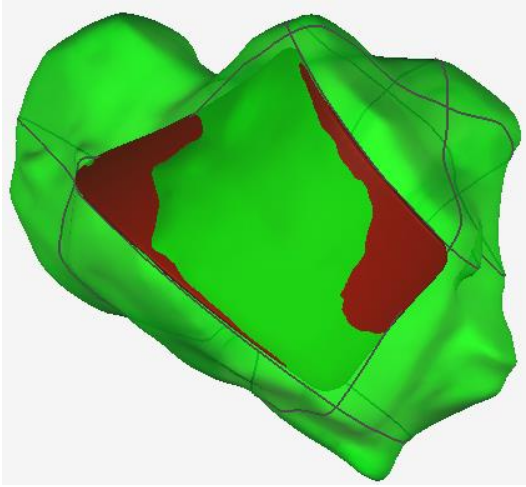

Figure 58: Anatomical talar implant surface aligned on talus for kinematic analysis.

Notice that the second set of implants are different from the first set as they were made from dimensions taken only from the CAD5L model and not from the average of all of the models described above. The first set was used to run the distance mapping analysis and the second set was used to run the kinematic analysis.

Tibial Surface Implant Positioning

The tibial aspect of the implant surface design also consisted of two implantation methods. The first method is as follows. For the Inman, Conic and cylindrical implant surfaces, the tibial aspect of the implant was first moved so that it was registered to the corresponding talar implant surface using the Geomagic Global Registration tool. It was then moved in the direction normal to its top surface in order to be moved at an offset to the surface of the talar implant surface.

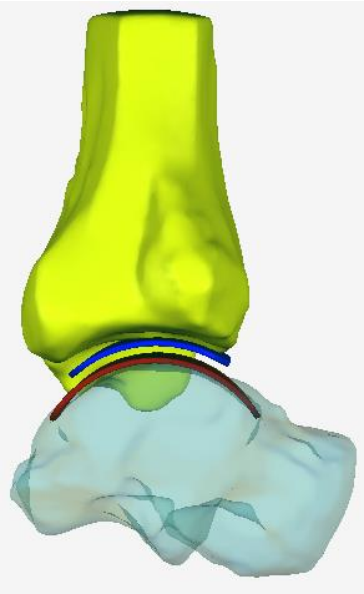

Figure 59: Inman tibial implant surface (blue) aligned on tibia for distance mapping analysis.

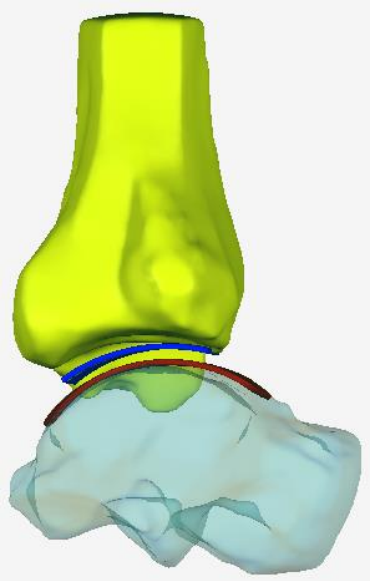

Figure 60: Conic tibial implant surface (blue) aligned on tibia for distance mapping analysis.

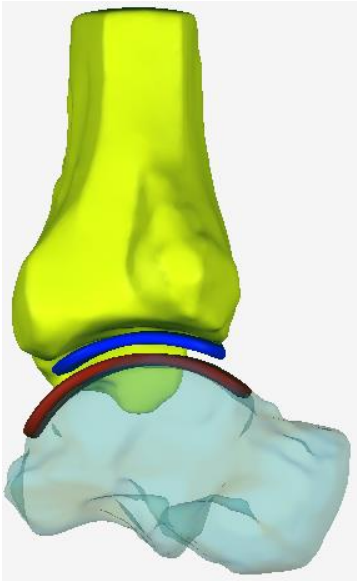

Figure 61: Cylindrical tibial implant surface (blue) aligned on tibia for distance mapping analysis.

The Anatomical implant surface design was placed on the tibia using the global registration feature in Geomagic and also by using the cuts as a guide. The implant surface was not lowered into the bone but was placed to sit on top of the bone.

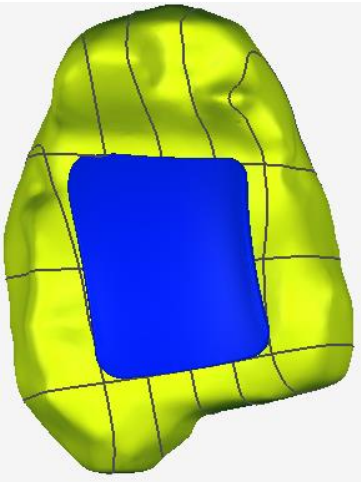

Figure 62: Anatomical tibial implant surface (blue) aligned on tibia for distance mapping analysis.

The second implantation method is as follows. For the Inman, Conic and cylindrical implant surfaces, the tibial aspect of the implant was first moved so that it was registered to the corresponding talar implant surface using the Geomagic Global Registration tool. It was then imported into Adams and moved in the direction normal to the top surface of the respective talar implant at the location of center of mass. The implant surface designs were moved by a distance until it penetrated the tibia while not going under it.

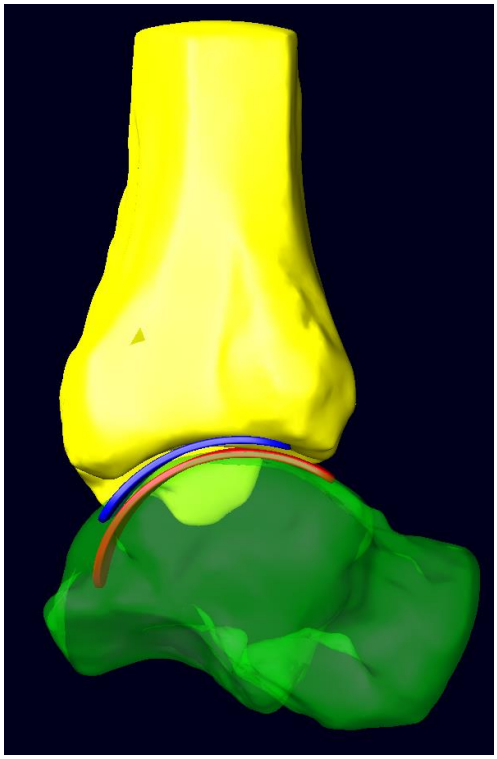

Figure 63: Inman tibial implant surface (blue) aligned on tibia for kinematic analysis.

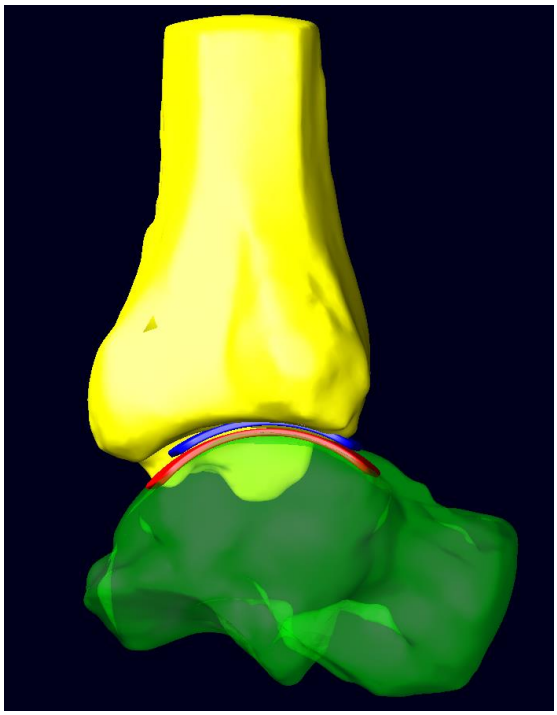

Figure 64: Conic tibial implant surface (blue) aligned on tibia for kinematic analysis.

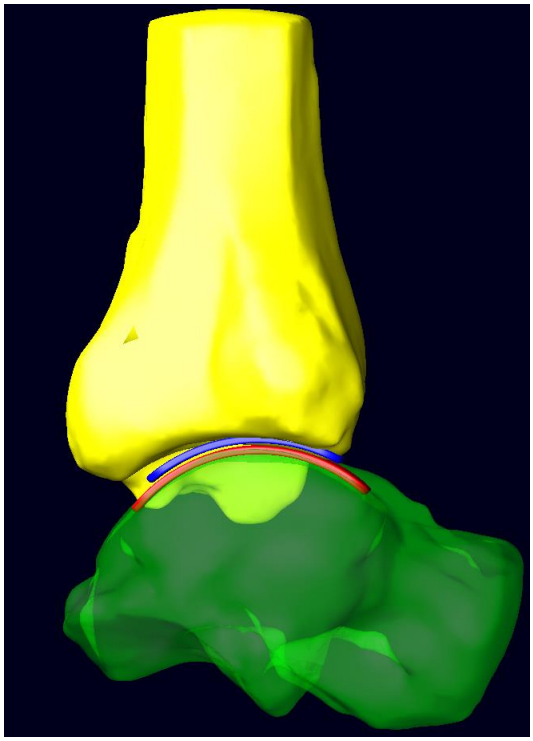

Figure 65: Cylindrical tibial implant surface (blue) aligned on tibia for kinematic analysis.

The Anatomical implant surface design was placed on the tibia using the global registration feature in Geomagic and also by using the cuts as a guide. The implant surface was lowered into the bone so that it replaces the location of the current bone without being too high above it or too low below it.

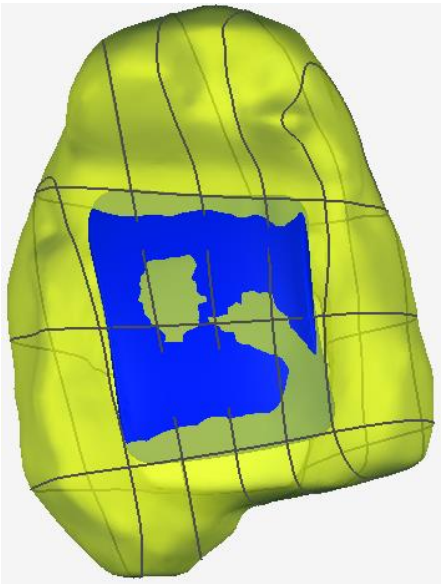

Figure 66: Anatomical tibial implant surface (blue) aligned on tibia for kinematic analysis.

Running Adams Simulation Models

The two sets of four implant designs, along with the natural ankle models, were run in Adams for distance mapping and kinematic analysis. The first set of implants and the six natural ankle models were run in Adams in order to obtain the positions of the bones and the implant surfaces in the different positions when a moment is applied. This first set was used for distance mapping analysis. These models were set to run for 15 seconds with 150 total calculation steps. This provided adequate quantitative results and optimized performance speed. The model was run in dorsi and plantar flexion, inversion and eversion, internal and external rotation, all at separate instances. A moment torque of 8 N*m was used for the three applied moments.

The second set of implant designs and the CAD5L model were run in Adams for kinematic analysis and comparison. Kinematic analysis included comparing the range of motion, the moment coupling, and the ligament strains for the different configurations. The models were set to run for 15 seconds with 150 total calculation steps. This provided adequate

quantitative results and optimized performance speed. The model was run in dorsi and plantar flexion, inversion and eversion, internal and external rotation, all at separate instances. In order to obtain a larger range of motion in the Adams model for kinematic analysis and comparison, a moment torque of 10 N*m was used for the three applied moments.

Distance Mapping

Distance mapping was done in Geomagic Qualify by creating points of the test object and mapping the distance of those points onto the reference object. For example, mapping the distance of the tibia and fibula onto the talus in neutral position would be done by first converting the tibia and the fibula into points. This was done by exporting the test object's wrap files from Adams into STEP files and then importing it into Geomagic where they can be used to create the points.

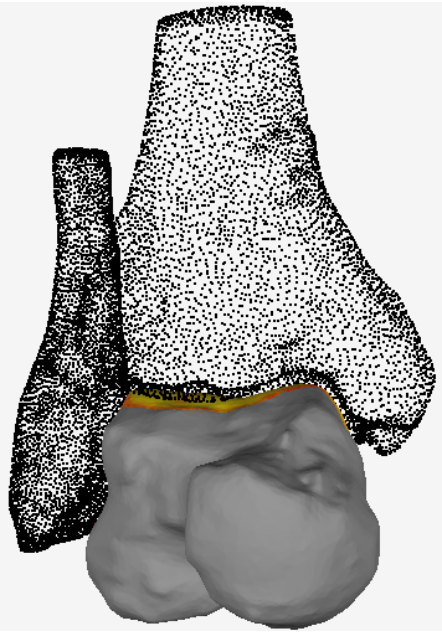

Figure 67: Object points of tibia and fibula mapped onto the talus for distance mapping analysis.

After this the points were mapped onto the reference object using the 3-D Analyze feature of Geomagic. The critical angle was set to 45° and the maximum deviation was 5.00mm. It was noted that changing the critical angle did not yield different results and thus the choice of critical angle seemed to be arbitrary.

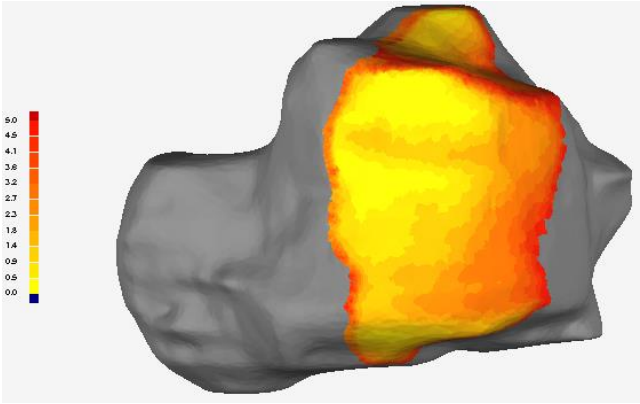

Figure 68: Results of distance mapping analysis (tibia and fibula mapped on talus in neutral position).

The results showed in a color spectrum that was averaged to show trends and areas of proximity or contact. The scale used to map the distances always had a maximum value of 5.00 mm and a minimum of 0.00 mm. The numbers of color segments used to create the mapping was 24.

Chapter 4: Results

Measurements of talus and tibia

Siegler Method Talar and Tibial Measurements

From the measurements of the CAD5L talar dome the medial condyle was found to have a radius of curvature of 26.0 mm and the lateral condyle was found to have a radius of curvature of 19.1 mm. Going posterior to anterior the radius of curvature of the talar dome was found to be 57.8 mm, 42.2 mm, 32.8 mm, 59.7 mm, and 48.6 mm. The skewedness of the axis of the line connecting the medial and lateral best fit circles compared to the line perpendicular to the center of the medial best fit circle was found to be skewed 15.5^{o} posteriorly in the transverse plane and 14.6^{o} superiorly in the coronal plane.

From the measurements of the CAD5L tibial plafond the medial condyle was found to have a radius of curvature of 34.0 mm and the lateral condyle was found to have a radius of curvature of 27.2 mm. Going posterior to anterior the radius of curvature of the tibial plafond was found to be 34.6 mm, 44.3 mm, 36.2 mm, 33.7 mm, and 31.3 mm. The skewedness of the axis of the line connecting the medial and lateral best fit circles compared to the line perpendicular to the center of the medial best fit circle was found to be skewed 14.7^{o} posteriorly in the transverse plane and 11.6^{o} superiorly in the coronal plane.

Table 1 below summarizes the measurements of all of the seven models used to gather data on the measurements of the tibial plafond.

Table 1: Summary of tibial radii of curvature in the sagital and coronal planes for all seven bone models.

Radius of curvature on Tibia (mm)							
	CAD3R	**CAD4L**	**CAD5L**	**CAD5R**	**CAD6R**	**SAHA**	**SIEGLER**
Posterior	27.5	65.9	34.6	36.9	63.6	50.5	56.3
	33.8	40.9	44.3	43.3	44.1	43.6	73
to	38.6	36.9	36.2	39.2	40.2	47	70.1
	40.8	39.9	33.7	50	48.3	46.7	51.5
Anterior	31.9	31.1	31.3	86.9	26.9	34.4	32.9
Medial	30.1	30.3	34.0	38.2	24.8	18.0	24.9
Lateral	19.6	15.2	27.2	20.5	21.7	17.6	26.9

Inman, Conic and Cylindrical Method Talar Measurements

For the Inman model, the measurements of the CAD5L talar dome the medial condyle was found to have a radius of curvature of 35.4 mm and the lateral condyle was found to have a radius of curvature of 40.0 mm.

For the Conic model, the measurements of the CAD5L talar dome the medial condyle was found to have a radius of curvature of 44.3 mm and the lateral condyle was found to have a radius of curvature of 38.4 mm.

The Cylindrical model used the average radius of curvature for the medial and lateral best fit circles of the Conic measurements (40.4 mm).

Adams Simulation Models Results

The results of the Adams models outputted three different parameters. The first is range of motion, the second is kinematic coupling and the third is ligament strains.

Range of Motion

The range of motion was quantified as the rotation about a specific axis when the respective 10 N*m moment was applied. The figures below display the angles as which each model moved when a specific torque was applied.

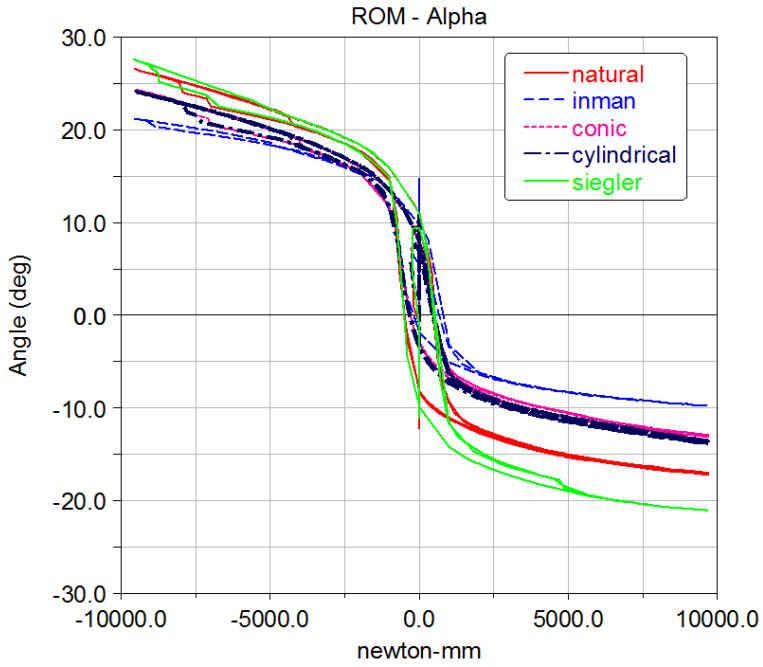

Figure 69: Range of motion of ankle joint complex in dorsi and plantar flexion vs the moment applied.

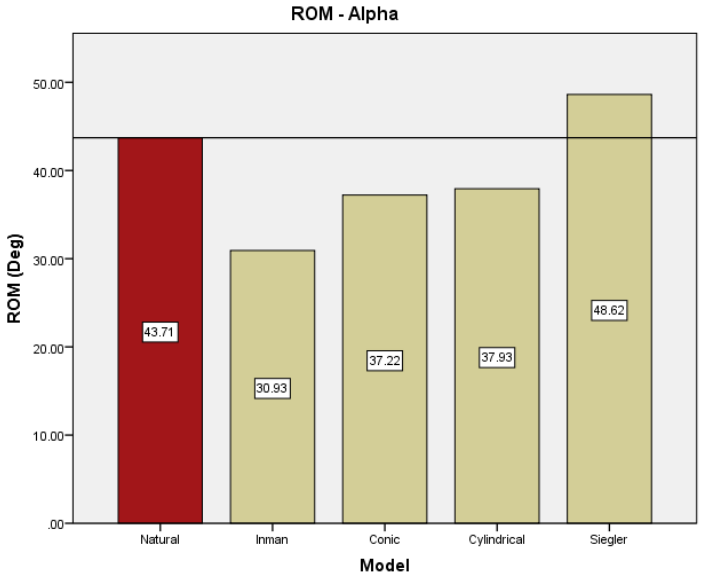

Figure 70: Range of motion of Alpha for the five different models.

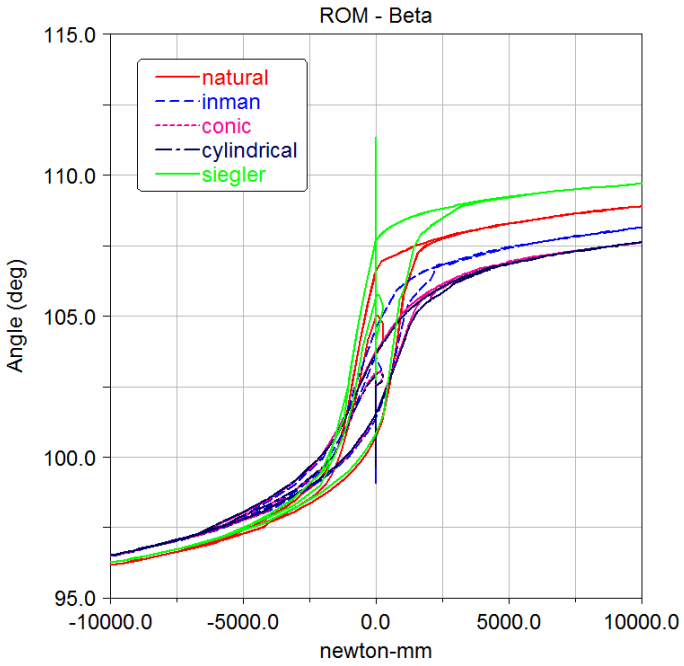

Figure 71: Range of motion of ankle joint complex in inversion and eversion vs the moment applied.

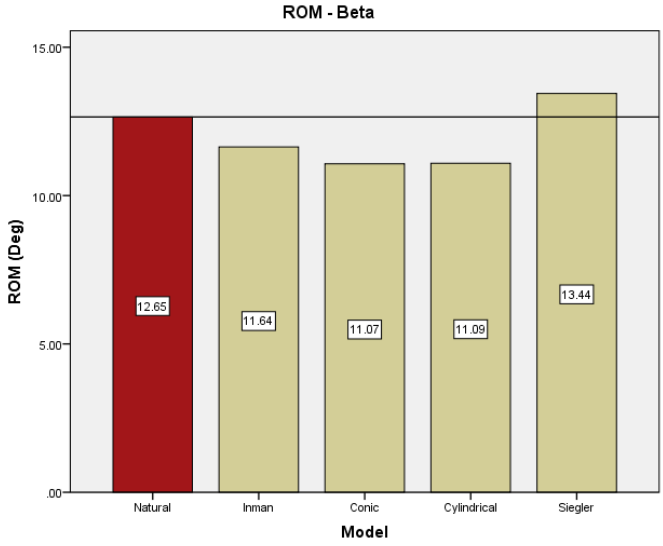

Figure 72: Range of motion of Beta for the five different models.

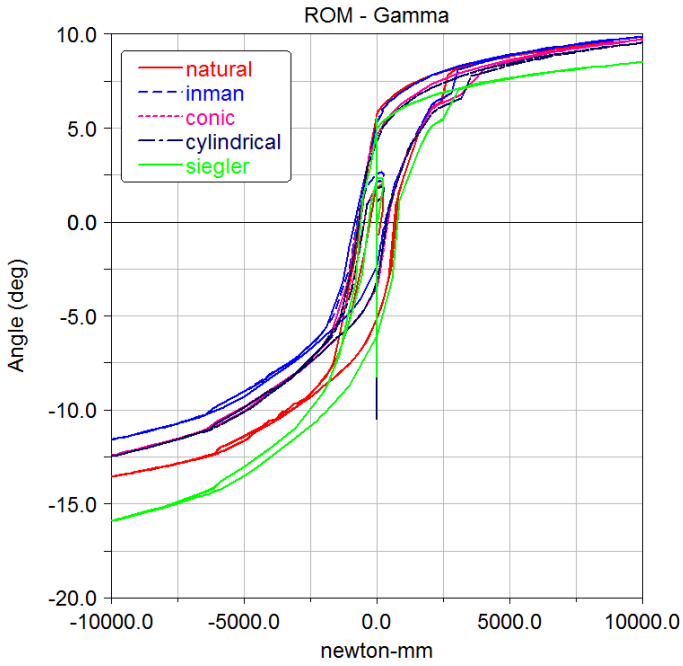

Figure 73: Range of motion of ankle joint complex in internal and external rotation vs the moment applied.

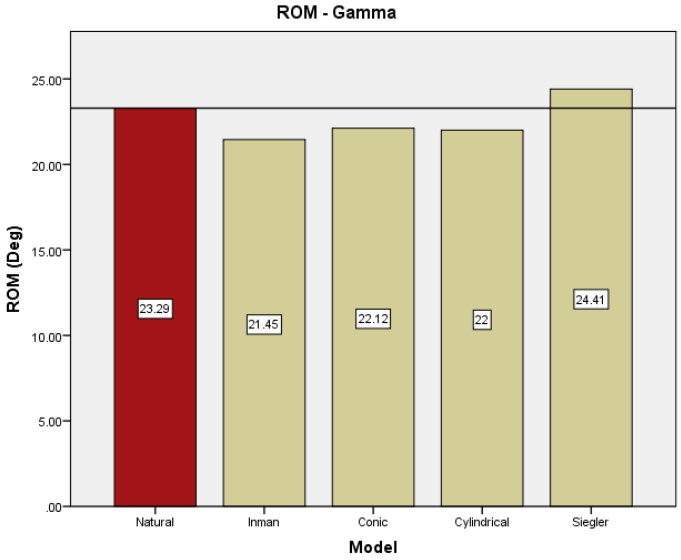

Figure 74: Range of motion of Gamma for the five different models.

Coupling

The kinematic coupling is displayed to show the coupling of motion across the three different rotational ranges of motion.

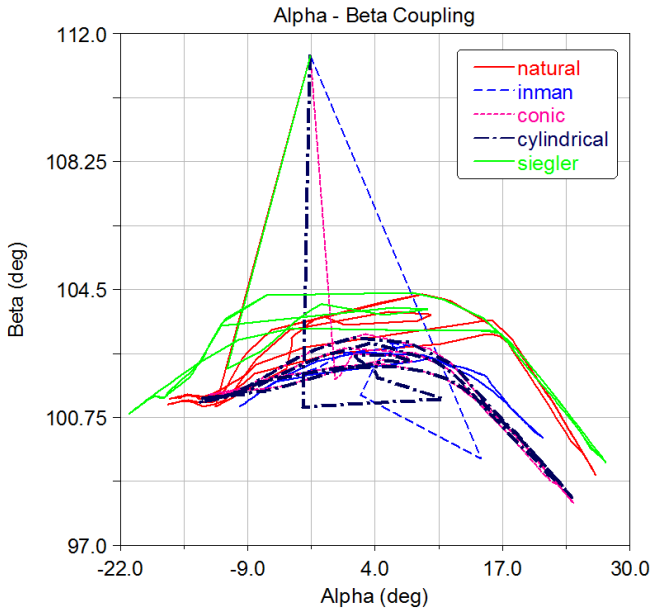

Figure 75: Coupling of Alpha and Beta.

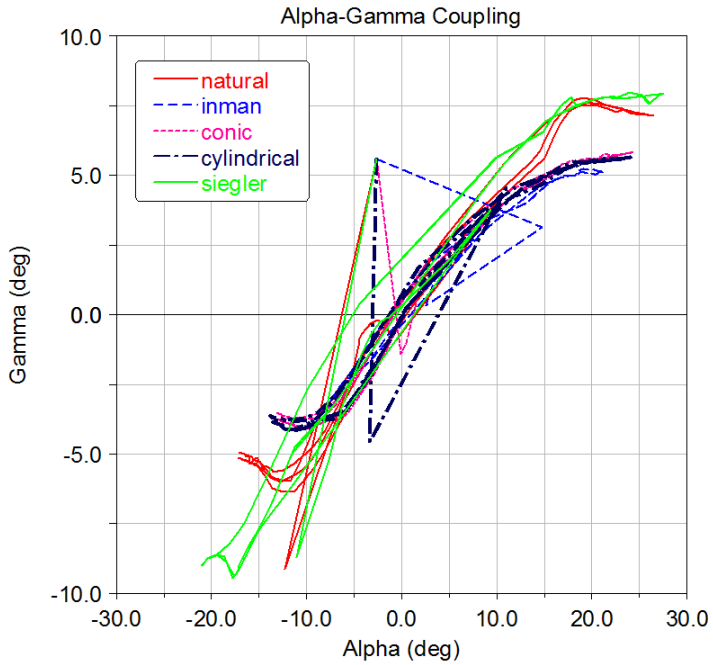

Figure 76: Coupling of Alpha and Gamma.

Kinematic coupling was more tightly regulated with the Inman, Conic and Cylindrical models compared to the Natural and Anatomical models. There was wiggle room in the Natural and Anatomical model that produced a plateau in the Alpha-Beta coupling diagrams between the -10^{o} to 15^{o} Alpha range of motion.

The Alpha-Gamma coupling was similar across the five models with the exception at the extremes of the Alpha range of motion where the Anatomical model was closer to the coupling found in the Natural model.

<u>Ligament Strains</u>

Table 2 summarizes the ligament strains experienced in each model compared to the Natural model. The biggest differences were observed in the ATFL and ATTL during the Alpha motion and the TSL regarding the Gamma motion.

Table 2: Summary of ligament strains for the four models relating to the Natural model. A plus sign indicates that the ligament was strained earlier in the motion and/or applied a greater force. A negative sign indicates that the ligament was strained later in the motion and/or applied a lower force. Multiple pluses or negatives indicate a higher level of difference from the Natural model.

	Alpha				**Beta**				**Gamma**			
Ligament	Inman	Conic	Cylindrical	Anatomical	Inman	Conic	Cylindrical	Anatomical	Inman	Conic	Cylindrical	Anatomical
ATFL	++	++	++	-	+	+	+	/	+	+	+	-
ATTL	++	++	++	/	- -	- -	- -	/	/	/	/	/
CFL	+	+	+	-	/	/	/	/	/	+	+	/
PTFL	+	+	+	/	/	/	/	/	/	/	/	+
PTTL	+	+	+	-	/	/	/	/	+	+	+	-
TCL	+	+	+	-	/	+	+	/	/	/	/	+
TSL	/	/	/	/	+	+	+	-	++	++	++	--

Ligament strains were measured to evaluate the effect of the different designs on the ligaments.

The ATFL was strained earlier in the plantar flexion motion in the Inman, Conic and cylindrical models compared to the Anatomical model; producing the same force as the Natural ankle approximately 10^{o} earlier. In the Beta, or inversion motion, the ATFL was experiencing similar forces in the Inman, Conic and Cylindrical models approximately 3^{o} earlier than in the Natural and Anatomical models. In the Gamma or internal rotation motion, the ATFL was experiencing similar forces in the Inman, Conic and Cylindrical models approximately 3^{o} earlier than in the Natural and Anatomical models.

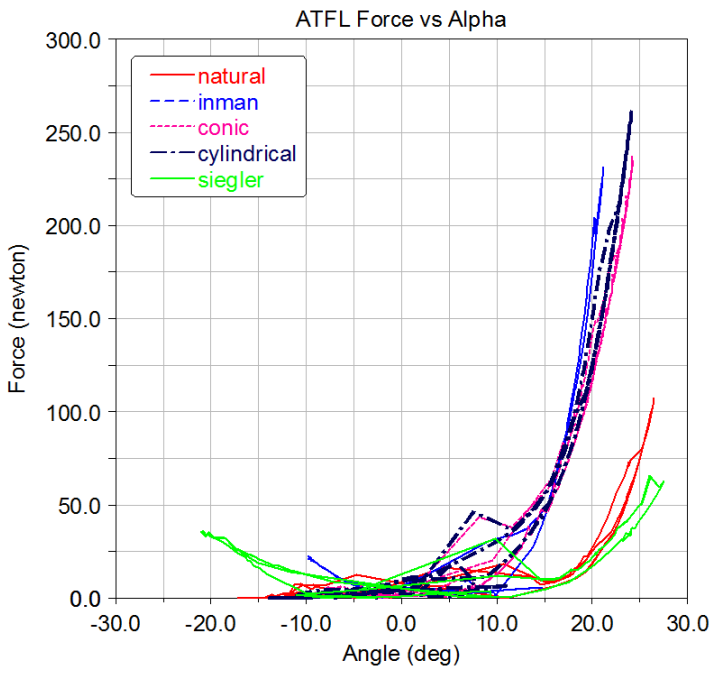

Figure 77: ATFL Force generation vs Alpha.

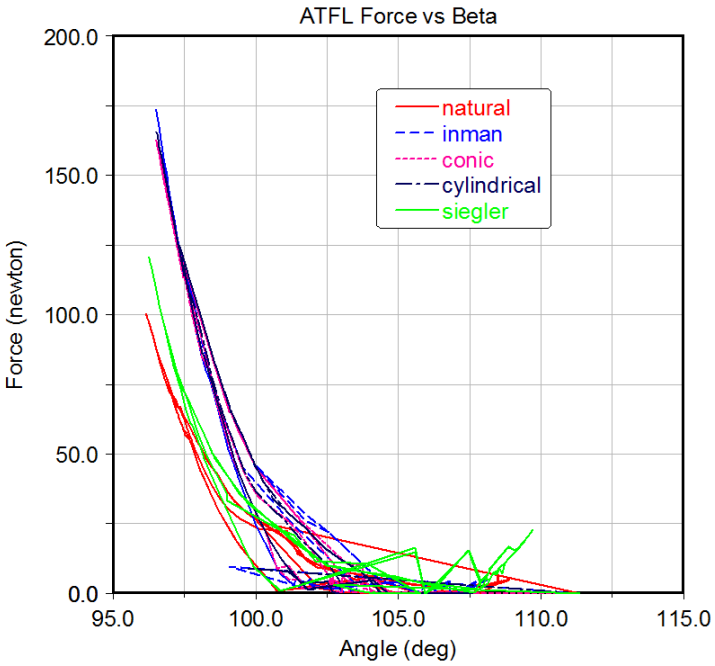

Figure 78: ATFL Force generation vs Beta.

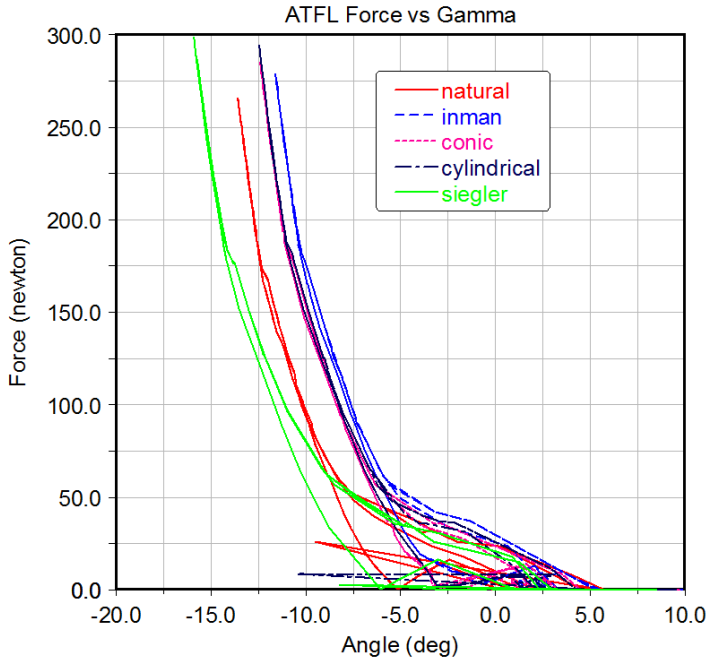

Figure 79: ATFL Force generation vs Gamma.

The ATTL was strained earlier in the plantar flexion motion in the Inman, Conic and cylindrical models compared to the Anatomical model; producing the same force as the Natural

ankle approximately 15-18^{o} earlier. In the Beta, or inversion motion, the ATTL was experiencing forces in the Inman, Conic and Cylindrical models approximately 30 N lower than in the Natural and Anatomical models. In the Gamma or external rotation motion, the ATTL was experiencing similar forces in the Anatomical model approximately 2^{o} earlier than in the Natural, Inman, Conic and Cylindrical models.

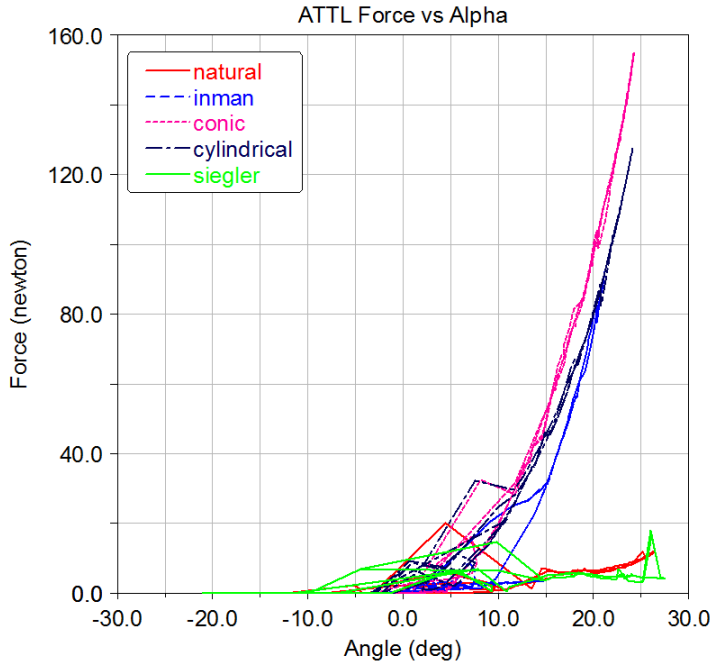

Figure 80: ATTL Force generation vs Alpha.

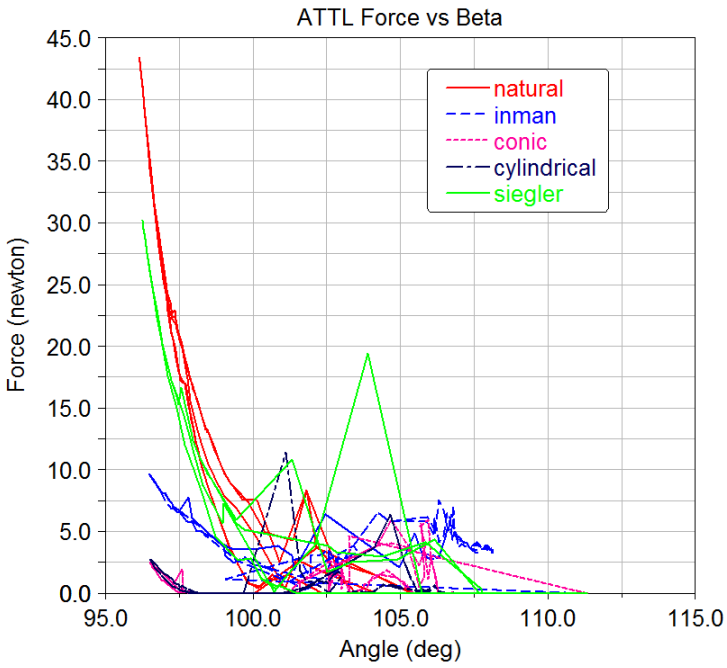

Figure 81: ATTL Force generation vs Beta.

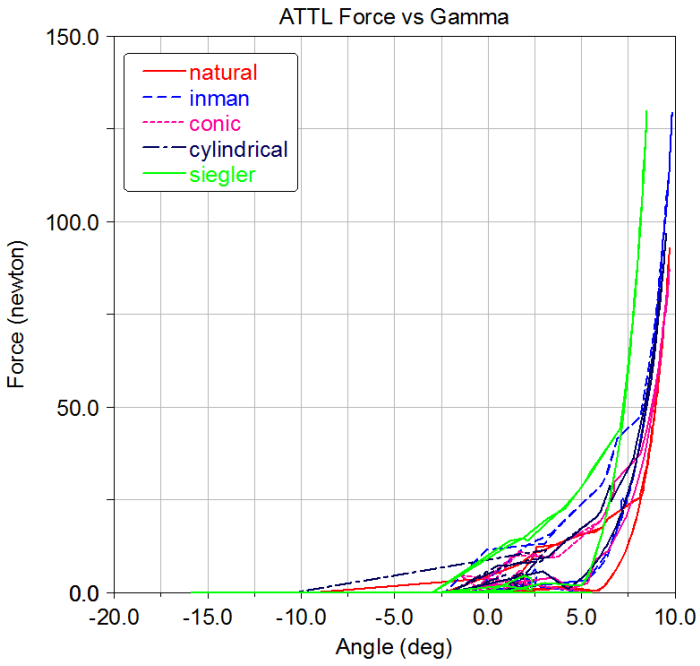

Figure 82: ATTL Force generation vs Gamma.

The CFL was strained earlier in the dorsiflexion motion in the Inman, Conic and cylindrical models compared to the Natural model; producing the same force as the Natural ankle approximately 4^{o} earlier. The Anatomical model did not strain the CFL as much as the Natural model and was only able to produce about half the force produced in the Natural model. In the Beta, or inversion motion, the CFL equally strained in all five models. In the Gamma or external rotation motion, the CFL was experiencing similar forces in the Conic and Cylindrical models approximately 2^{o} earlier than in the Natural, Inman and Anatomical models.

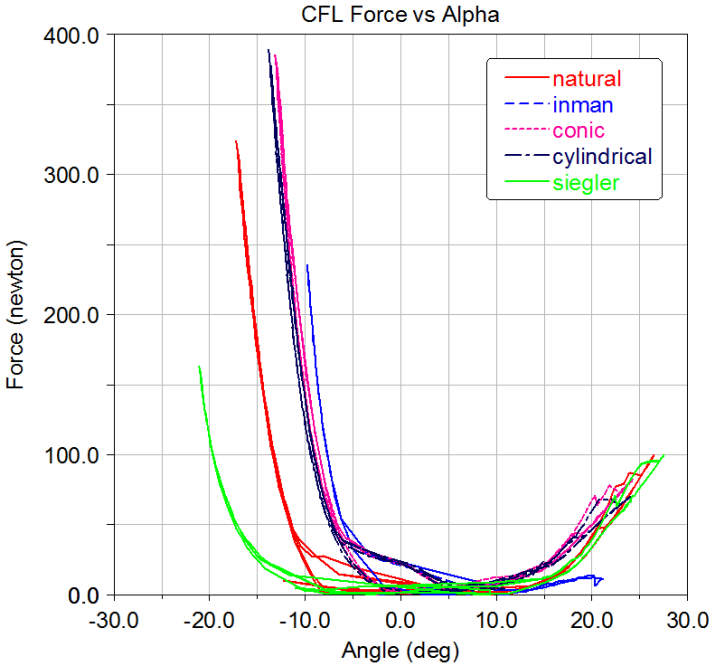

Figure 83: CFL Force generation vs Alpha.

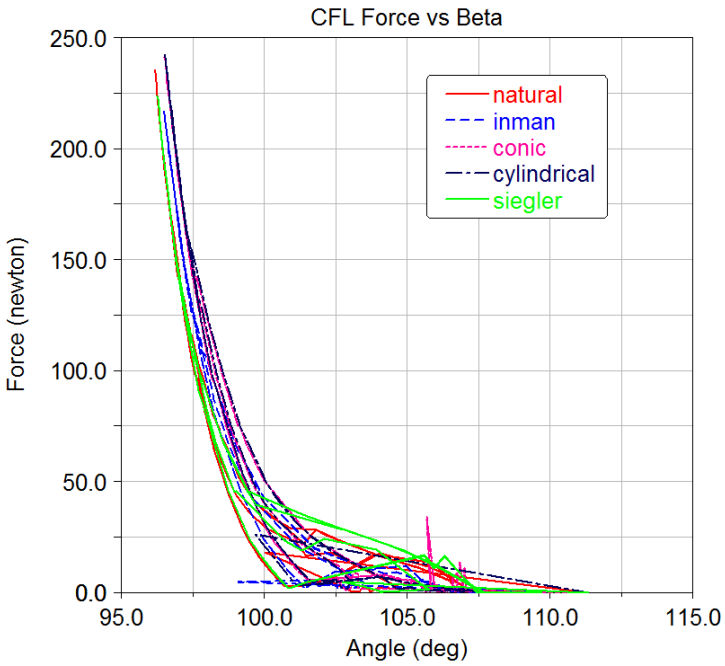

Figure 84: CFL Force generation vs Beta.

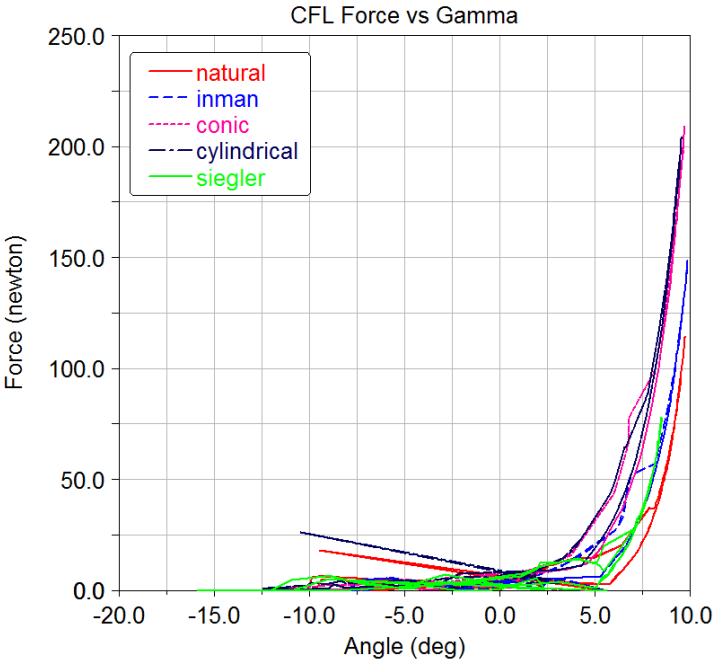

Figure 85: CFL Force generation vs Gamma.

The PTFL was strained earlier in the dorsiflexion motion in the Inman, Conic and Cylindrical models compared to the Natural and Anatomical models; producing the same force

as the Natural ankle approximately 3-6^{o} earlier. There was no discriminating differences or trends seen when plotting the PTFL Force vs Beta. In the Gamma or external rotation motion, the PTFL was experiencing similar forces in the Inman, Conic and Cylindrical models approximately 2^{o} earlier than in the Natural model; and approximately 5^{o} earlier than in the Anatomical model.

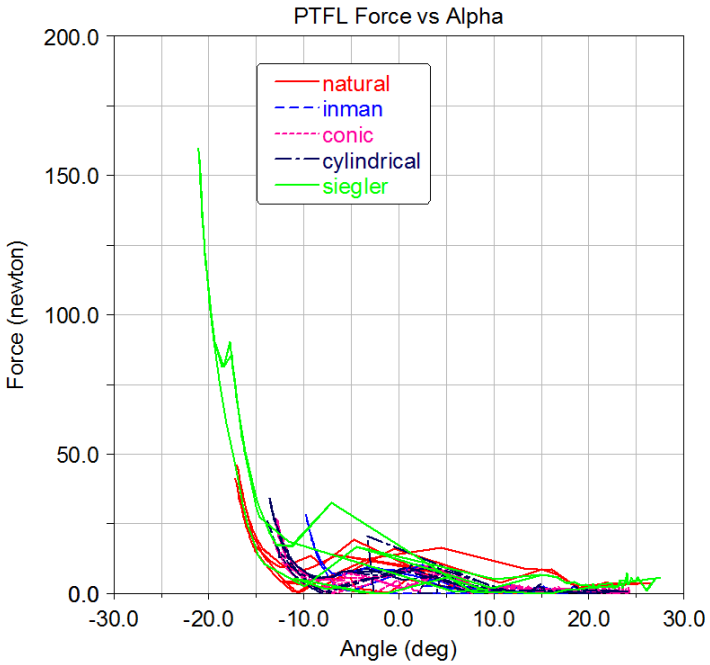

Figure 86: PTFL Force generation vs Alpha.

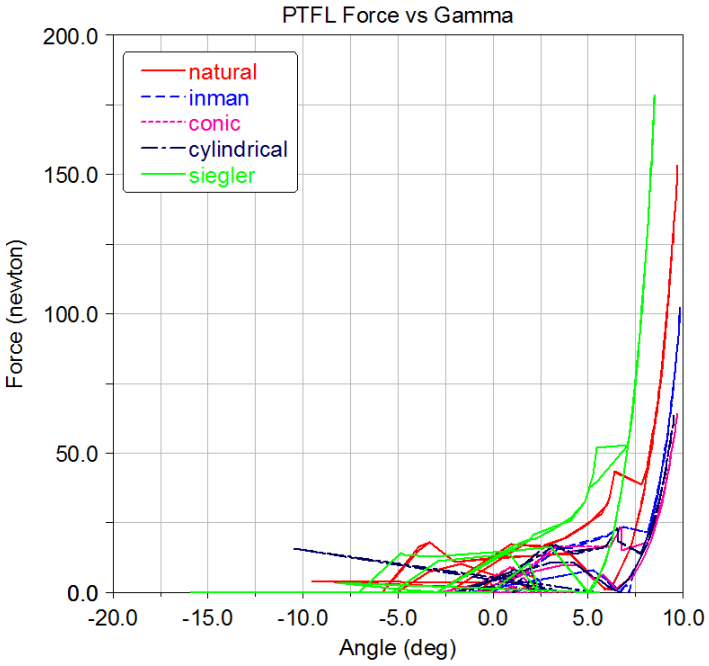

Figure 87: PTFL Force generation vs Gamma.

In the Alpha motion, specifically dorsiflexion, PTTL4 is less stressed in the Anatomical model and thus produces less force at increased angles of dorsiflexion. In plantar flexion, PTTL3 produces most of the force in the Anatomical model. This is similar to the Natural model. In the Inman, Conic and Cylindrical models, PTTL4 produces force at smaller angels of dorsiflexion and PTTL1 shares the force generation with PTTL3 in plantar flexion. In the Beta or inversion motion PTTL1 displayed slight difference in force production as the Beta angle decreased and shows that the Anatomical model is the one most close to the Natural model. In the Gamma motion, specifically internal rotation, PTTL1 produces most of the force when the ankle is rotated internally followed by the third and fourth PTTLs together. This is true for the Natural and Anatomical models but not the Inman, Conic and Cylindrical models where force is mainly generated by PTTL4 flowed by the first then the third when the ankle is internally rotated. The

contribution of the fourth and third PTTLs decreases for the Anatomical model compared to the Natural model.

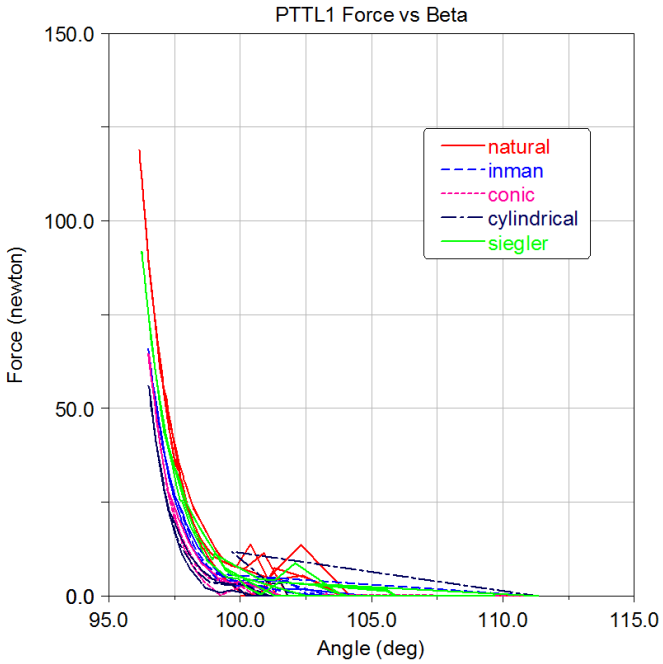

Figure 88: PTTL1 Force generation vs Beta.

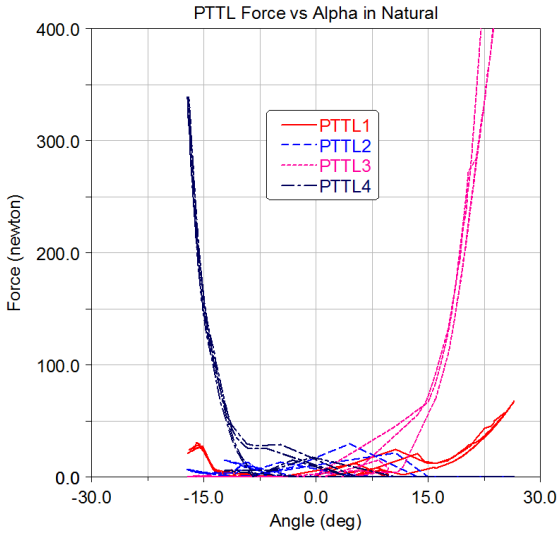

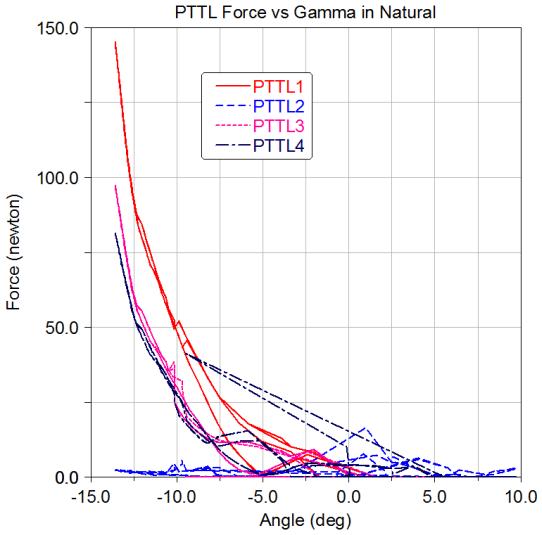

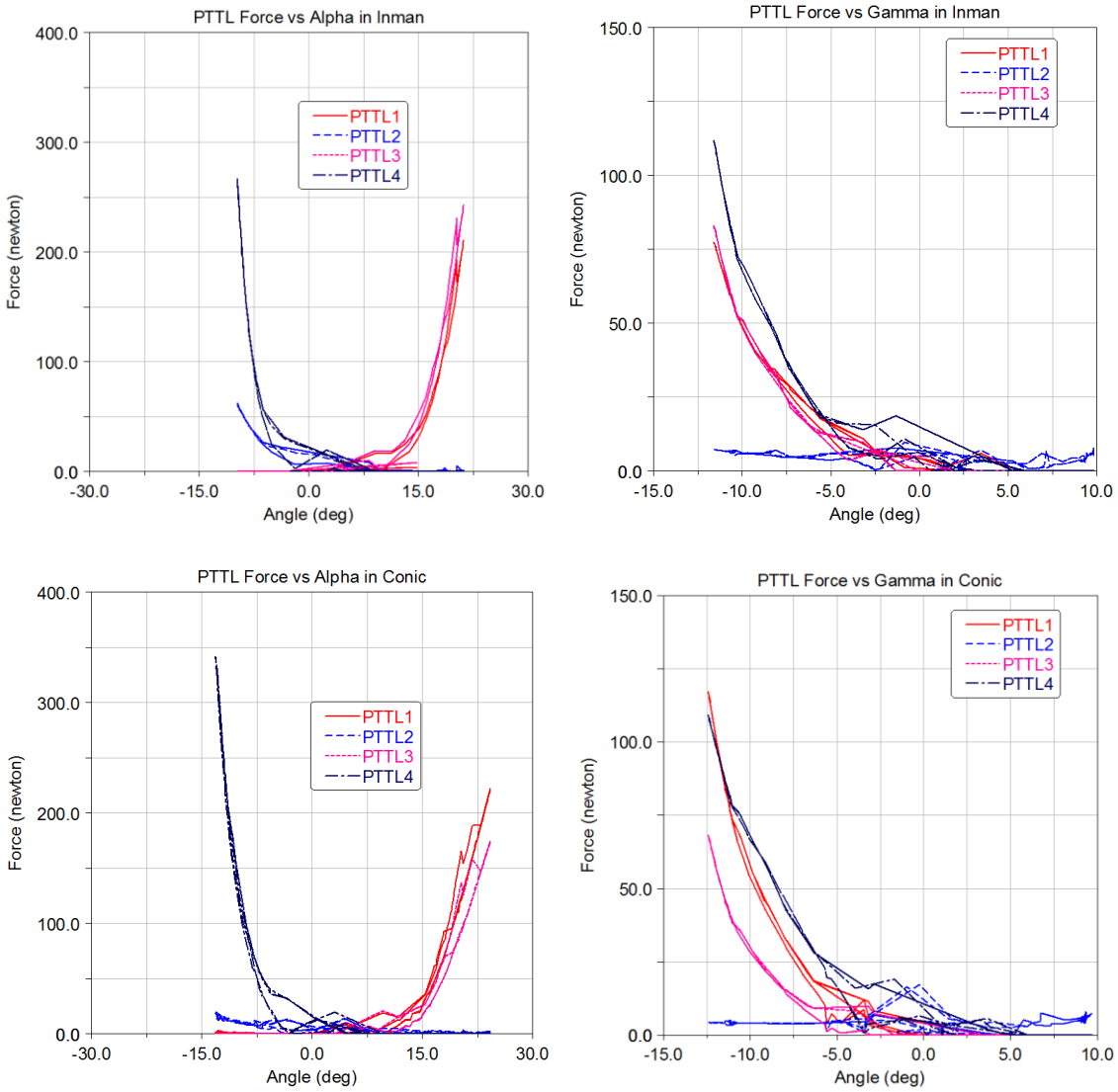

Figure 89: PTTL1-PTTL4 force generation vs Alpha and Gamma for all five models. Continued on next page.

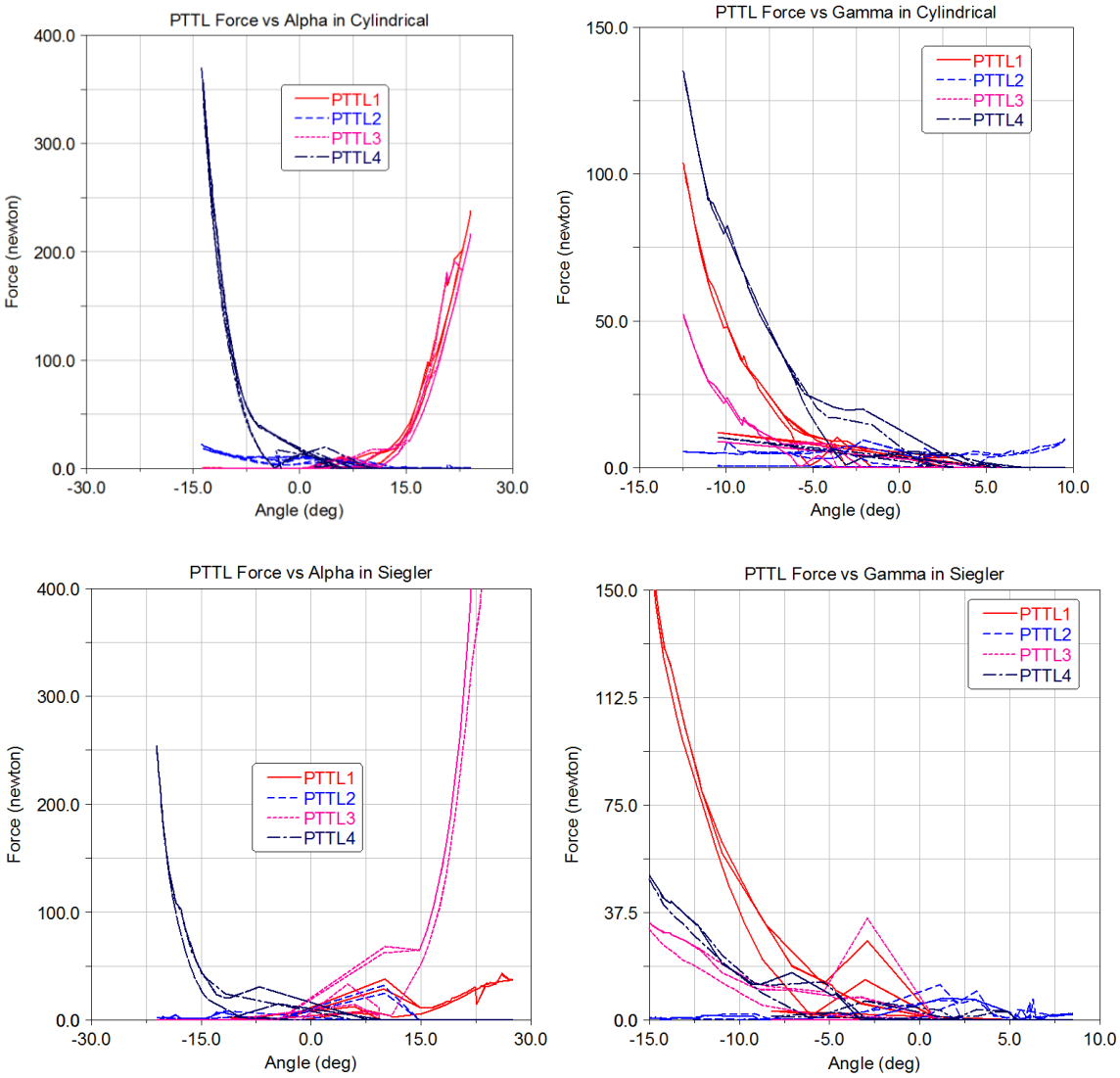

Figure 89 (Continued): PTTL1-PTTL4 force generation vs Alpha and Gamma for all five models.

The TCL was strained earlier in the dorsiflexion motion in the Inman, Conic and cylindrical models compared to the Natural model; producing the same force as the Natural ankle approximately 5^{o} earlier. The Anatomical model produced the same force as the Natural ankle approximately 4^{o} later. In the Beta, or eversion motion, the TCL was experiencing similar forces in the Conic and Cylindrical models approximately 2.5-3^{o} earlier than in the Natural, Inman and Anatomical models. In the Gamma or external rotation motion, the TCL was

experiencing similar forces in the Anatomical model approximately 2.5^{o} earlier than in the Natural, Inman, Conic and Cylindrical models.

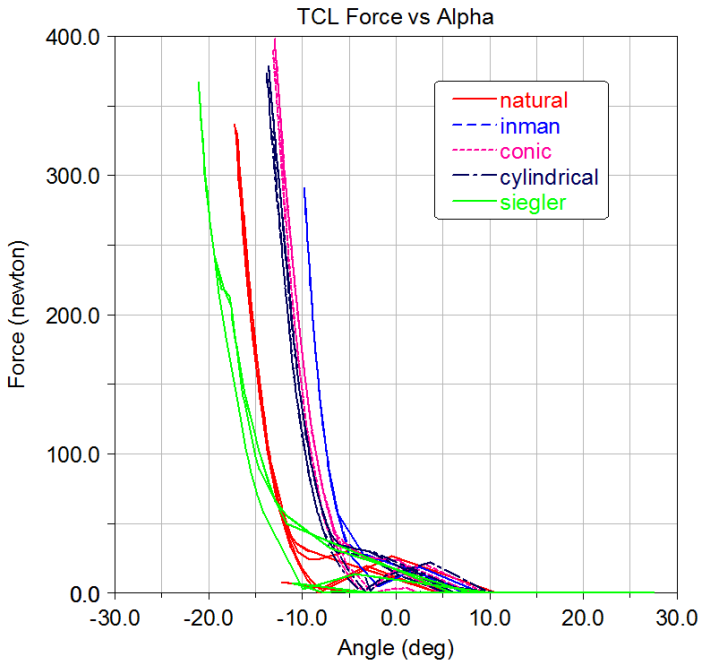

Figure 90: TCL force generation vs Alpha.

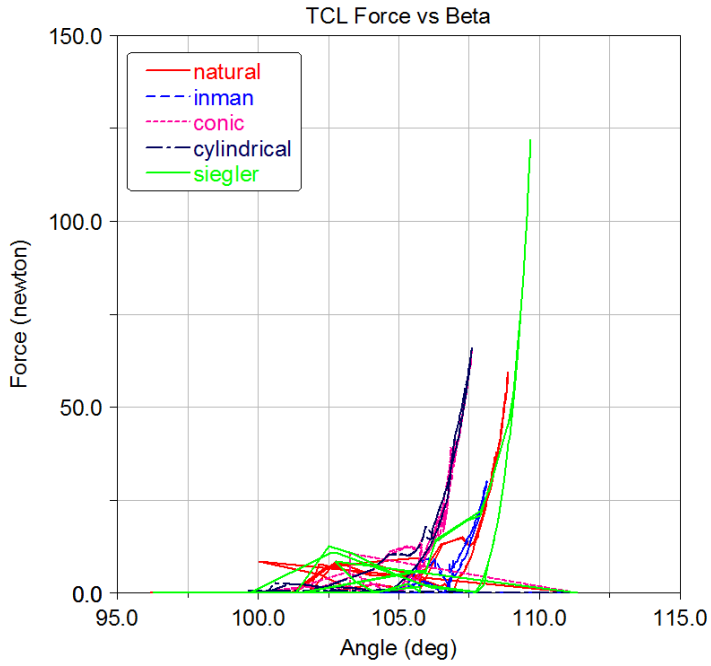

Figure 91: TCL force generation vs Beta.

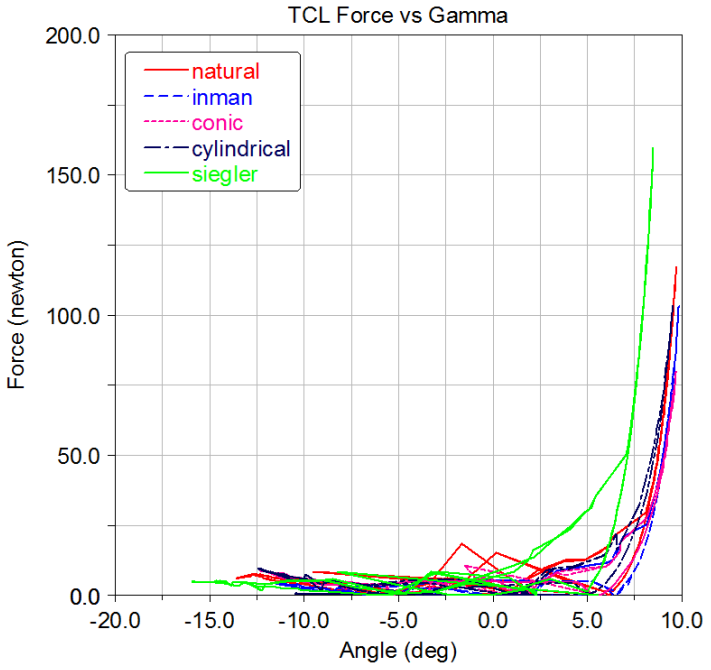

Figure 92: TCL force generation vs Gamma.

The TSL produced similar forces as the ankle went into plantar flexion for all of the five models. In the Beta, or eversion motion, the TSL was experiencing similar forces in the Inman,

Conic and Cylindrical models approximately 2-3^{o} earlier than in the Natural model; while the TSL in the Anatomical model was experiencing the same forces approximately 2^{o} later. In the Gamma motion, both internal and external rotation, the TSL was experiencing more forces in the Inman, Conic and Cylindrical models compared to the Natural and Anatomical models. The Anatomical model did not display any parabolic behavior in the relationship between the TSL force generation and the Gamma angle.

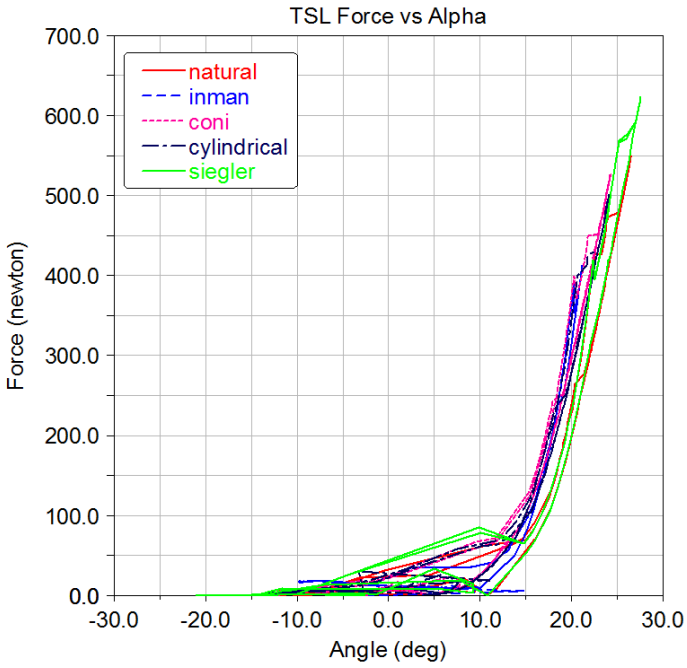

Figure 93: TSL force generation vs Alpha.

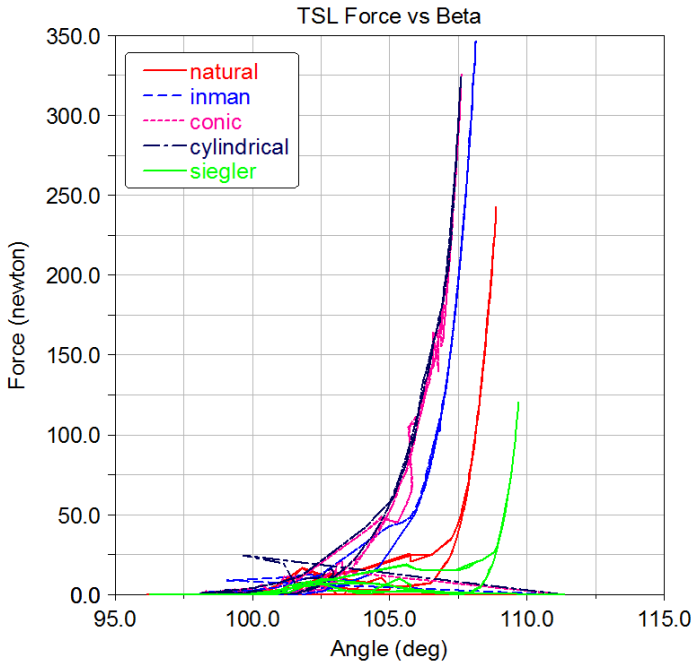

Figure 94: TSL force generation vs Beta.

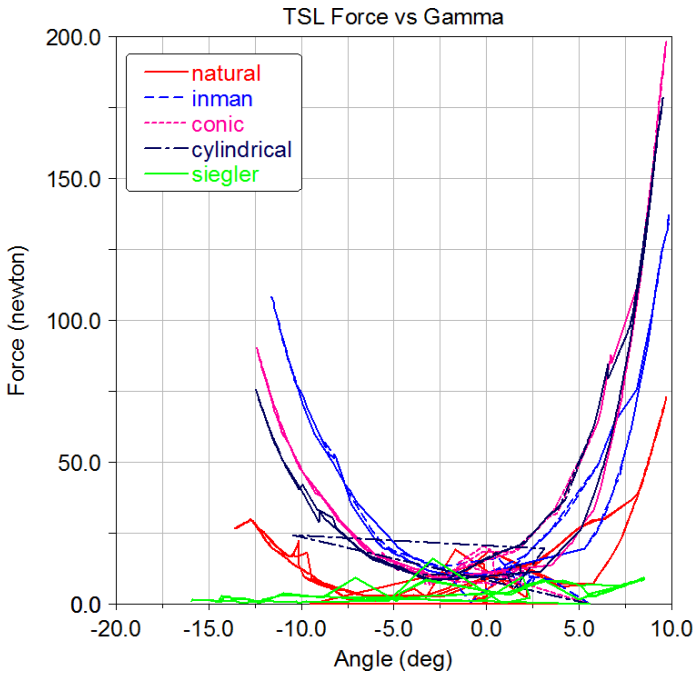

Figure 95: TSL force generation vs Gamma.

Distance Mapping Results

Summary of Distance mapping Results

In the Alpha motion the Natural and Anatomical models displayed contact between the talus and the tibia that started from the most anteromedial aspect of the talus and moved posterolateral. This was also evident in the Inman and Cylindrical models but with heavy penetration, especially at the anteromedial aspects, along with limited contact separation at the posterior aspect in the dorsiflexed position; up to 4.5 mm for both the Natural and Anatomical models and up to 2.5 mm for the Inman, Conic and Cylindrical models. The Conic model displayed similar results to the Cylindrical model but with more penetration and posteromedial rather than posterolateral contact when in plantar flexion.

In the Beta direction the Natural model displayed penetration and contact between the tibia and the talus in the anteromedial condyle of the talus and tibia in inversion and then at the center and anterolateral condyle of the talus and tibia in eversion. The Inman and Conic models displayed penetration and contact at the anteromedial aspects of the implant surface when in inversion and contact on the entire anterior aspect of the implant surface when in eversion. The Cylindrical model displayed a similar behavior to that of the Inman and Conic models but with little to no penetration at the contact points. The Anatomical model displayed penetration and contact on the anteromedial aspect of the implant surface when in inversion and increased anteromedial penetration and entire lateral contact when in eversion.

While in inversion, up to 4mm of separation was observed between the lateral aspects of the talus and tibia for both the Natural and Anatomical models. For the Inman, Conic and Cylindrical models approximately 2.5 mm of separation was observed at the posterolateral aspects of the implant surface.

In the Gamma direction the Natural model displays contact and penetration across the anterior aspect of the talus and the tibia when in internal rotation and the contact remained while in external rotation. Similarly, the Inman and Conic models display contact and penetration across the anterior aspect of the talar and tibial implant surfaces when in internal rotation and the contact remains with increasing penetration when in external rotation. The Cylindrical model displays little change in contact from neutral position when in internal rotation but also displays increased penetration and contact at the entire anterior aspect of the talar and tibial implant surface when in external rotation. The Anatomical model displays contact and penetration at the anteromedial aspect of the implant surface when in internal rotation and increase anteromedial penetration with contact through the entire anterior part of the implant surface when in external rotation. The penetration seen in the Anatomical model is less than that in the Inman, Conic and Cylindrical model.

Natural Distance Mapping Results

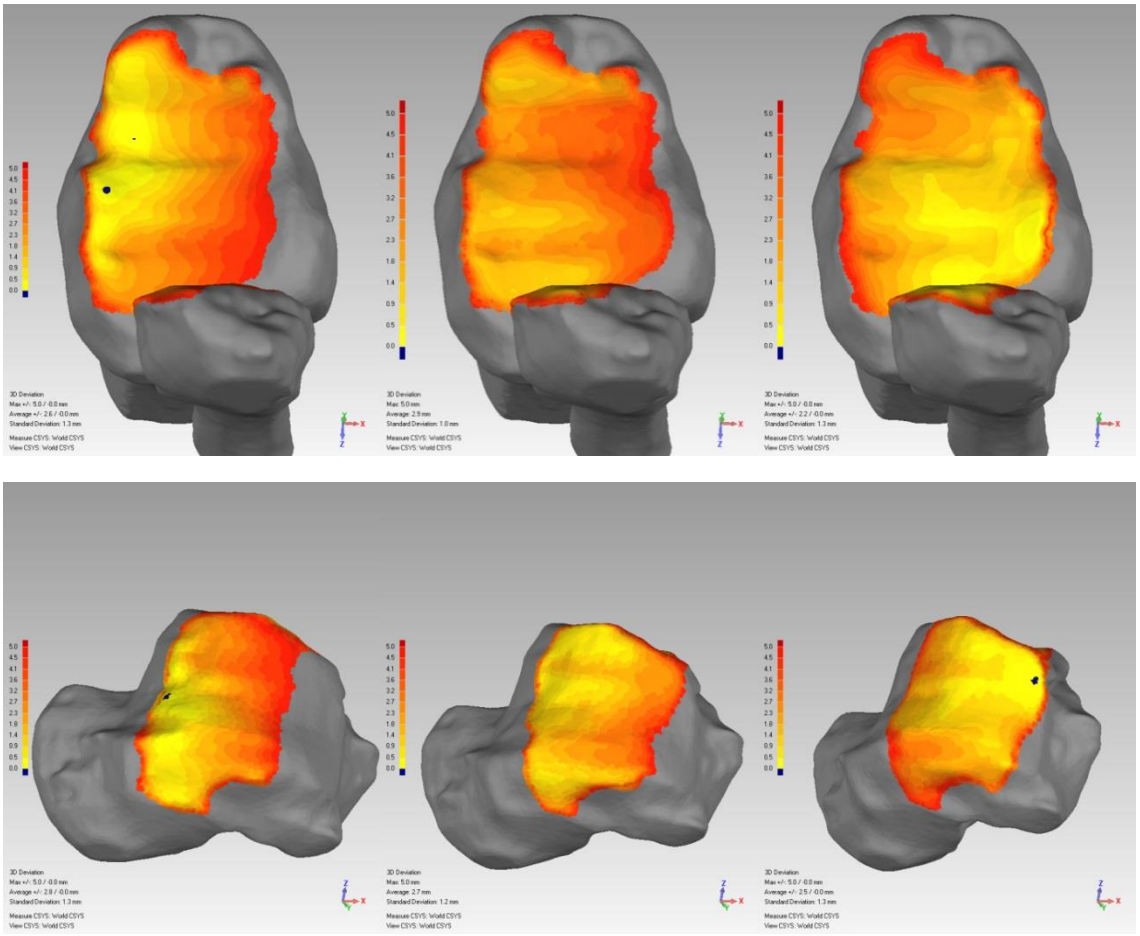

Figure 96: Distance mapping of dorsiflexion (left) to neutral (center) to plantarflexion (right) of the Natural model.

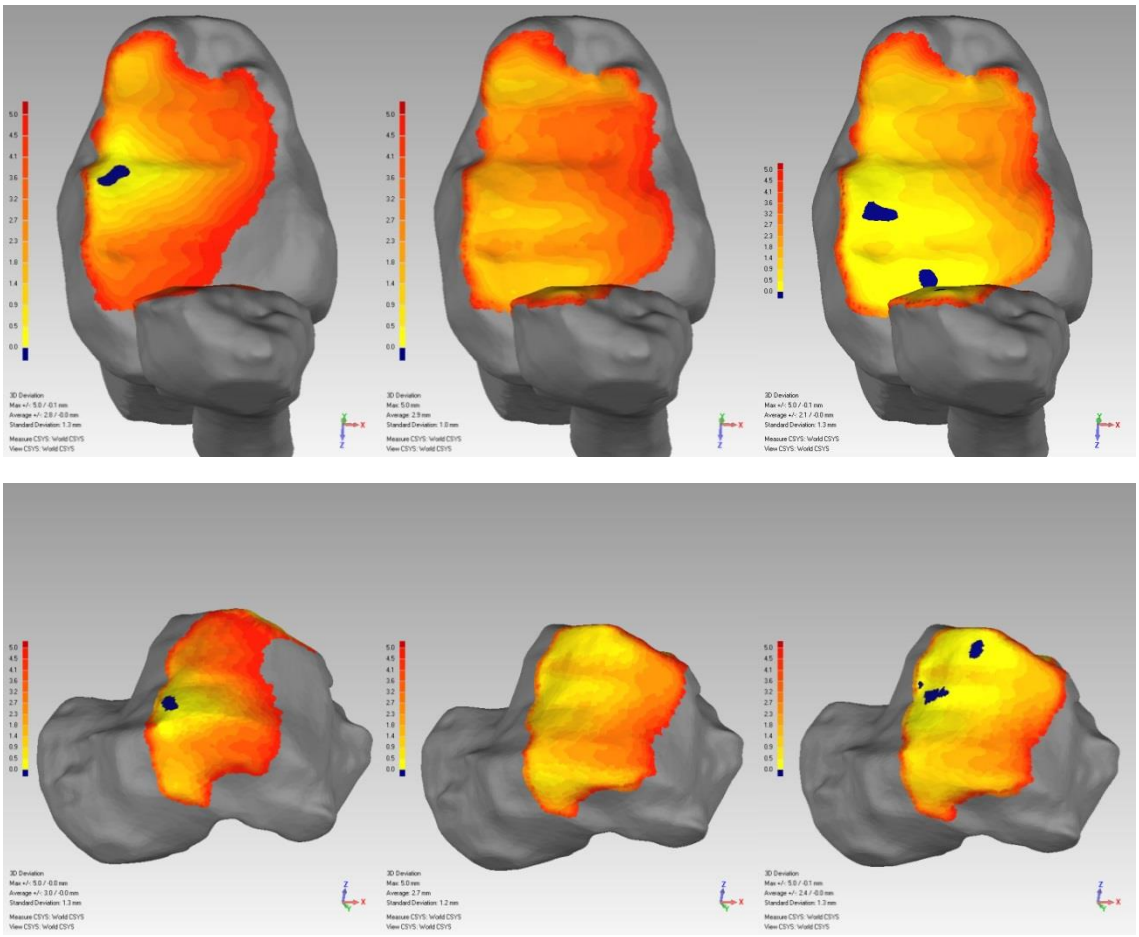

Figure 97: Distance mapping of inversion (left) to neutral (center) to eversion (right) of the Natural model.

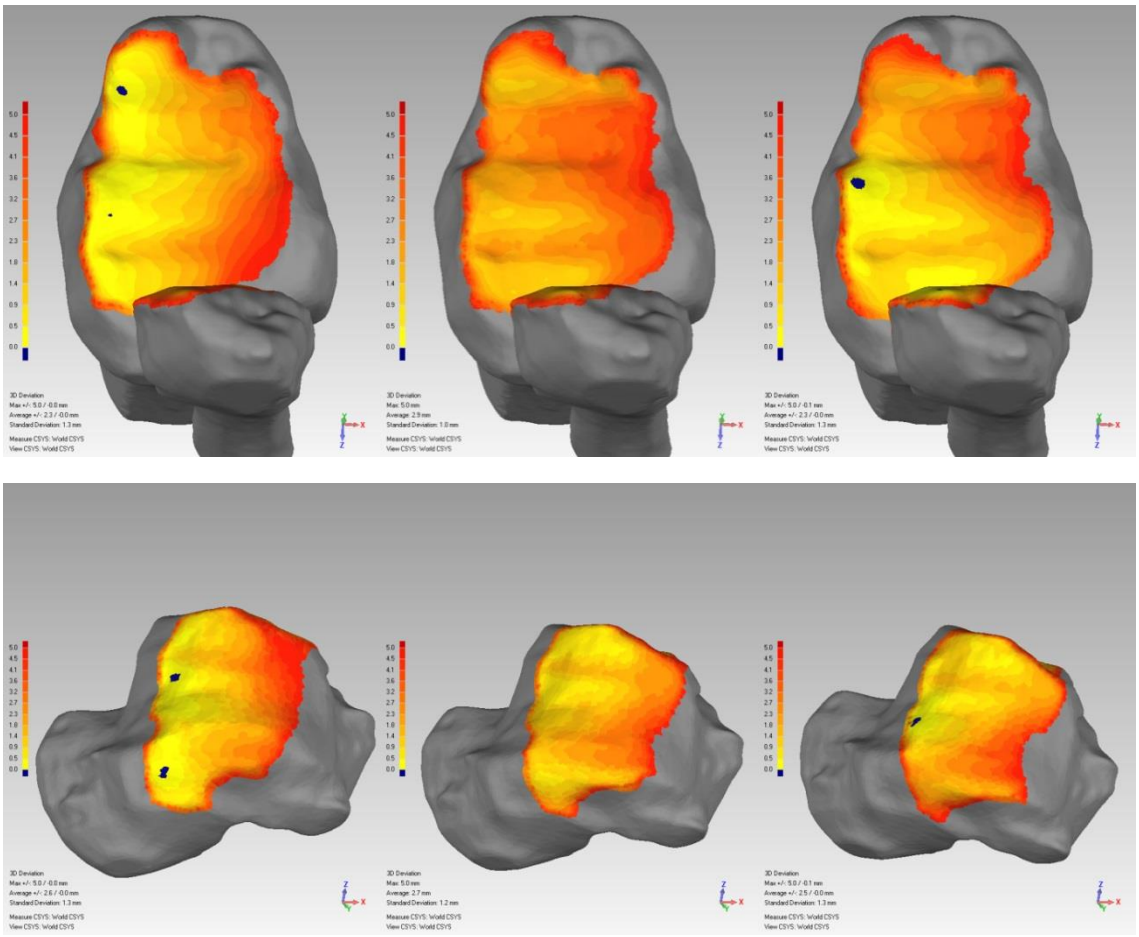

Figure 98: Distance mapping of internal rotation (left) to neutral (center) to external rotation (right) of the Natural model.

Inman Distance Mapping Results

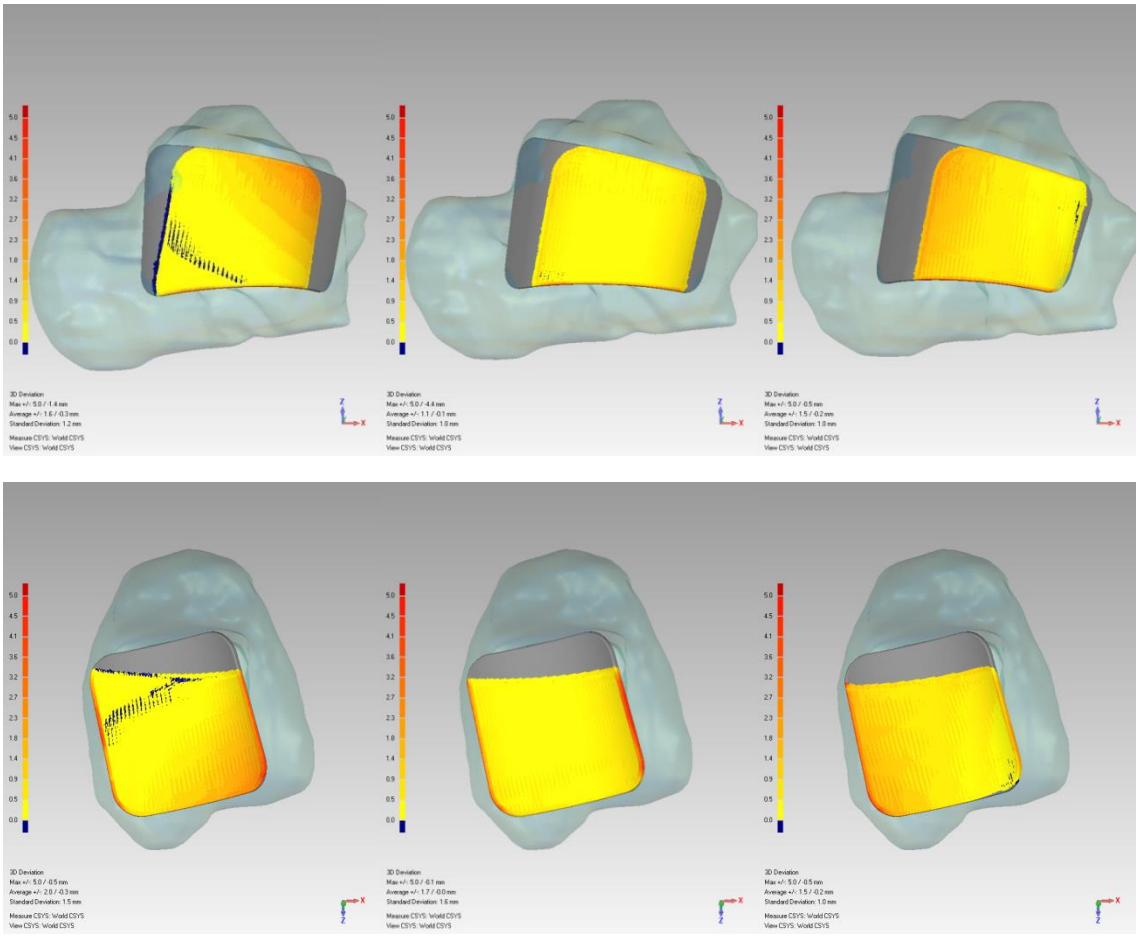

Figure 99: Distance mapping of dorsiflexion (left) to neutral (center) to plantarflexion (right) of the Inman model.

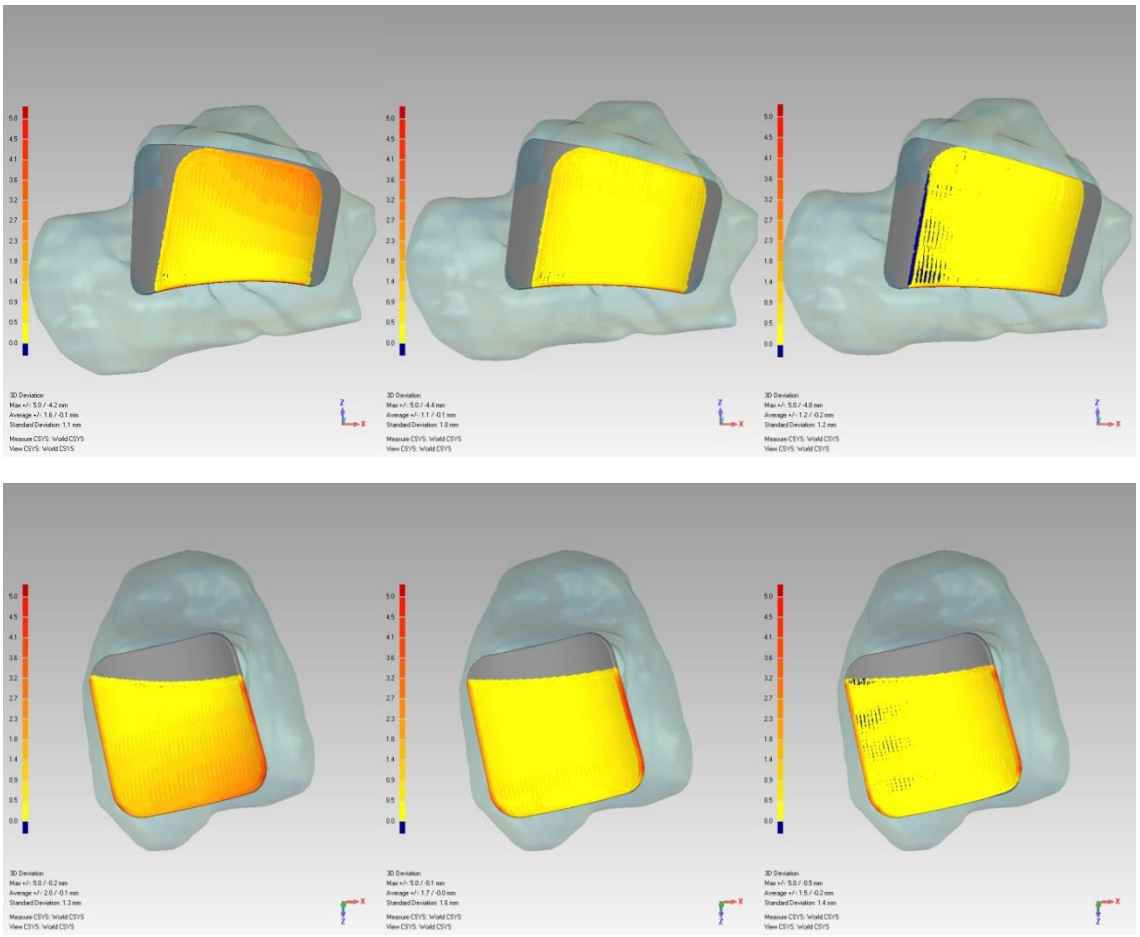

Figure 100: Distance mapping of inversion (left) to neutral (center) to eversion (right) of the Inman model.

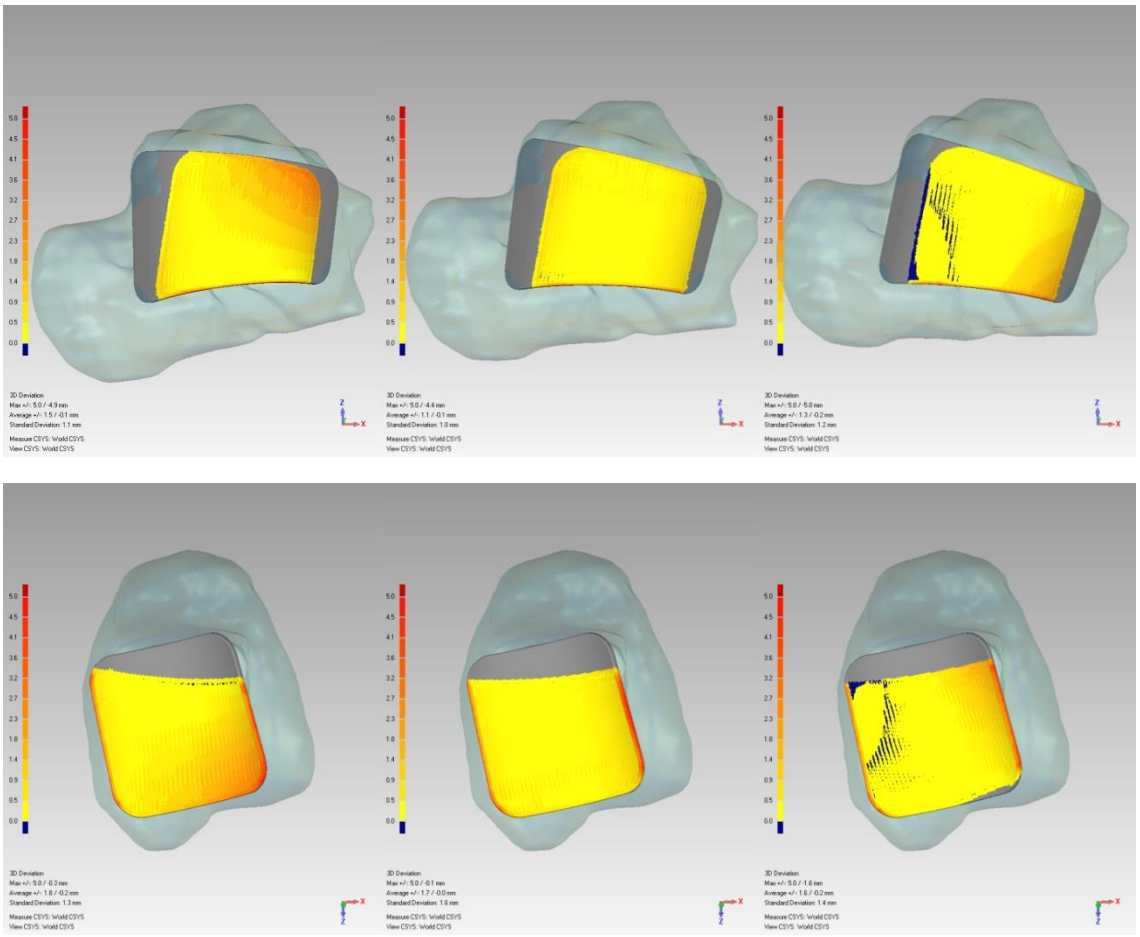

Figure 101: Distance mapping of internal rotation (left) to neutral (center) to external rotation (right) of the Inman model.

Conic Distance Mapping Results

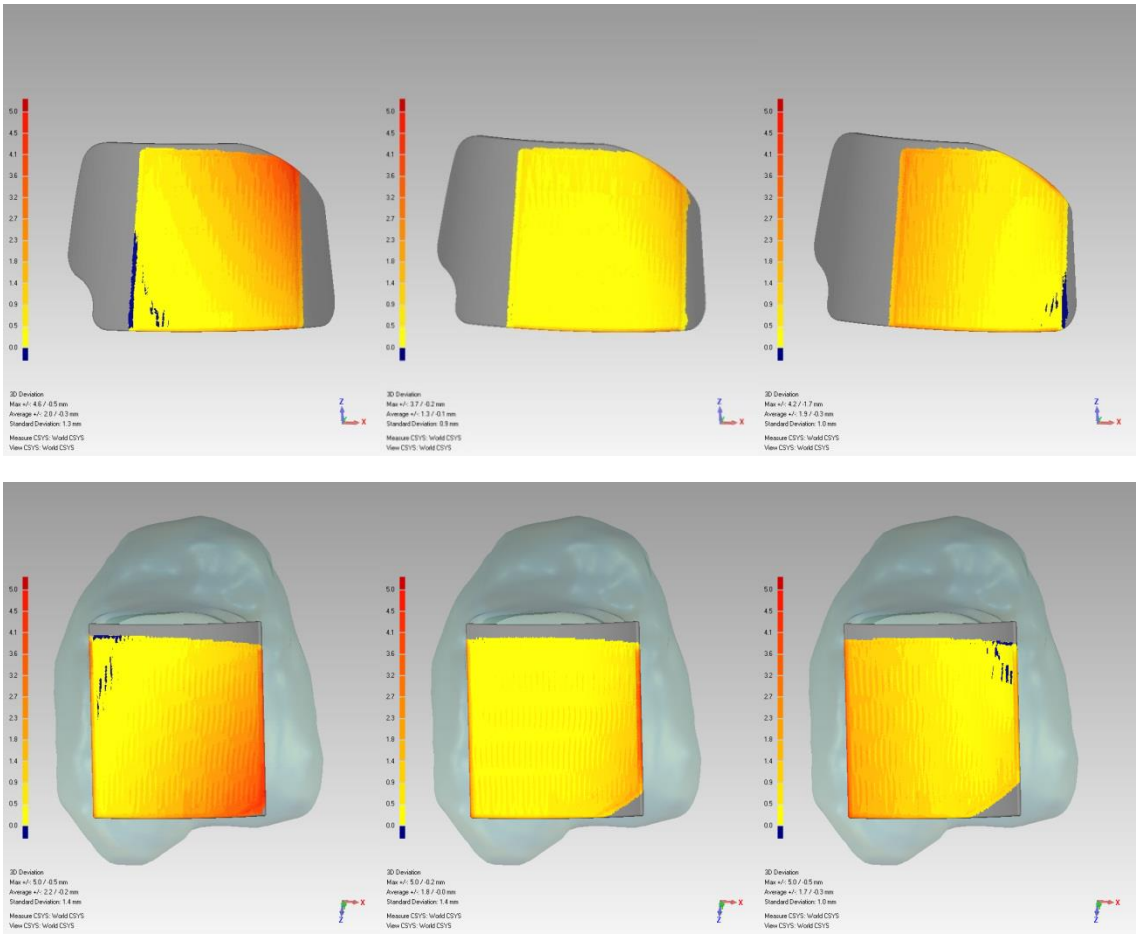

Figure 102: Distance mapping of dorsiflexion (left) to neutral (center) to plantarflexion (right) of the Conic model.

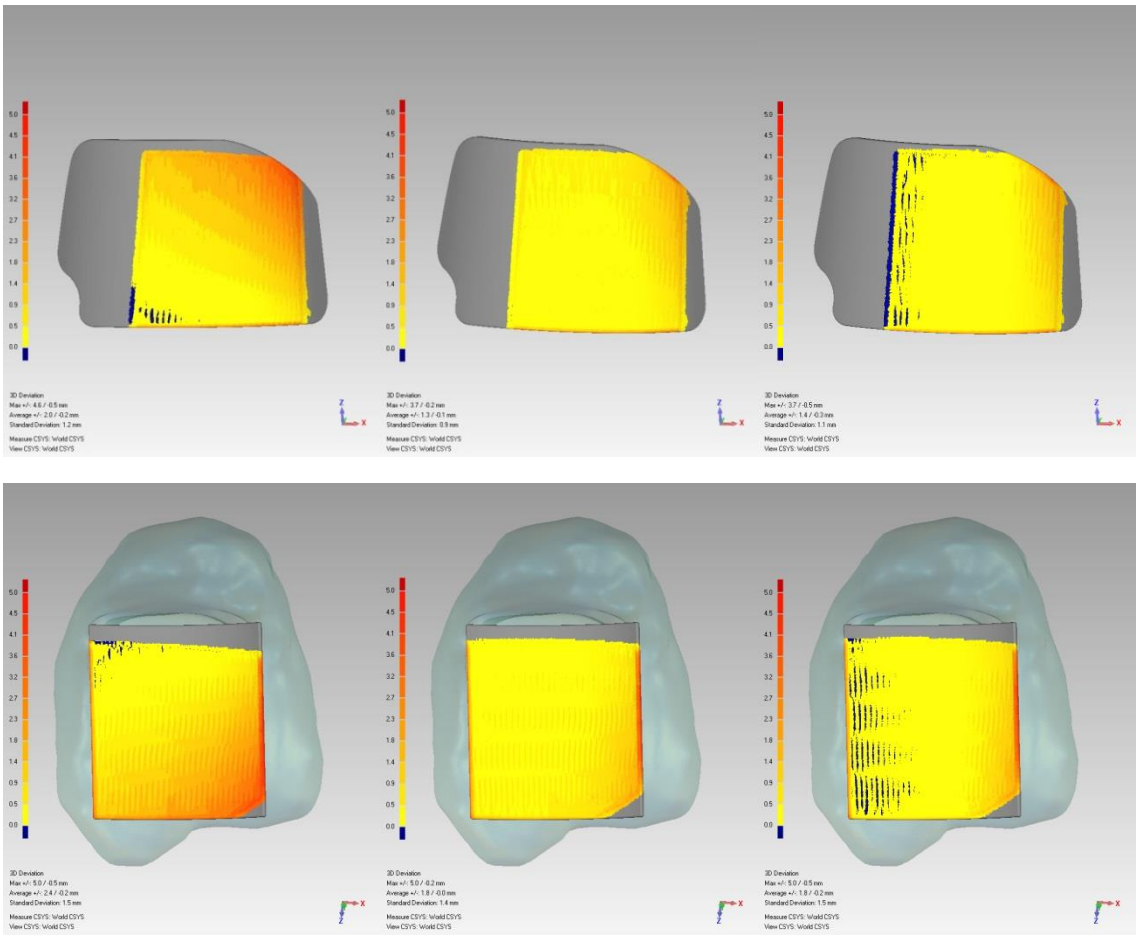

Figure 103: Distance mapping of inversion (left) to neutral (center) to eversion (right) of the Conic model.

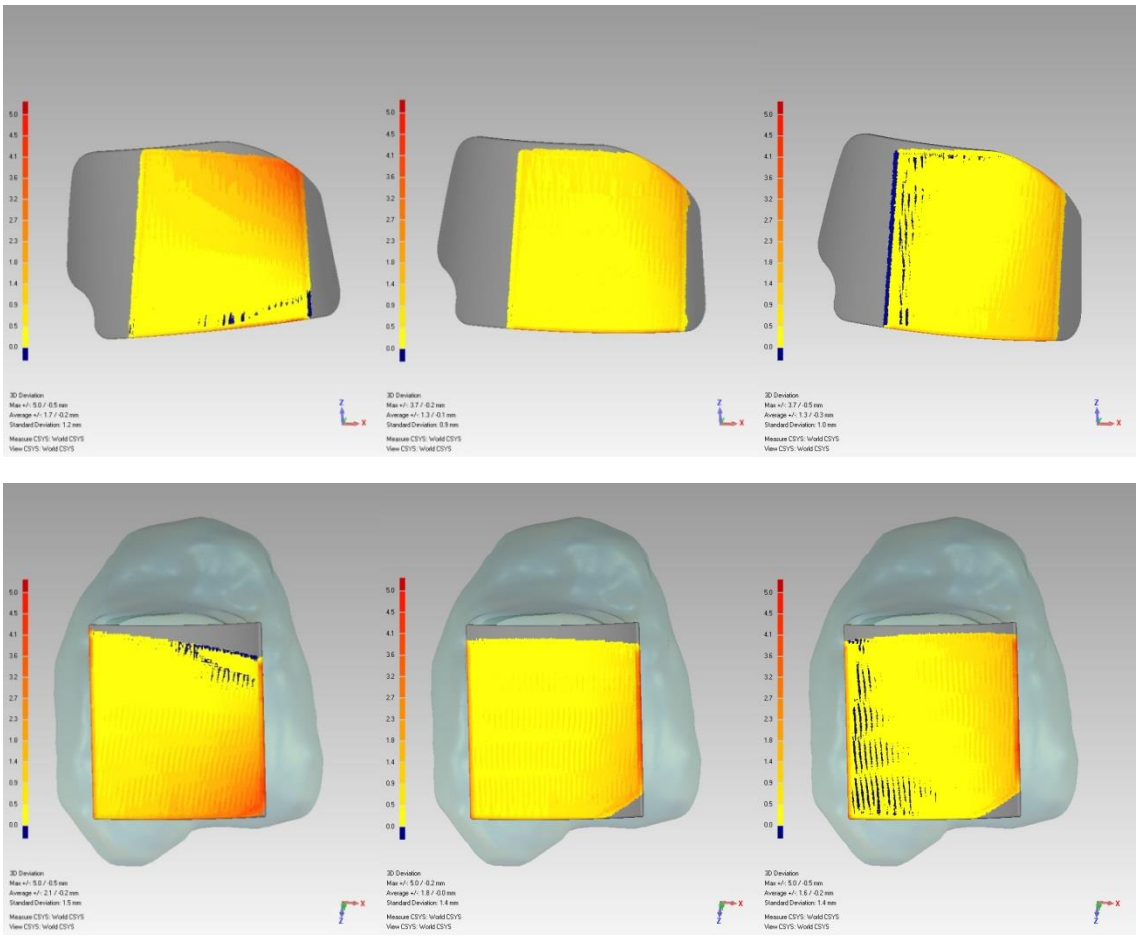

Figure 104: Distance mapping of internal rotation (left) to neutral (center) to external rotation (right) of the Conic model.

Cylindrical Distance Mapping Results

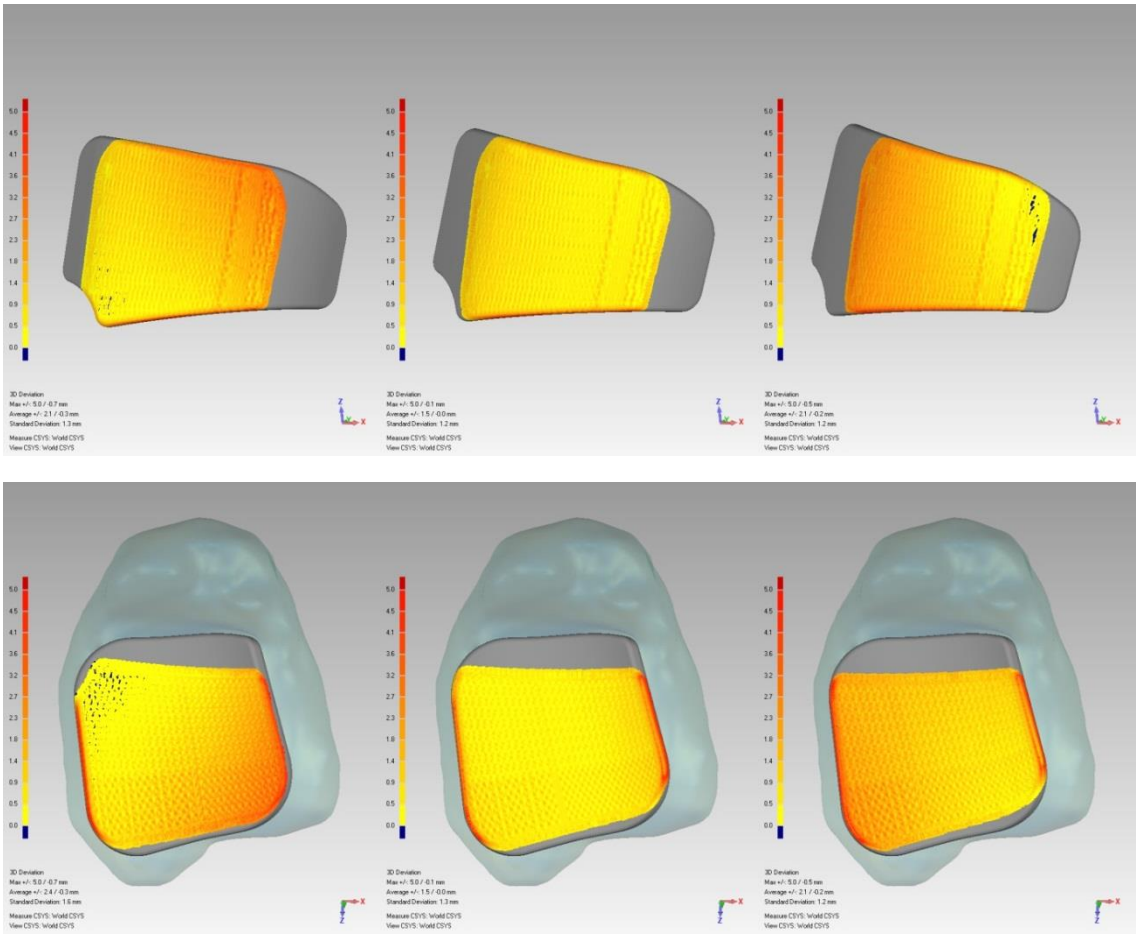

Figure 105: Distance mapping of dorsiflexion (left) to neutral (center) to plantarflexion (right) of the Cylindrical model.

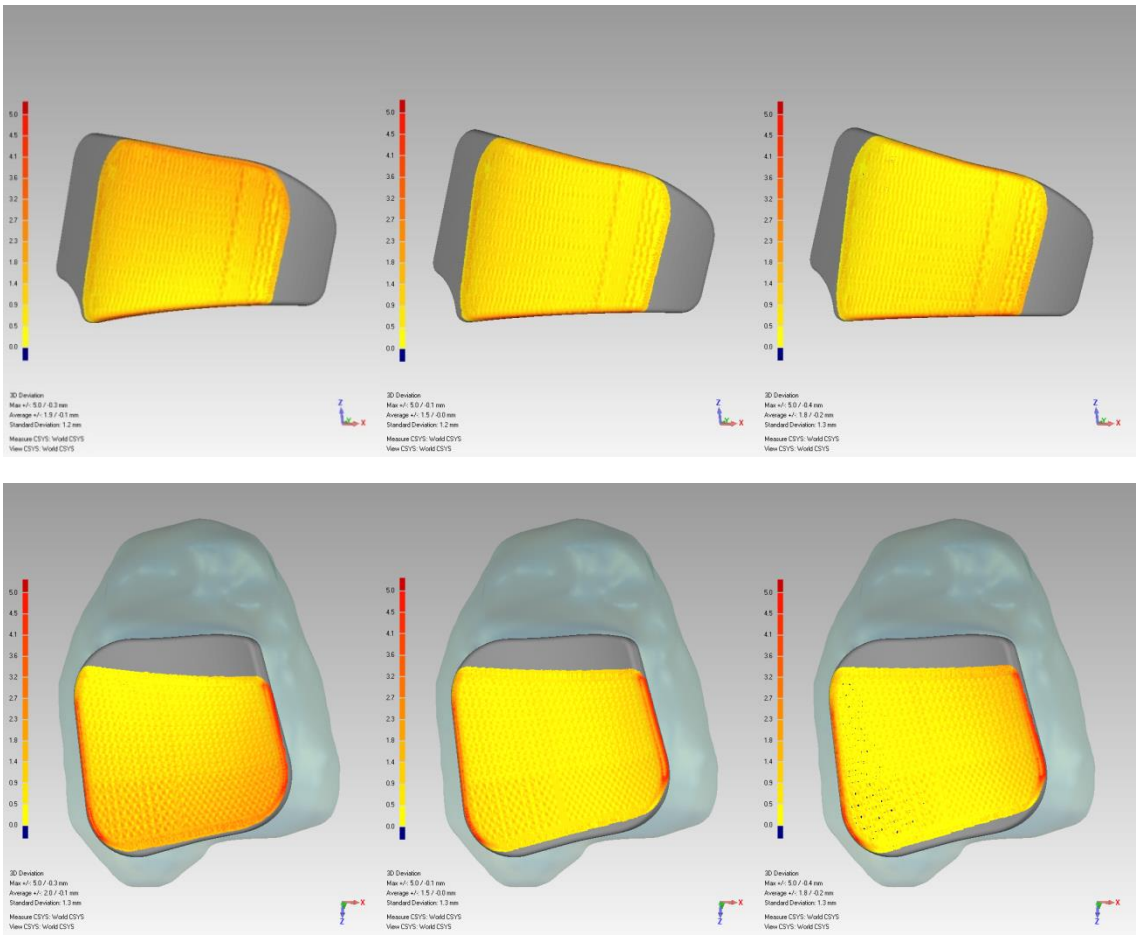

Figure 106: Distance mapping of inversion (left) to neutral (center) to eversion (right) of the Cylindrical model.

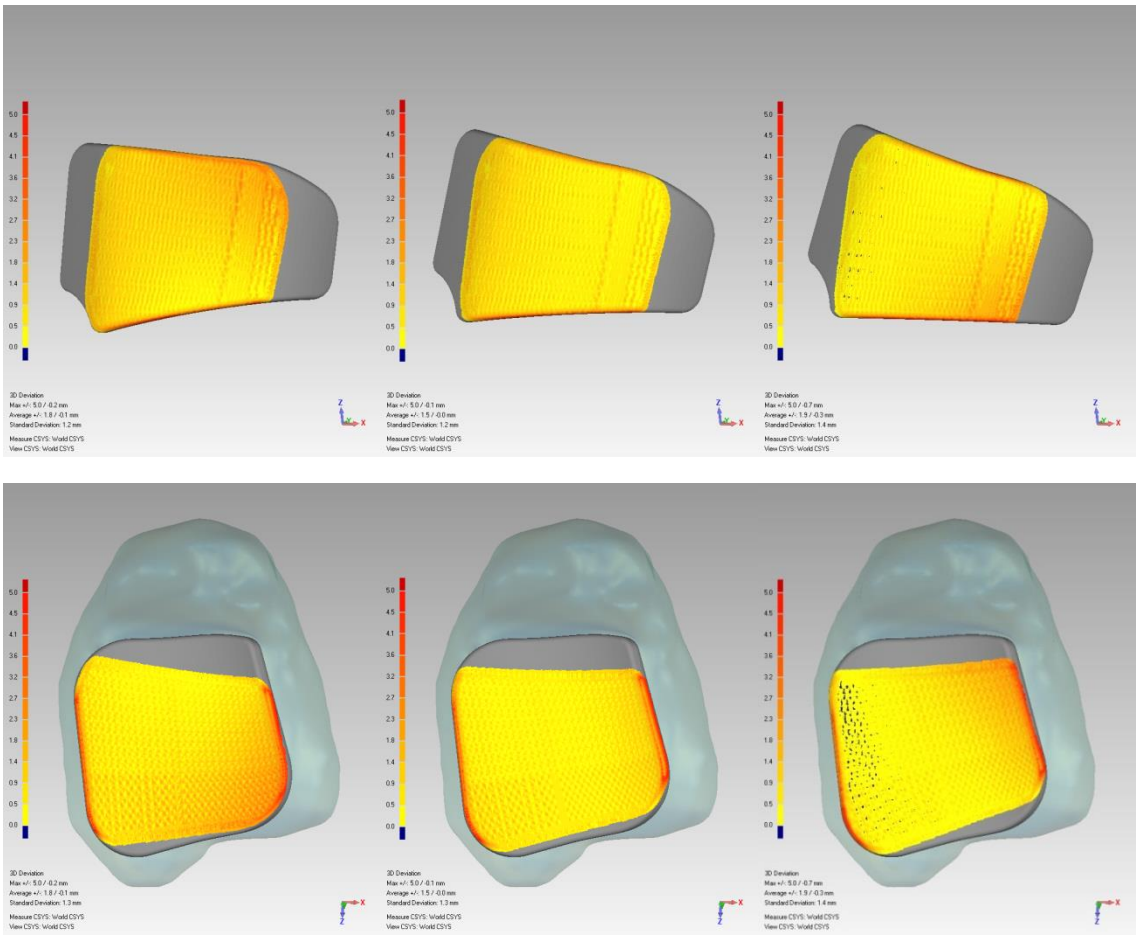

Figure 107: Distance mapping of internal rotation (left) to neutral (center) to external rotation (right) of the Cylindrical model.

Anatomical Distance Mapping Results

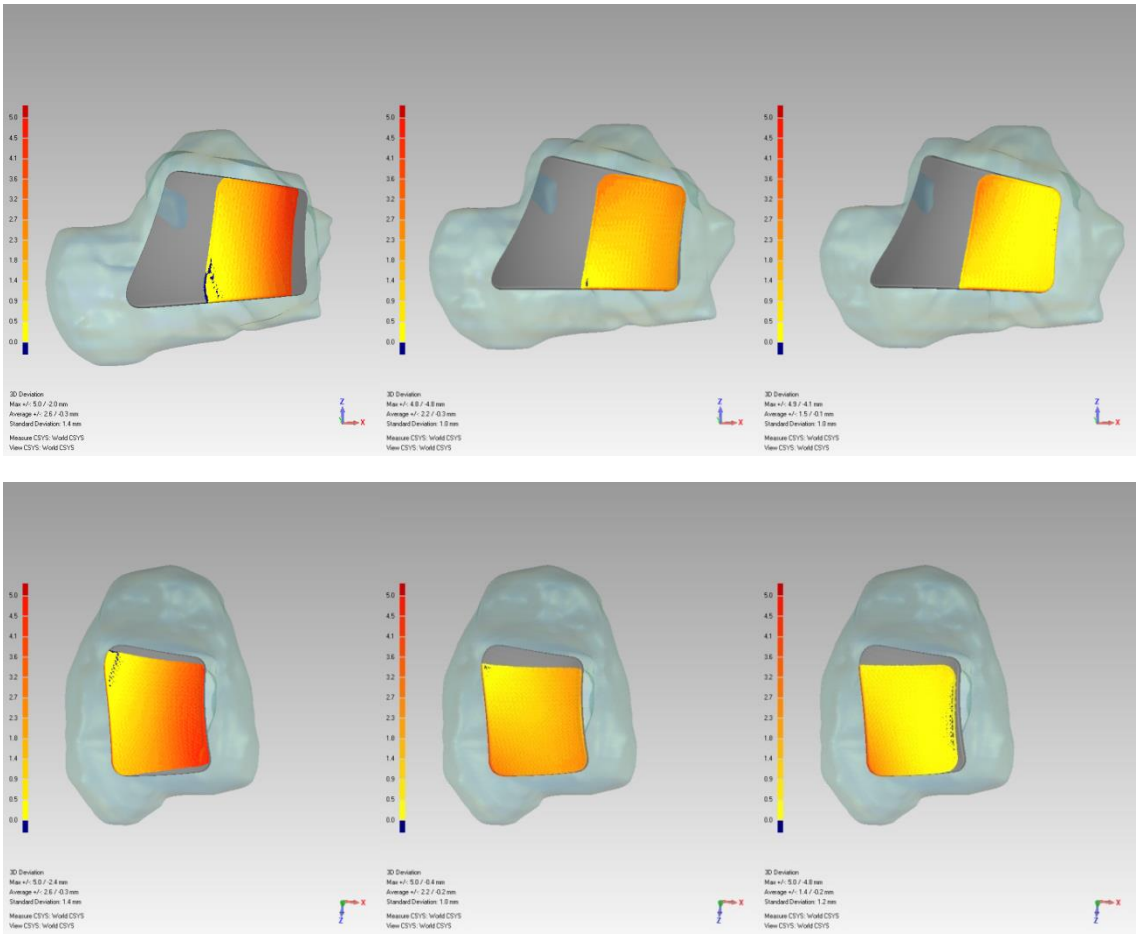

Figure 108: Distance mapping of dorsiflexion (left) to neutral (center) to plantarflexion (right) of the Anatomical model.

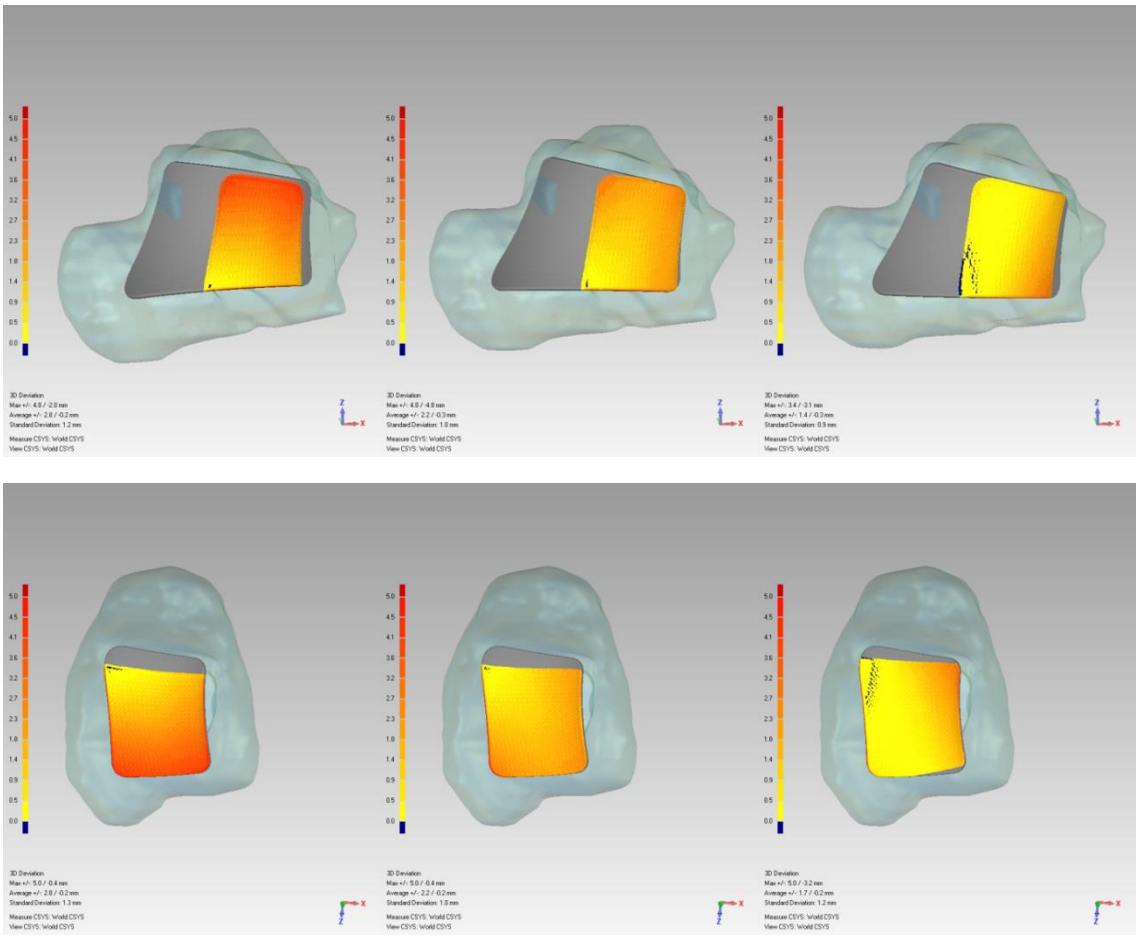

Figure 109: Distance mapping of inversion (left) to neutral (center) to eversion (right) of the Anatomical model.

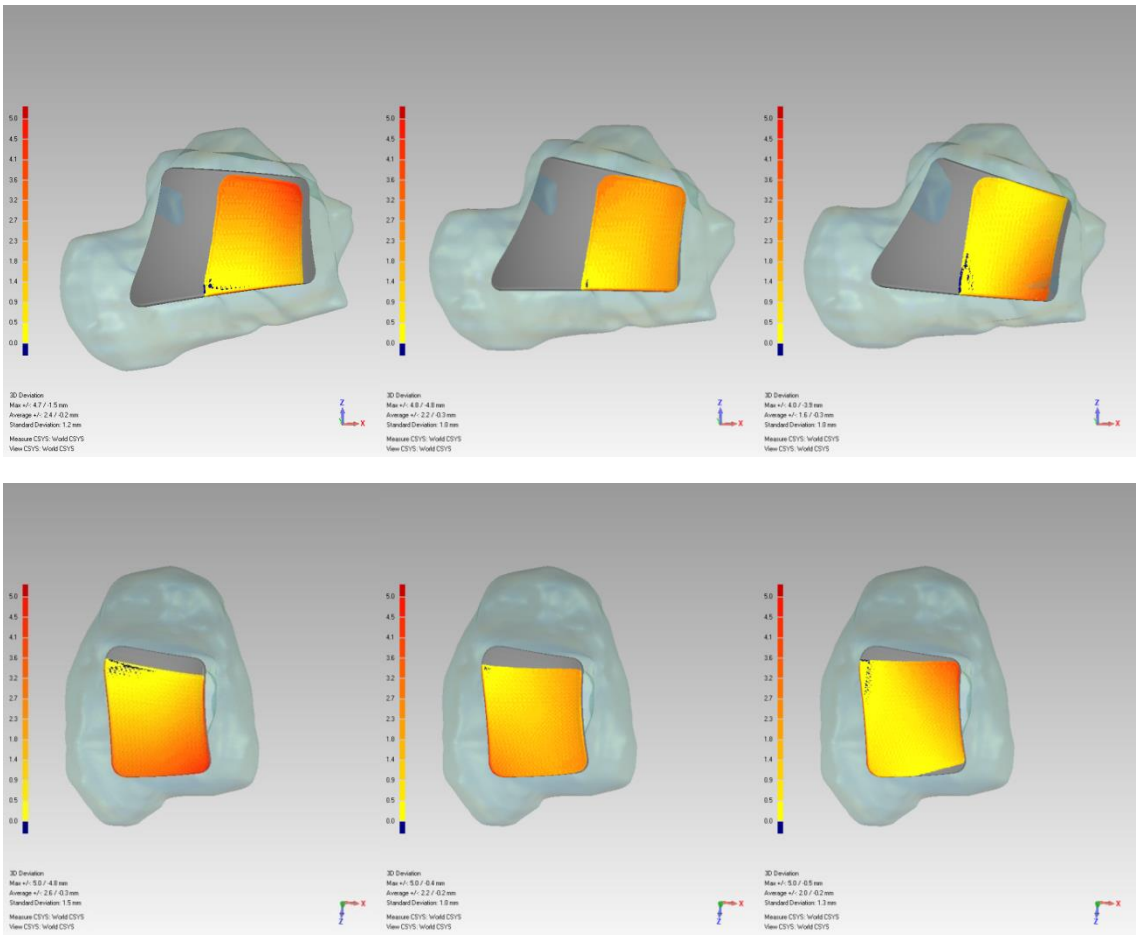

Figure 110: Distance mapping of internal rotation (left) to neutral (center) to external rotation (right) of the Natural model.

Chapter 5: Discussion

To evaluate the four different implant surface models, range of motion, kinematic coupling, ligament forces, and distance mapping of the articulating surfaces were used.

Range of motion was simply used to evaluate the ability of the implant design to allow the ankle to rotate in its three different axis of rotation, namely Alpha, Beta and Gamma. The goal was to accurately test the range of motion the four different implant surface designs offered without having outside factors affect the results. One of the factors that can affect range

of motion other than surface morphology is the placement of the implant surface. If the implant surface is sitting too high it may cause increased tension in the ligaments and thus reduce the total range of motion, and sitting too low would cause excess slack in the ligaments allow for a greater range of motion. To counteract this, the implantation method used was consistent through all of the implant surfaces so as to limit the effect of implant surface positioning on the range of motion. Since the methodology of positioning, or “implanting”, these surface designs was not 100% accurate but relied to some extent on the human eye, a small error can be introduced in the results of this study. This however can be dismissed since the method used for positioning the surface designs was consistent across all models, and since the point of the results is to compare them to one another and not make a judgment or a conclusion based on their individual values separately. From the results of the study, the Anatomical surface design was found to allow for more range of motion compared to the Inman, Conic, Cylindrical surface models, and even the natural ankle model. This could be due to two main reasons. The first is the idea that the Anatomical implant surface was sitting further into the bone compared to the others because of the saddle in its geometry. Since the implant surface was fit to be halfway between fully above and below the respective bone, it was pushed further into the bone because the saddle gave it more height and increased the distance it would have to travel into the bone to get halfway into the bone. This leads to less initial tension in the ligaments and allow for more range of motion. However, the results of the distance mapping can be used to contest this argument, which brings us to the second reason why the Anatomical design has more range of motion. The second reason is the saddle and skewedness geometry of the tibial and talar implant surfaces. Recall that in the coronal plane the tibia had a smaller curvature than the talus, but a larger curvature in the sagittal plane. This tells us that in the sagittal plane the talus fits into the tibia and in the coronal plane the tibia fits into the talus. This bi-directional fit

is replicated with the Anatomical model and is shown to behave similar to the Natural model when analyzed through the distance maps. For example, the results of the distance maps for the rotational movement about the Alpha axis display that the Natural and Anatomical models had separation between the talar and tibial aspects that were up to approximately 4 mm, while the remaining models only had up to approximately 2.5 mm in separation. Keep in mind that the positioning of the implant for the distance mapping tests were done by simply laying the implant surfaces lie on top of the respective bone and not penetrate into it whatsoever. This separation hints to the idea that the Anatomical implants are not simply sliding over one another but that the center of rotation moves and allows the implant to swing over and create and fill space in between the two articulating surfaces. This type of kinematic motion is not possible with symmetrical cones and especially with a cylinder. This is why there are larger amounts of contact in those implant surface designs and a resulting penetration that is a product of the articulations in the model attempting to swing over one another.

Kinematic coupling was a measure of the coupling found between two ranges of motion of the ankle. Coupling was observed between Alpha-Beta, and Alpha-Gamma, but not between Beta-Gamma. Between Alpha and Beta there is a hyperbolic relationship concaves with a plateau near the neutral position. In both the Natural and Anatomical models there is little to no coupling for the first 10^{o} of dorsiflexion and the first 15^{o} of plantar flexion. After that the Natural and Anatomical models couple their motion into inversion for both the dorsi and plantar flexion, but more so for plantar flexion. This is similarly seen in the Inman, Conic and Cylindrical models as well but without the plateaued region near the neutral position that contain the little to no coupling of motion. Between Alpha and Gamma there is a more linear coupling motion for all models, for when the ankle goes from dorsiflexion to plantar flexion it is coupled with external rotation. In other words, when the ankle goes into dorsiflexion from neutral it internally rotates

and when it goes into plantar flexion from neutral it externally rotates. One difference from among the five models is that the Natural and Anatomical models allowed for greater range of motion and displayed a coupling that occurred over a larger range of motion. The Inman, Conic and Cylindrical models also ceased to couple the Alpha motion with the Gamma motion approximately 5^{o}, in the Alpha direction, earlier. This displays the stiffness these models add compared to the Natural and Anatomical models.

One thing to note about the two coupling situations is the fact that the coupling did not change between the Inman and Conic models. Recall that the Inman and Conic designs are opposites of one another; they are both symmetrical cones where the Inman design apexes medially and the Conic design apexes laterally. One would expect to see opposite coupling from these two models but surprisingly they are similar. This hints to the idea that the ligaments play a larger role in this coupling motion and one would expect to see a difference between the ligaments reaction between the different models, especially between the Anatomical, Inman and Conic models. The distance mapping also supports this idea. When looking at the areas of contact and penetration on the Inman and Conic implant surfaces during plantar flexion, it can be noticed how the area of penetration on the Inman surface is more posterolateral where on the Conic surface it is more posteromedial. This is because the implant surface is being forced to move in the way of the natural ankle and the two different apexed cones display different areas of contact based on their apex, namely the Inman apexes medial and has contact laterally and the Conic apexes laterally and has contact medially. Also, when the Inman, Conic and Cylindrical implant surface designs are implemented in an actual implant, the two articulating surfaces will be under an axial load during motion that will force the two surfaces to be flush on one another and thus may change the kinematic behavior and even ligament strains. This was not done in the numerical model as the surfaces began to penetrate excessively and the model collapsed

when an axial load was applied. Future work is currently ongoing where a few of the implant surface designs will be 3-D printed and implanted into cadavers to test for kinematic behavior in vivo.

When looking at the ligament forces it is important to keep in mind the role of each ligament, its location and the motion causing the force in it. Recall the role of the ATFL, which is to prevent anterior drawer of the ankle and also control inversion and internal rotation. When going into plantar flexion, this ligament was tensioned 10^{o} earlier in the Inman, Conic and Cylindrical models compared to the Natural and Anatomical models. This could be due to the fact that the coupling found between plantar flexion and inversion in the Inman, Conic and Cylindrical models occurred faster leading to faster ligament loading. Simply applying an inversion or internal rotation moment without a plantar flexion moment did not expose a difference in the ATFL force production similar to that of when plantar flexion was added.

The ATTL is part of the deltoid ligament and plays a role in the stabilizing the ankle joints. From the results of the model simulation runs it can be easily noticed that the ATTL is highly strained when the ankle goes into plantar flexion in the Inman, Conic and Cylindrical models compared to the Natural and Anatomical Models where the ligament is only slightly strained. This could be a result of the coupling between Alpha and Beta occurring too early in the Inman, Conic and Cylindrical models compared to the Natural and Anatomical models. When going into inversion the ATTL experiences forces in the Natural and Anatomical models while in the Inman, Conic and Cylindrical models there is minimal force generation from the ATTL. This again can be contributed to the fact that the Inman, Conic and Cylindrical models coupled the plantar flexion motion with inversion faster than the Natural and Anatomical models allowing opposite effects on the loading behavior of the ATTL.

The CFL prevents the motion of the ankle in dorsiflexion, inversion and external rotation. When the ankle went into dorsiflexion and coupled with internal rotation the CFL experienced higher forces in the Inman, Conic and Cylindrical models compared to the Natural model, and less loading in the Anatomical model compared to the Natural model. This could be, once again, the result of the tighter Alpha-Beta coupling found in the Inman, Conic and Cylindrical models compared to the Natural and Anatomical models. Also, in plantar flexion, the coupled inversion led to some loading of the CFL but not to the same extent as going into dorsiflexion because of the coupled external rotation with plantar flexion that gave the CFL some slack.

The PTFL prevents motion in the external rotation and dorsiflexion direction. When the ankle went into dorsiflexion and coupled with internal rotation, the PTFL experienced forces earlier in the Inman, Conic and Cylindrical models compared to the Natural and Anatomical model due to the stronger coupling of dorsiflexion and inversion in the Inman, Conic and Cylindrical models, giving the PTFL some slack. One thing to note is the amount of force generated in the Anatomical model was at least three times larger than any of the other models. This however was a result of the increased range of motion offered by this model and not because the model forced this strain. In other words the Anatomical model allowed the ankle to rotate more internally, giving the PTFL a chance to generate more force as it undergoes lager strains. As the ankle went into external rotation the PTFL experienced forces 5^{o} earlier in the Anatomical model and 2^{o} earlier in the Natural model compared to the Inman, Conic and Cylindrical models. This can be attributed to the results that described a stronger coupling of Alpha with Beta in the Inman, Conic and Cylindrical models which provides some slack to the PTFL.

The TSL resists motion into eversion and external and internal rotation. The TSL experienced forces in the Inman, Conic and Cylindrical models earlier than in the Natural and Anatomical models when an eversion moment is applied. This is supported by the distance mapping of the articulating surfaces when going from neutral into eversion. The Inman, Conic and Cylindrical models do not display the same amount of distance change when going from neural to eversion as the Natural and Anatomical models do. As the ankle goes into eversion the saddle geometry found in the Natural and Anatomical models allow for the ankle to translate superiorly and thus give slack to the TSL whereas the Inman, Conic and Cylindrical models do not provide that range of motion. A similar trend is seen in the plot of the TSL force vs Gamma. The translational degree of freedom offered by the Natural and Anatomical models allow for the TSL to experience less strains when the ankle moves into internal and external rotation.

Chapter 6: Conclusions

From the results of this study it can be concluded that morphological features of the talocrural joint play a significant role in the kinematic behavior of the joint. Allowing at least two degrees of freedom, range of motion was found to be higher in the novel implant surface design when compared to traditional and currently used implant designs in current medicine. Kinematic coupling was not found to be different across the five models due to improper articulations between the surfaces. This suggested that ligament forces played also role in the coupling behavior and that. Distance mapping was used to support the idea that morphological features of the implant had an effect on the kinematic behavior of the ankle. Ligaments of the ankle joint were more properly strained in the novel implant surface design than in the current

implant designs, when compared to the native ankle. Finally, distance mapping of the articulating surfaces displayed how the novel implant surface design allowed for similar trends of contact as the native ankle throughout the different motions of the ankle.

List of References

[1] H. C. M.J. Seo, "The Assessment of Ankle Joint Forces During The Postural Balance Control Movement," *Engineering in Medicine and Biology,* September 4 2005.

[2] A. Jariwala, 2S. Sripada, 2A. Pillai, "Total Ankle Replacement: A Review," *American Medical Journal,* vol. 4, January 17 2013.

[3] A. Lundberg, "Kinematics of the ankle and foot: In vivo roentgen stereophotogrammetry," *Wallin 8t Dalholm* vol. 60, 1989.

[4] B. Hintermann, *Total Ankle Arthroplasty: historical overview, current concepts and future perspectives*: Springer Wien New York.

[5] J. B. Stiehl, & Inman, V. T., *Inman's joints of the ankle*. Baltimore: Williams & Wilkins, 1976.

[6] J. T. Sorin Siegler, Damani Seale, David Pedowitz, "New Observations on The Morphology of The Talar Dome and Its Relationship To Ankle Kinematics," *Clinical Biomechanics,* vol. 29, 2014.

[7] Orthopod, "Lateral Ligaments," in *Website*, ed, 2002.

[8] Becuo. *Instability of the Ankle*. Available: http://becuo.com/deltoid-ligament-mri

[9] M. K. Richard J de Asla, Lu Wan, Harry E Rubash, Guoan Li, "Function of anterior talofibular and calcaneofibular ligaments during in-vivo motion of the ankle joint complex," *Journal of Orthopaedic Surgery and Research,* vol. 4, March, 16 2009.

[10] I. T. J. O. Rasmussen, J. Hedeboe, "An analysis of the function of the posterior talofibular ligament," *International Orthopaedics,* vol. 7, 1983.

[11] H.-S. W. Hyung-Jin Won, Chang-Seok Oh, Seung-Ho Han, In-Hyuk Chung, Jin-Suck Suh, Woo-Chun Lee, "Posterior tibiotalar ligament: An anatomic study correlated with MRI," *Clinical Anatomy,* vol. 27, 2014.

[12] B. G. Hintermann, Pau, "Techniques in Foot & Ankle Surgery," *Special Focus: Advances in Medial Ankle Instability,* vol. 13, 2014.

[13] W. J. S. E. S. Grood, "A Joint Coordinate System for the Clinical Description of Three Dimensional Motions: Applications to the Knee," *Journal of Biomechanical Engineering,* vol. 105, 1983.

[14] C. W. Imhauser, "The Development and Evaluation of a 3-Dimensional, Image-Based, PatientSpecific, Dynamic Model of the Hindfoot," Doctor of Philosophy, Drexel University, 2004.

[15] J. J. O. C. A. Leardini, F. Catani, S. Martelli, S. Giannini, "The kinematics of the ankle in the sagittal plane," *Journal of Biomechanics,* 1998.

[16] S. Siegler, "The three-dimensional kinematics and flexibility characteristics of the human ankle and subtalar joints--Part I: Kinematics.," *Journal of Biomechanical Engineering,* vol. 110, 1988.

[17] J. J. O. C. Alberto Leardini, Sandro Giannini, "Biomechanics of the natural, arthritic, and replaced human ankle joint," *Journal of Foot and Ankle Research,* vol. 7, 2014.

[18] N. Meyers, "Methodology for Designing and Evaluating a Total Ankle Replacement Using a Subject-Specific Numerical Model of the Hind Foot," Master's of Science, Mechanical Engineering, Drexel University, 2013.

[19] D. S. Nawoczenski, Charles L; Cook, Thomas M, "The effect of foot structure on the three-dimensional kinematic coupling behavior of the leg and rear foot," *Physical Therapy,* vol. 78, 1998.